

TAG
106
CER-87/88-2



copy 2

**PLUME BEHAVIOR FROM TALL STACKS
AT SAVANNAH RIVER LABORATORY
AIKEN, SOUTH CAROLINA**

Prepared by

David E. Neff
Robert N. Meroney



**FLUID MECHANICS AND
WIND ENGINEERING PROGRAM**

COLLEGE OF ENGINEERING

**COLORADO STATE UNIVERSITY
FORT COLLINS, COLORADO**

**PLUME BEHAVIOR FROM TALL STACKS
AT SAVANNAH RIVER LABORATORY
AIKEN, SOUTH CAROLINA**

Prepared by

David E. Neff
Robert N. Meroney

Final Report
(August 1986 - July 1987)

Fluid Mechanics and Wind Engineering Program
Department of Civil Engineering
Colorado State University
Fort Collins, CO 80523

for

E. I. Dupont Company
Savannah River Laboratory
Aiken, South Carolina

CSU Contract No. 5-36439

July 1987

CER87-88RNM-DEN2

EXECUTIVE SUMMARY

Title Plume Behavior from Tall Stacks
at Savannah River Laboratory
Aiken, South Carolina

Contractor Civil Engineering Department
Colorado State University
Fort Collins, Colorado 80523

Principal Investigators R. N. Meroney and D. E. Neff

Report Period August 1, 1986 - July 31, 1987

Objective The objective of this study is to physically model, at a reduced scale, the plant stack plume released at three different heights for the L and P reactor complexes at the Savannah River Project for a combination of different wind speeds, wind directions, and atmospheric stabilities.

Results A 1:400 scale model of the L-reactor complex was tested under conditions of neutral atmospheric stability. 1:1000 scale models of the L and P reactor complexes were tested for three different wind directions and stack heights under conditions of neutral, stable, and unstable atmosphere stability. For each atmospheric stability class, data was obtained for passive plumes without the presence of a reactor complex at the three different stack heights. Mean velocity and temperature profiles along with turbulence measurements of all three velocity components are reported for all atmospheric stability classes tested.

Technical Approach Small scale models (1:400, 1:1000) of the L and P nuclear power plant complexes were constructed and placed within a wind tunnel capable of simulating the turbulent character of the atmospheric surface winds. Simulate gases were released at their properly-scaled values from the plant stack models. Video tapes were recorded when these plumes were made visible with smoke. Hydro-carbon tracers in the plumes were measured at 144 or more different locations downwind of the power plant complex for 56 different test conditions.

TABLE OF CONTENTS

<u>Section</u>		<u>Page</u>
	EXECUTIVE SUMMARY.....	i
	TABLE OF CONTENTS.....	ii
	LIST OF TABLES.....	iii
	LIST OF FIGURES.....	iv
	LIST OF SYMBOLS.....	vi
1.0	INTRODUCTION.....	1-1
2.0	MODELING OF PLUME DISPERSION.....	2-1
	2.1 FLUID MODELING OF THE ATMOSPHERIC BOUNDARY LAYER.....	2-2
	2.1.1 Partial Simulation of the Atmospheric Boundary Layer.....	2-3
	2.1.2 Performance of Prior Fluid Modeling Experiments.....	2-7
	2.2 PHYSICAL MODELING OF BLUFF BODY AERODYNAMICS....	2-10
	2.2.1 Simulation Criteria.....	2-11
	2.2.2 Performance of Prior Fluid Modeling Experiments.....	2-18
	2.3 PHYSICAL MODEL OF PLUME MOTION.....	2-18
	2.4 MODELING OF PLUME DISPERSION AT SAVANNAH RIVER SITES.....	2-20
3.0	DATA ACQUISITION AND ANALYSIS.....	3-1
	3.1 WIND-TUNNEL FACILITY.....	3-1
	3.2 WIND AND TEMPERATURE PROFILE MEASUREMENTS.....	3-2
	3.3 POWER PLANT MODEL.....	3-7
	3.4 FLOW VISUALIZATION TECHNIQUES.....	3-8
	3.5 CONCENTRATION MEASUREMENTS.....	3-8
	3.5.1 Gas Chromatograph.....	3-8
	3.5.2 Sampling System.....	3-9
	3.5.3 Test Procedure.....	3-10
4.0	TEST PROGRAM AND DATA.....	4-1
	4.1 VELOCITY AND TEMPERATURE PROFILES.....	4-1
	4.2 CONCENTRATION DATA RESULTS.....	4-2
	4.3 VISUAL PLUME RESULTS.....	4-3
5.0	DISCUSSION.....	5-1
	5.1 APPROACH WIND CONDITIONS.....	5-1
	5.2 VISUALIZATION RESULTS.....	5-2
	5.3 CONCENTRATION RESULTS.....	5-4
	REFERENCES.....	R-1
	TABLES.....	T-1
	FIGURES.....	F-1

LIST OF TABLES

<u>Table</u>		<u>Page</u>
1	Model Test Conditions.....	T-1
2	Field Test Conditions.....	T-2
3	Visualization Test Log.....	T-3
4	Bulk Richardson Number Calculations.....	T-4
5-1 to 5-3	Concentration Measurement Results (Neutral, 1:1000 scale).....	T-5
6-1 to 6-3	Concentration Measurement Results (Stable, 1:1000 scale).....	T-8
7-1 to 7-3	Concentration Measurement Results (Unstable, 1:1000 scale).....	T-11
8	Concentration Measurement Results (1:400 scale).....	T-14
9	Neutral Wind Profile Data.....	T-15
10	Stable Wind Profile Data.....	T-16
11	Unstable Wind Profile Data.....	T-17

LIST OF FIGURES

<u>Figure</u>		<u>Page</u>
1	Meteorological Wind Tunnel.....	F-1
2	Wind Tunnel Configuration for Unstable Flow.....	F-2
3	Savannah River Power Plant.....	F-3
4	Savannah River Plant Site Map.....	F-4
5	Longitudinal Velocity and Turbulent Intensity Profiles (Neutral Stability).....	F-5
6	Longitudinal Velocity and Turbulent Intensity Profiles (Stable Stability).....	F-6
7	Longitudinal Velocity and Turbulence Intensity Profiles (Unstable Stability).....	F-7
8	Turbulence Intensity Profiles (Neutral Stability).....	F-8
9	Turbulence Intensity Profiles (Stable Stability).....	F-9
10	Turbulence Intensity Profiles (Unstable Stability)....	F-10
11	Reynolds Stress Profiles.....	F-11
12	Temperature Profile (Stable Stability).....	F-12
13	Temperature Profile (Unstable Stability).....	F-13
14	Vertical Concentration Profiles of Neutral Flow at 1 and 4 km (Runs 4, 5,6).....	F-14
15	Vertical Concentration Profiles of Stable Flow at 1 and 4 km (Runs 25, 26, 27).....	F-15
16	Vertical Concentration Profiles at Unstable Flow at 1 and 4 km (Runs 36, 37, 38).....	F-16
17	Vertical Concentration Profiles of Stable and Unstable Flow at 10 km (Runs 25, 26, 27 and 36, 37, 38).....	F-17
18	Longitudinal Concentration Profiles, Neutral Flows Maximum Ground Level Values (Runs 1, 4, 7, 9, 12, 14 and 4, 5, 6).....	F-18
19	Longitudinal Concentration Profiles, Stable Flows Maximum Ground Level Values (Runs 17, 20, 23, 25, 28, 30 and 20, 21, 22).....	F-19

<u>Figure</u>		<u>Page</u>
20	Longitudinal Concentration Profiles, Unstable Flows Maximum Ground Level Values (Runs 33, 36, 39, 41, 44, 46 and 36, 37, 38).....	F-20
21-1 to 21-27	Concentration Contour Plots.....	F-21

LIST OF SYMBOLS

Dimensions are given in terms of mass (m), length (L), time (t), moles (n), and temperature (T).

<u>Symbol</u>	<u>Definition</u>	<u>Code</u>
@	at	
C_p	Specific heat capacity at constant pressure	$[L^2 t^{-2} T^{-1}]$
g	Gravitational acceleration	$[L t^{-2}]$
g'	$(= g(\rho_s - \rho_a)/\rho_a)$ gravitational parameter	$[L t^{-2}]$
H	Height	[L]
k	Thermal conductivity	$[m L T^{-1} t^{-3}]$
L	Length	[L]
P	Pressure	$[m L^{-1} t^{-2}]$
Q	Volumetric rate of gas flow	$[L^3 t^{-1}]$
\bar{R}	Universal gas constant	$[n m^{-1} L^2 t^{-1} T^{-1}]$
T	Temperature	[T]
ΔT	Temperature difference across some reference layer	[T]
u_*	Friction velocity	$[L t^{-1}]$
U, u	Mean velocity	$[L t^{-1}]$
W, w	Plume vertical velocity	$[L t^{-1}]$
x	General downwind coordinate	[L]
y	General lateral coordinate	[L]
z	General vertical coordinate	[L]
z_o	Surface roughness parameter	[L]
ν	Kinematic viscosity	$[L^2 t^{-1}]$
ρ	Density	$[m L^{-3}]$
χ	Mole fraction of gas component	--
Ω	Angular velocity of earth - 0.726×10^{-4} (radians/sec)	$[t^{-1}]$

Subscripts

a	Air
bg	Background
g	Gas
H	Evaluated at height H
E	On centerline
m	Model
mea	Measured
p	Prototype
r	Reference conditions
s	Source gas

Superscripts

$\overline{()}$	Mean of a quantity
$()'$	Fluctuating part of a quantity
$()^\cdot$	Quantity per unit time
$()''$	Quantity per unit area

Dimensionless Parameters

Re	Reynolds number
Ri	Bulk Richardson number
Ro	Rossby number
Pr	Prandtl number
Ec	Eckert number
Ma	Mach number
M	Mass flux ratio
F	Momentum flux ratio
Fr	Densimetric Froude number
Fr _s	Densimetric Froude number relative to inertia of the plume
•	
Fr	Flux Froude number
V	Volume flux ratio
SG	Specific gravity
K	Dimensionless concentration

1.0 INTRODUCTION

The Savannah River Laboratory (SRL) Meteorological Group is studying the environmental effects of gases released from five tall stacks located around the SRL facility. These studies are related to the mitigation of effects in case of serious accidents. Preliminary studies suggest that significant safety improvements can be made by replacing current 62 m stacks with taller stacks to 152 m. Gaussian plume models have been used to evaluate plume rise and ground level concentrations. These plume models are too simplistic to accurately evaluate:

- a. Plume interaction with buildings and facilities near stacks,
- b. Effect of irregular terrain or roughness on plume rise, growth, and consequent ground-level concentrations,
- c. Effect of unstable thermal stratification on near stack plume rise and subsequent ground-level concentrations, and
- d. Effect of stable thermal stratification on off-site and site-boundary ground-level concentrations.

This study uses a wind tunnel model of two different Savannah River reactor complexes to evaluate the safety improvements obtained by replacing the current stack with taller ones. Wind-tunnel models are more accurate in predicting the previously mentioned effects than existing Gaussian models.

Reduced scale models of the Savannah River L and P reactor plant complexes were constructed and placed within the Meteorological Wind Tunnel facility at Colorado State University. Plant stack plume concentrations were measured for fifty-six different test conditions. These covered combinations of two model scales, two reactor complexes, and three wind directions under stable, unstable and neutral atmospheric stabilities.

Section 2.0 discusses the physics of modeling plumes at reduced scales, Section 3.0 describes the data acquisition technique used to perform this study, Section 4.0 lists the test program results, and Section 5.0 is a discussion of selected data.

2.0 MODELING OF PLUME DISPERSION

To obtain a predictive model for a specific plume dispersion problem, one must quantify the pertinent physical variables and parameters into a logical expression that determines their interrelationships. This task is achieved implicitly for processes occurring in the atmospheric boundary layer by the formulation of the equations of conservation of mass, momentum and energy. These equations with site and source conditions and associated constitutive relations are highly descriptive of the actual physical interrelationship of the various independent variables (space and time) and dependent variables (velocity, temperature, pressure, density, concentration, etc.).

These generalized conservation statements subjected to the typical boundary conditions of atmospheric flow are too complex to be solved by present analytical or numerical techniques. It is also unlikely that one could create a physical model for which exact similarity exists for all the dependent variables over all the scales of motion present in the atmosphere. Thus, one must resort to various degrees of approximation to obtain a predictive model. At present, purely analytical or numerical solutions of boundary layer, wake, and plume dispersion are unavailable because of the classical problem of turbulent closure (Hinze, 1975). Boundary layer wind tunnels are capable of physically modeling plume processes in the atmosphere under certain restrictions. These restrictions are discussed in the next sections.

2.1 FLUID MODELING OF THE ATMOSPHERIC BOUNDARY LAYER

The atmospheric boundary layer is that portion of the atmosphere extending from ground level to a height of approximately 1000 meters within which the major exchanges of mass, momentum, and heat occur. This region of the atmosphere is described mathematically by statements of conservation of mass, momentum and energy (Cermak, 1975). The mathematical requirements for rigid laboratory-atmospheric-flow similarity may be obtained by fractional analysis of these governing equations (Kline, 1965). This methodology is accomplished by scaling the pertinent dependent and independent variables and then casting the equations into dimensionless form by dividing by one of the coefficients (the inertial terms in this case). Performing these operations on such dimensional equations yields dimensionless parameters commonly known as:

Reynolds number	$Re = (UL/\nu)_r$	= $\frac{\text{Inertial Force}}{\text{Viscous Force}}$
Bulk Richardson number	$Ri = [(Lg\Delta T/T)/U^2]_r$	= $\frac{\text{Gravitational Force}}{\text{Inertial Force}}$
Rossby number	$Ro = (U/L\Omega)_r$	= $\frac{\text{Inertial Force}}{\text{Coriolis Force}}$
Prandtl number	$Pr = [\nu/(k/\rho C_p)]_r$	= $\frac{\text{Viscous Diffusivity}}{\text{Thermal Diffusivity}}$
Eckert number	$Ec = [U^2/C_p(\Delta T)]_r$	

For exact similarity between different flows which are described by the same set of equations, each of these dimensionless parameters must be equal for both flow systems. In addition to this requirement,

there must be similarity between the surface-boundary conditions and the approach flow wind field.

Surface-boundary condition similarity requires equivalence of the following features:

- a. Surface-roughness distributions,
- b. Topographic relief, and
- c. Surface-temperature distribution.

If all the foregoing requirements are met simultaneously, all atmospheric scales of motion ranging from micro to mesoscale could be simulated within the same flow field. However, all of the requirements cannot be satisfied simultaneously by existing laboratory facilities; thus, a partial or approximate simulation must be used. This limitation requires that atmospheric simulation for plume dispersion must be designed to simulate most accurately those scales of motion which are of greatest significance for transport and dispersion of plumes.

2.1.1 Partial Simulation of the Atmospheric Boundary Layer

For the case of the interactions between buildings and structures near a lakeshore and the atmospheric boundary layer, several of the aforementioned parameters are unnecessarily restrictive and may be relaxed without causing a significant effect on the resultant concentration field. The Rossby number magnitude controls the extent to which the mean wind direction changes with height. The effect of Coriolis-force-driven lateral wind shear on wind flow is only significant when heights are of the same order of magnitude as the boundary layer height. The Eckert number (in air $Ec = 0.4 Ma^2 (T_r/\Delta T_r)$, where Ma is the Mach number) is the ratio of energy dissipation to the convection of energy. In both the atmosphere and

the laboratory flow, the wind velocities and temperature differences are such that the Eckert number is very small; hence, it is neglected. Prandtl number equality guarantees equivalent rates of momentum and heat transport. Since air is the working fluid in both the atmosphere and the laboratory, Prandtl number equality is always maintained.

The approach flow Richardson number (Ri) and Reynolds number (Re) determine the kinematic and dynamic structure of turbulent flow within a boundary layer. This influence is apparent in the variations that occur in the spectral distribution of turbulent kinetic energies with changing Ri and changing Re.

The Reynolds Number

Re equality implies $u_m = (L_p/L_m)u_p$. Re equality at a significantly reduced length scale would cause the model's flow velocity to be above sonic; hence, its equality must be distorted. A reduced Re changes only the higher frequency portion of an Eulerian-type description of the spectral energy distribution. Unfortunately, there is no precise definition as to which portion of an Eulerian Spectrum is dominant in dispersing ground-level or elevated plumes over moderate travel distances.

Most investigators use a minimum Reynolds number requirement based on rough-walled pipe measurements; i.e., $Re = u_* z_o / \nu > 2.5$, where u_* , the friction velocity, and z_o , the roughness length, are derived from a log-linear fit to a measured mean velocity profile. The value 2.5 is an empirically determined constant. At Re below 2.5, it is observed that the mean velocity profiles in turbulent pipe flow lose similarity in shape and deviate from the universal curve of a rough wall turbulent boundary layer. For Re above 2.5, it is observed that the surface drag coefficient (and thus the normalized mean

velocity profile) is invariant with respect to increasing Re . For Re between 0.11 and 2.5, the velocity profiles are characteristic of smooth wall turbulent boundary layers. For values below 0.11, the growth of a laminar sublayer on the wall is observed to increase with decreasing Re .

Extrapolation of results from pipe flow measurement to flat plate boundary layers may cause a shift in the magnitude of the minimum Re requirement, but it is generally felt that this shift is small. Precise similarity in the universal form of mean wind shear may be necessary for invariance with respect to the surface drag coefficient, but this does not necessitate that precise similarity must exist for the invariance of the wind field and dispersion. It is the distribution of turbulent velocities which has the greatest effect on the wind field and dispersion. It is the mean wind shear, however, which generates the turbulent velocities. It is possible that the specification of a minimum Re of 2.5 is overly conservative. The criteria, $Re > 2.5$, for example, is not applicable for flow over complex terrain or building clusters.

The Richardson Number

Although most wind-tunnel investigations are conducted with neutrally stratified boundary layers, there are circumstances when the stratification of the atmosphere must be considered. In particular, air pollution and dispersion problems are often critical during stratified conditions. Unstable stratification may be expected to mitigate hazards by accelerating plume dilution, whereas stable stratification may permit high concentrations to persist. The stability state of the atmosphere is typically characterized by the Richardson number.

The atmospheric gradient Richardson number can be computed from averaged quantities through the equation

$$Ri = \frac{g}{T} (\Gamma_d - \Gamma) \left(1 + \frac{0.07}{B} \right) \left[\left(\frac{\partial u}{\partial z} \right)^2 + \left(\frac{\partial v}{\partial z} \right)^2 \right] \quad (1)$$

where Γ and Γ_d are the actual and dry adiabatic potential temperature lapse rates, and $B = [c_p(T_2 - T_1)] / [(z_2 - z_1)(q_2 - q_1)]$ is the Bowen ratio of sensible to latent heat flux at the surface. The Ri number can be taken to represent the ratio of the relative importance of convective and mechanical turbulence. Negative Ri numbers of large value indicate strong convection and weak mechanical turbulence; zero Ri numbers imply purely mechanical turbulence. Positive Ri numbers less than some critical value, $Ri_{critical}$, suggest the presence of mechanical turbulence damped by the density-induced buoyancy forces; for larger positive Ri numbers, turbulence essentially disappears, since the stratification overpowers production by wind shear. The critical Richardson number has a value near 0.25.

Other stability parameters which are frequently used are the flux Richardson number, the bulk Richardson number, the Ekman stability parameter, or the Monin-Obukhov similarity length:

The flux Richardson number:
$$Ri_f = \frac{g \overline{w't'}}{T \overline{u'w'} (du/dz)}$$

The bulk Richardson number:
$$Ri_b = \frac{gz^2 (dT/dz - \Gamma)}{T u^2}$$

The Ekman stability parameter:
$$f = \frac{ku_*}{f_c L_{mo}}$$

The Monin-Obukhov length:

$$L_{mo} = \frac{-T u_*^3}{k g \overline{w't'}}$$

The Richardson Ri, number, is a local parameter rather than a global one since it is based on local flow conditions, but it is inherently related to other parameters such as the Monin-Obukhov stability length. Snyder (1981) calculated typical values for the various stability parameters. Golder (1972) considered the relationships among different stability parameters in the surface layer, and he produced figures to show the relationship between Ri, Ri_b and z/z₀. Ri always approaches zero as z goes to zero at the surface, where mechanical turbulence production due to shear is a maximum.

Richardson numbers characteristic of non-neutrally stable conditions can be obtained in wind-tunnel facilities that control air and floor temperatures. Wind-tunnel temperatures are generally controlled through upstream heat exchangers, injecting of heated air, or the use of a thermal boundary layer permitted to grow over long segments of heated or cooled surfaces (Plate and Cermak, 1963; Teunissen, 1975; Ogawa et al., 1985; Schon and Mery, 1971). Water channels maintain stratification using either heat or, more frequently, layered salt water (Hunt et al., 1978; Snyder et al., 1979).

2.1.2 Performance of Prior Fluid Modeling Experiments

Meroney et al. (1978) summarized experimental data available from field and laboratory studies for neutral airflow over hills, ridges, and escarpments. Wind-tunnel model measurements were performed to study the influence of topography profile, surface roughness and stratification on the suitability of various combinations of these

variables. Detailed tables of velocity, turbulence intensity, pressure, spectra, etc., were prepared to guide numerical model design and experimental rule of thumb restrictions. Cases included hill slopes from 1:2 to 1:20, neutral and stratified flows, two- and three-dimensional symmetric ridges, six alternate hill and escarpment shapes, and a variety of windward versus leeward slope combinations to evaluate ridge separation characteristics. The laboratory data were validated by comparison with field measurements for flow in the Rakaia Gorge, New Zealand, and over Kahuku Point, Oahu, Hawaii, (Meroney et al., 1978; Chien, Meroney and Sandborn, 1979).

Local heating and cooling of coastline or hill surfaces are the driving mechanisms for sea-land breezes, and anabatic and katabatic winds which may inhibit or enhance airflow over the land surface. Early laboratory work includes simulations of urban heat islands by Yamada and Meroney (1971) and Sethuraman and Cermak (1973), simulation of flow and dispersion at shoreline sites by Meroney et al. (1975a), and simulation of dispersion effects of heat rejected from large industrial complexes by Meroney et al. (1975b).

Meroney (1980) compared three model/field investigations of flow over complex terrain, suggested performance envelopes for realizable modeling in complex terrain, and discussed recent laboratory studies which provide data for valley drainage flow situations. Not all of the model/field comparison experiments performed in the past were successful. Many early studies had model approach flow velocity exponents near zero, were modeled as neutral flows when the field observed strong stratification effects, or simulated unrealistic boundary layer depths, integral scales, or turbulence intensities which did not match their atmospheric counterpart. But few studies

claimed unreasonable correlation, and some were strongly self-critical. Nonetheless, most studies accomplished their prestated limited objectives. It would appear that the simulation hypothesis developed in the last few years is appropriate for physical modeling of flow over complex terrain when appropriate care is taken to simulate the approach flow conditions and to maintain simulation parameters equal between model and prototype.

Arya and Plate (1969), Arya (1975) performed velocity, temperature, and turbulence measurements in the lowest 15 percent of a 70 cm deep boundary layer over a smooth surface, where conditions ranged from unstable to moderately stable ($-0.3 < z/L_{mo} < 0.3$). Free stream flow speeds varied from 3 to 9 m/s, and temperature differences were about 40°C across the boundary layer. Cermak, Shrivastava and Poreh (1983) reported mean velocity and turbulence measurements made for a variety of simulated atmospheric boundary layers over different surface roughness. Free stream flow speeds varied from 2.4 to 3.0 m/s and temperature differences were from 150° to -80°C across the boundary layer. Poreh and Cermak (1984) reproduced unstable lapse conditions including mixed layers and elevated inversions. They reproduced the characteristics of convective boundary layer turbulence measured in the atmosphere.

Diffusion studies made by Chaudhry and Meroney (1973) in stable boundary layers investigated previously by Arya (1969) have shown agreement of experimental results with Lagrangian similarity theory. Horst (1979) tested Lagrangian similarity predictions of crosswind-integrated ground concentration against the Prairie Grass diffusion experiment (Barad, 1958) and an experiment at Idaho Falls (Islitzer and Dumbauld, 1963). He reported good agreement for all stabilities

at distances x/z_0 out to 2×10^5 . Poreh and Cermak (1984, 1985) released plumes in their modeled mixing layer. Their plumes exhibited the plume lofting typical of ground sources and the descent typical of elevated sources, predicted from water tank experiments by Willis and Deardorff (1974, 1976, 1978) and numerically by Lamb (1982).

Staff at the Fluid Mechanics Laboratory at the Ecole Centrale de Lyon have studied unstable wind-tunnel boundary layers and compared them with the atmospheric boundary layer (Schon and Mery, 1971). Flow speeds were typically 2 to 4 m/s and the floor temperature was maintained 50°C above ambient. Comparisons with the Kansas data (Haugen et al., 1971) were quite satisfactory, but longitudinal turbulence intensities exhibited a slight Reynolds number dependence, and spectral energy was too low in the high frequency portions of the spectra. The most unstable flow they studied had a Monin-Obukhov scale length of about -1 m at model scales, or -500 to -1000 when scaled to the atmosphere.

2.2 PHYSICAL MODELING OF BLUFF BODY AERODYNAMICS

The interaction of an approach wind field with bluff bodies or structures constructed on the earth's surface is broadly termed "Building Aerodynamics." In a review article on this subject, Meroney (1982) discusses the character of bluff body flow about rectangular buildings and cylindrical cooling towers. Defects in velocity profiles can easily persist from 10 to 15 building heights downwind. Field and laboratory measurements of plume dispersion about the Rancho Seco Nuclear Power Station in Sacramento, California, confirm that cooling tower wake effects persist for significant downwind distances under a variety of stratification conditions (Allwine, Meroney and Peterka, 1978; Kothari, Meroney and Bouwmeester, 1981).

2.2.1 Simulation Criteria

Often atmospheric turbulence may cause only weak effects compared to the turbulence generated by buildings, obstacles, and terrain. Yet the magnitude of the perturbations depends upon the incident flow turbulence scale and intensity, details of the obstacle shape and surface roughness, and size of the obstacle compared to the boundary layer depth. Geometrical scaling implies that the ratio of the building height to length scale must be matched and, of course, that all other building length scales be reduced to this same ratio.

Several questions should be considered when modeling flows which include surface obstacles:

- a. What size obstacles should be disregarded?
- b. What detail or roughness on an obstacle need be included?
- c. To what upwind distance should all obstacles be included?
- d. At what point does the size of a modeled obstacle become too big for the wind tunnel (i.e., blockage effects)?
- e. What is the effect on the flow field of mismatching obstacle and approach flow length scales?
- f. What is the minimum allowable model obstruction Reynolds number?

Obstacle sizes to be disregarded:

Boundary layer studies of rough surfaces reveal that if protuberances are of a size k , such that $u_*k/\nu < 5$, they will have little effect on the flow in a turbulent boundary layer. Thus, assuming a laboratory wind speed of 1 m/s and a typical friction coefficient $C_f/2 = (u^*/u)^2 = 0.0025$, obstacles of size less than 2 mm would go unnoticed.

Required obstacle surface detail or roughness:

Another question that always arises is "How much detail is required for the building or obstacle model? The answer is, of course, dependent upon the size of the protuberance compared to the plume and the dominant eddies of mixing. If the obstruction is large enough to modify the separated wake over the main obstacle, then it must be included. Often an equivalent obstacle surface roughness suffices. Snyder (1981) concludes a generic surface roughness criterion might be $u_* k / \nu > 20$. For a 1 m/s laboratory flow this results in model roughness elements equal to about 6 mm. But since the exterior flow is usually highly turbulent, the body typically includes a highly unsteady wake, and the u_* value to be used should be that acting on the building surface, rather than that of the approach flow. Hence, even this roughness may be unnecessarily large.

Upstream fetch to be modeled:

Suppose there is another building, tree line, fence, cooling tower, or obstacle some distance, s , upstream of a meteorological measurement location; is it necessary to include this obstacle in the wind-tunnel model? Hunt (1974) showed that the velocity deficit in the wakes of cubes and cylinders is given approximately by:

$$DU_{mx}/U(h) = A (s/h)^{-3/2} \quad (2)$$

downwind of the separation bubble, where DU_{mx} is the maximum mean velocity deficit created by the obstacle, h is the height of the obstacle, S is the distance downstream of the obstacle, and A is a constant dependent upon the obstacle shape, orientation, boundary layer thickness, etc. Typically, $A = 2.5$, but it may range from 1.5

to 5.0. If we desire that the velocity at the spill site be within 3 percent of its undisturbed value, Snyder (1981) recommends that any upstream obstacle as high as $s/20$ be included upstream in the model of the spill site. If the obstacle's width is much greater than its height (for example, a fence or ridge), one should include it in the physical model if its height is greater than $s/100$.

Blockage effects:

Because of the influence of wind-tunnel walls on the behavior of the flow past models, it is desirable to use small models or big tunnels, or both. On the other hand, larger models are not only easier to work with, but they may be needed for similarity reasons to achieve large enough Reynolds numbers. It is possible to identify three different types of effects of wind-tunnel constraints. The first is the simple "solid blockage" effect which arises because the fluid stream is unable to expand laterally as it normally would in unconfined flow. The second effect, called "wake blockage", results because the accelerated flow between an obstacle and the tunnel walls continues to "pinch" the wake flow region and reduce its normal lateral rate of growth. The third effect is produced by the growth of boundary layers on the tunnel walls which produce "wall boundary interference." Tunnel blockage can cause separation and reattachment locations to vary, produce higher velocities, larger wake turbulence, and modify the dispersion patterns in the vicinity of obstructions.

The ratio of the cross-sectional area of a model obstacle to that of the tunnel is called the "blockage ratio," BR. Mass continuity produces an average velocity speed-up of $S = BR/(1-BR)$. Although wind tunnels with adjustable ceilings can compensate to some extent by raising the roof locally; this is not a perfect solution to the

problem. Measurements on building and cooling tower models placed in different size wind-tunnel test sections reveal major changes in the character of pressure distributions, separation, and wake growth in the presence of flow restricted by wind-tunnel side walls (Farell et al., 1977).

Blockage corrections, which are conventionally applied in aeronautical tunnels, cannot usually be applied to the typical asymmetric model configuration placed against the wall of a meteorological wind tunnel (Ranga Raju and Singh, 1976). Conventional wisdom now suggests the "rule of thumb" that blockage ratios greater than five percent should be avoided.

Simulation of the flow over sharp-edged obstacles:

A number of authors have discussed flow studies about simple cubical or rectangular sharp-edged obstacles. An extensive review about such flow fields and the subsequent character of diffusion near obstacles has been provided by Hosker (1984). Peterka, Meroney and Kothari (1985) describe typical flow deviations which result from the presence of a sharp-edged building.

Consider the main features of the flow around a sharp-edged building. Typically, when the approach flow is normal to the building face, the flow separates from the ground upwind of the building and produces a "horseshoe"-shaped vortex which wraps around the base of the building. The surface streamline reattaches on the front of the building, and fluid parcels move up and down the building's forward face. An elevated streamline flows over the obstacle, dips down behind, and stagnates on the surface at the end of the recirculating cavity immediately downwind of the building. Sometimes separation streamlines from the forward building edges reattach to the same face,

yet in other cases the streamlines enter the downwind cavity and mingle with the other recirculating fluid. Air which enters the cavity departs through turbulent mixing across the dividing streamlines, mingles with downwind-pointing vortices and is ejected laterally out of the cavity, or leaves suddenly during an exhalation when the entire cavity appears to collapse and then reform.

When a building is oriented obliquely to the wind, flow over the front side walls does not separate, but strong recirculation occurs on the downwind faces. Flow over the roof often produces counter-rotating "delta-wing" vortices which increase mixing over the top and in the wake of the building. These vortices can cause reattachment of the flow in the middle of the roof and serious plume downwash in the near wake. Other features of the flow near the building include vertical vortices produced by the vertical corners of the building.

Golden (1961) measured the concentration patterns above the roof of model cubes in a wind tunnel. Two sizes of cubes were used to vary the Reynolds number from 1000 to 94,000. The concentration isopleths in the fluid above the cube roof showed only slight variations over the entire range of Reynolds numbers studied. The maximum concentration on the roof itself was found to vary strongly with Reynolds numbers less than 11,000, but to be invariant with Reynolds numbers between 11,000 and 94,000. Frequently, modelers quote Golden's experiments as justification for presuming dispersion invariance when obstacle Reynolds numbers exceed 11,000. However, Golden's "11,000 rule" is limited to the measurement of concentrations at only one point on the roof of smooth-walled cubes placed in a uniform approach flow of very low turbulent intensity. It is probably quite conservative because the shear and high turbulence in a simulated

atmospheric boundary layer are likely to further reduce the critical Reynolds number. Indeed, Halitsky (1968) observed that for dispersion in the wake region, no change in isoconcentration isopleths from passive gas releases was found to occur for values of Reynolds number as low as 3300.

Flow around sharp-edged obstacles will remain kinematically similar at very low Reynolds numbers. Wake width variation will be minimal, and obstacle generated turbulence scales and intensity will only vary slowly as Reynolds number decreases. Gas clouds dispersing in this environment will remain similar at very low model speeds.

Simulation of flow over rounded obstacles:

Flow around a smooth cylinder is Reynolds number dependent. This dependence reflects changes in the nature of the boundary layer that forms over the cylinder and its behavior in the vicinity of the flow separation. At low Reynolds numbers, the boundary layer is laminar, and separation occurs easily under the influence of even modest positive pressure gradients. At higher Reynolds numbers, the boundary layer becomes turbulent and flow separation is delayed; i.e., the flow can move farther along a curved surface without separation. At prototype scales, obstacles are large enough that only turbulent separation occurs. However, model flows are usually at such low Reynolds numbers that the local boundary layer growing over a curved surface would be laminar. Most modelers attempt the reproduction of full-scale similarity around curved surfaces by artificially roughening the model surface to force transition to turbulence in these laminar boundary layers. This can be done by providing the surface with special (or artificial) roughness elements, for example, sandpaper, thin wires, or grooves. The height of the roughness, k ,

should be such that $Uk/\nu > 400$ and $k/R < 0.01$, where U is the mean wind speed at obstacle height, and R is the characteristic obstacle radius of curvature. Szechenyi (1975) studied flows about rough circular cylinders and determined that as Reynolds number decreases, roughening the surface becomes less effective. Fage and Warsap (1929) considered the effect of increasing the surface roughness of cylinders on their drag coefficient. Eventually, even ridiculously large roughness is ineffective.

Niemann and Ruhwedel (1980) compared pressures and forces about a 1:333 scale model to a full-scale hyperbolic cooling tower shell. They roughened their model with vertical ribs of height 0.09 mm and width 0.77 mm, producing a roughness coefficient of $k/2R = 0.0006$ and roughness Reynolds number, $Re_k > 270$. They found meridional forces on the cooling tower model and prototype were similar. Model Reynolds numbers were between 4.5×10^5 and 6.0×10^5 , and this corresponding to $U_m > 45$ m/s. But again these speeds are much higher than is appropriate for current measurements.

Halitsky et al. (1963) examined dispersion about a smooth-model nuclear reactor containment building (a hemisphere fitted on a vertical cylinder) and found a critical Reynolds number greater than 79,000. (Yet this critical Reynolds number was for flow very close to the vessel wall. The behavior of concentration isopleths further downwind is likely to be less Reynolds number dependent.)

Although the details of fluid motions around rounded obstacles vary significantly with Reynolds number, the gross features of the flow do not change. Even small models at low wind speeds will produce horseshoe-shaped ground vortices, elevated pairs, and regular vortex

shedding. If the internal boundary layer over the obstacle is laminar, then the wake region will be broader and less intense.

2.2.2 Performance of Prior Fluid Modeling Experiments

A number of studies have been performed in the CSU Fluid Dynamics and Diffusion Laboratory to establish the effect of buildings and meteorological masts on flow fields. Hatcher et al. (1977) examined flow and dispersion in stratified flow downwind of the Experimental Organic Cooled Reactor, Idaho Falls; Allwine et al. (1978) studied the Rancho Seco Reactor, Sacramento; Kothari et al. (1981) studied the Duane Arnold Energy Center, Iowa. In each case field measurements were compared to laboratory measurements with good agreement. Specific effects of the structure of a meteorological mast on instrumentation response were reported by Hsi and Cermak (1965).

2.3 PHYSICAL MODEL OF PLUME MOTION

In addition to modeling the turbulent structure of the atmosphere in the vicinity of a test site it is necessary to properly scale the plume source conditions. One approach would be to follow the methodology used in Section 2.1; i.e., writing the conservation statements for the combined flow system followed by fractional analysis to find the governing parameters. An alternative approach, the one which will be used here, is that of similitude (Kline, 1965). The method of similitude obtains scaling parameters by reasoning that the mass ratios, force ratios, energy ratios, and property ratios should be equal for both model and prototype. When one considers the dynamics of gaseous plume behavior the following nondimensional parameters of importance are identified.*

*The scaling of plume Reynolds number is also a significant parameter. Its effects are invariant over a large range. This makes it possible to accurately model its influence by maintaining model tests above a minimum plume Reynolds number requirement.

$$\text{Mass Flux Ratio (M)} = \frac{\text{mass flow of plume}}{\text{effective mass flow of air}} = \frac{\rho_g W_g A_g}{\rho_a U_a A_a}$$

$$= \left[\frac{\rho_s Q}{\rho_a U_a L^2} \right] @ \text{ source}$$

$$\text{Momentum Flux Ratio (F)} = \frac{\text{inertia of plume}}{\text{effective inertia of air}} = \frac{\rho_g W_g^2 A_g}{\rho_a U_a^2 A_a}$$

$$= \left[\frac{\rho_s Q^2}{\rho_a U_a^2 L^4} \right] @ \text{ source}$$

Densimetric Froude

$$\text{No. relative to the inertia of air (Fr)} = \frac{\text{effective inertia of air}}{\text{buoyancy of plume}} = \frac{\rho_a U_a^2 A_a}{g(\rho_g - \rho_a)V_g}$$

$$= \left[\frac{U_a^2}{g \left(\frac{\rho_s - \rho_a}{\rho_a} \right) L} \right] @ \text{ source}$$

Densimetric Froude No.

$$\text{relative to inertia of the plume (Fr}_g\text{)} = \frac{\text{inertia of plume}}{\text{buoyancy of plume}} = \frac{\rho_g W_g^2 A_g}{g(\rho_g - \rho_a)V_g}$$

$$= \left[\frac{Q^2}{g \left(\frac{\rho_s - \rho_a}{\rho_s} \right) L^5} \right] @ \text{ source}$$

$$\text{Flux Froude No. (Fr)} = \frac{\text{momentum flux of air}}{\text{buoyancy momentum flux of plume}}$$

$$= \frac{\rho_a U_a^2 A_a}{Qg(\rho_g - \rho_a)(L/U_a)} = \left[\frac{U_a^3 L}{Qg \left(\frac{\rho_s - \rho_a}{\rho_a} \right)} \right] @ \text{ source}$$

$$\text{Volume Flux Ratio (V)} = \frac{\text{volume flow of plume}}{\text{effective volume flow of air}} = \frac{W_g A_g}{U_a A_a}$$

$$= \left[\frac{Q}{U_a L^2} \right] \quad @ \text{ source}$$

It is necessary to maintain equality of the plume's specific gravity, ρ_g/ρ_a , over the plume's entire lifetime to obtain simultaneous simulation of all of these parameters. Unfortunately a requirement for equality of the plume gas specific gravity for plume with significant buoyancy differences (i.e. $\rho_g \neq \rho_a$) leads to several complications in practice. These are:

- 1) Equality of the source gas specific gravity between a model and its atmospheric equivalent leads to a wind speed scaling of $u_m = (L_m/L_a)^{1/2} u_a$. For a significant range of atmospheric wind speeds this relationship leads to wind-tunnel speeds at which there is a possible loss of the Reynolds number invariance in the approach flow.
- 2) A thermal plume in the atmosphere is frequently simulated in the laboratory by an isothermal plume formed from a gas of appropriate molecular weight. Under certain situations of specific heat capacity mismatch, this practice will lead to a variation of the equality of plume density as the plume mixes with air.

It is important to examine each modeling situation and decide if an approximation to complete plume behavior may be employed without a significant loss in the similarity of the modeled plume structure.

2.4 MODELING OF PLUME DISPERSION AT SAVANNAH RIVER SITES

The previous sections have described in general terms the scaling laws that cover a large class of fluid modeling applications. The intent of this section is to specifically address the modeling techniques used in the present study.

In order to obtain a proper wind-tunnel scaling of the Savannah River sites surface layer winds the approach flow characteristics must

be similar. To insure similarity in both the mean velocity variation and turbulent character with height the wind tunnels surface roughness and vertical temperature gradients were adjusted.

For a neutral stability flow condition, a convenient parameter which characterizes the mean velocity variation with height is z_0 , the aerodynamic roughness height (Schlichting, 1968), as defined by log-linear description of velocity variation in a boundary layer. A convenient parameter which characterizes the scales of turbulent velocity fluctuations is Λ_i , the integral scale of turbulence (Hinze, 1975). The conditions in the wind tunnel were adjusted until both of these length scales were in the same proportion to their atmospheric equivalents obtained from Counihan (1975) as the geometric length scale chosen for the model terrain construction. This optimal geometric length scale was chosen to be 1:1000.

For stable and unstable flow conditions equality of the Bulk Richardson number was of primary importance

$$(Ri)_m = (Ri)_p = \frac{g H^2 (\Delta T / \Delta Z - \Gamma)}{T u^2}$$

To achieve model Richardson numbers of similar magnitude as those observed at the Savannah River site at a length scale ratio of 1:1000 the model velocity must be lower than the field velocity and the model temperature gradient must be greater than the field gradient.

For plume similarity buoyancy scaling was not required since the Savannah River stack gases are released at near ambient temperatures. Thus the two primary scaling considerations were that the velocity ratio (wind speed at the stack height to stack gas exit velocity) be

equivalent and that the model stack gases be tripped turbulent within the stack. Since the model simulant gas density and the field stack gas density were equal, velocity ratio equality also guarantees momentum ratio equality.

Summarizing these comments into a model parameter decision process yields:

Neutral Stability

1. Maximum field dispersion distance of interest and size of the wind tunnel facility lead to a model-field length scale decision.
2. Model stack exit velocity is chosen so that plume is turbulent at exit; thus assuring plume Reynolds number independence.
3. Equality of model and field velocity ratios with known field ratio and model stack velocity yields model wind speed at stack height.
4. Wind-tunnel floor roughness is adjusted to produce proper scaled wind shear and turbulence structure.
5. Model wind speed and stack exit velocity are increased to assure Reynolds number independence of approach flow and stack flow.

Non-Neutral Stability

1. It is the same as for neutral flow.
2. It is the same as for neutral flow.
3. It is the same as for neutral flow.
4. Wind tunnel's approach flow temperature profile and floor roughness is adjusted to create desired Richardson number and thus properly scaled wind shear and turbulence.

5. If Richardson number magnitudes are insufficient when wind tunnel temperature boundary conditions are at their limit, then model wind speed must be reduced sacrificing plume Reynolds number independence or model-field length scale ratio must be reduced.

3.0 DATA ACQUISITION AND ANALYSIS

Laboratory measurement techniques are discussed in this section, along with conversion methods which provide a basis for interpretation of model data in terms of field equivalent quantities. Some of the methods used are conventional and need little elaboration.

3.1 WIND-TUNNEL FACILITIES

The experiments were performed in the Meteorological Wind Tunnel (MWT) shown in Figure 1. This wind tunnel, especially designed to study atmospheric flow phenomena, incorporates special features such as an adjustable ceiling, a rotating turntable, temperature controlled boundary walls, and a long test section to permit adequate reproduction of micrometeorological behavior. Mean wind speeds of 0.2 to 36 m/sec in the MWT can be obtained. Boundary-layer thickness up to 1.2 m can be developed "naturally" over the downstream 12 m of the MWT test section. Thermal stratification in the MWT is provided by the heating and cooling systems in the section passage and the test section floor. The flexible test section on the MWT roof is adjustable in height to permit the longitudinal pressure gradient to be set at zero.

During the neutral stability test series the following test section modifications were employed:

- Three inch diameter by three foot long honeycombed tubes were installed across the entrance of the tunnel test section.
- One centimeter high link chains were placed across the entire test section floor to insure the proper upwind roughness condition.
- The air flow and wall boundary temperatures were maintained at an isothermal condition of 22°C.
- The power plant model was placed 12 m downwind of the test section entrance at a location at which an equilibrium boundary layer had developed.

During the stably-stratified test series the following test section modifications were employed:

- The tunnel floor temperature was maintained at 0°C and the incoming air temperature was maintained at 48°C.

During the unstably stratified test series the following test section modifications were employed:

- The honeycomb flow straightener was moved to four meters upwind of the model.
- The 12 upwind cooling plates were arranged into the configuration shown in Figure 2 thus providing cooling to the air layer 15 cm to 55 cm above the ground levels.
- The air entering the test section was heated to 48°C.
- The aluminum floor 2 meters upwind of the model to 10 meters downwind was electrically heated. The leading portion of the aluminum floor (2 m upwind of model) was heated to ~110°C. The floor temperature from the leading edge (2 m upwind of model) to the end of the test section (10 m downwind of model) was maintained as a decreasing temperature from 110°C to 40°C.

3.2 WIND AND TEMPERATURE PROFILE MEASUREMENTS

Velocity measurements were made with single hot film and cross film anemometer systems from Thermo-System, Inc. (TSI). Temperature measurements were made with miniature thermocouples. Each of these instruments will be described in the following sections.

Velocity Standard

The velocity standard used in the present study consisted of a Matheson model 8116-0154 mass flowmeter, a Yellow Springs thermistor, and a profile conditioning section designed and calibrated by the FDDL staff at CSU. The mass flowmeter measures mass flow rate independent of temperature at the exit conditions, and the profile conditioning section forms a flat velocity profile of very low turbulence at the position where the probe is located. Incorporating a measurement of the ambient atmospheric pressure and a small profile correction factor

permits the calibration of velocity at the measurement station from 0.15-2.0 m/s ± 5 percent. These error bounds were determined by comparison to TSI's 1125 velocity calibrator system.

Single-Hot-Film Probe Measurements

Single-hot-film (TSI 1210 Sensor) measurements were used to document the longitudinal turbulence levels for the three different approach flow conditions and as an error estimator for the cross film measurements. During calibration of the single film probe anemometer voltages were digitized for several velocities covering the range of interest at a specific calibration temperature. These voltage-velocity $(E,U) \Big|_{T=T_{cal}}$ pairs were then regressed to the equation $E^2 = A + BU^c$ via a least squares approach to assumed values of exponent c . Convergence to the minimum square was accelerated by using the secant method to find the best new estimate of c .

To take measurements with this calibrated single film probe the anemometer voltage along with a temperature signal from a thermocouple mounted close to the sensor were digitized and stored on a disk file within an IBM AT computer. This voltage time series was converted to a velocity time series using the inverse of the calibration equation;

$$U = [(E^2 - A^*)/B^*]^{1/c}$$

where $A^* = A T_{factor}$,

$$B^* = B T_{factor}$$

$$T_{factor} = (T_{sensor} - T_{environment}) / (T_{sensor} - T_{calibration})$$

$T_{\text{environment}}$ was obtained by the appropriate conversions on the thermocouples time series. This velocity time series was then analyzed for pertinent statistical quantities, such as mean, mean square, etc. and tabulated at the computer.

The calibration curve yielded hot film anemometer velocities that were always within ± 2 percent of the known calibrator velocity. The accuracy of a single-hot-film during the measurement of turbulent flow quantities is dependent upon the flow regime being measured. During the present study the single-film probe was used in conditions of mean wind shear and temperature gradients. The errors associated with using an analytic correction for temperature effects on a hot wire are discussed in Thermo-Systems Anemometry News and should be accurate to within ± 5 percent. Considering the accumulative effect of calibrator, calibration curve fit and temperature correction errors the model velocity time series should be accurate to within ± 10 percent.

Cross-Film Probe Measurements

Cross-film (TSI 1241) measurements were used to document longitudinal, lateral and vertical turbulence levels for all approach flow conditions.

During calibration of the 1241 X-film probe it was placed at the nozzle of the calibrator with the probe support axis parallel to air flow. In this position the angle between each sensor and the flow vector is 45° thus, the yaw angles for each sensor are 45° . The voltage from each anemometer channel were digitized for several velocities covering the range of interest. These voltage-velocity pairs ($E_i, U_i; i = 1,2$), at a fixed angle, were fit to the equation

$$E_{i,j}^2 = A_i + B'_i(U_j)^{c_i} ; \quad i = 1,2; j = 1,n$$

where $B'_i = B_i(\cos^2\phi_i + k^2\sin^2\phi_i)^{c_i/2}$

ϕ_i = yaw angle between velocity vector and film i.

k = yaw factor

n = number of calibration points

via a least squares fit with the secant method to find the best new estimate of exponent, c_i . Note that if the yaw factor, k, equals zero then a simple cosine law dependence of heat flux exists. To determine the yaw factor, k, the air velocity was set at a constant value, and the probe was rotated about its third axis so that voltage samples could be taken for a wide range of yaw angle variation on both films. These voltage-yaw angle pairs, $(E_i, \phi_i; i = 1,2)$ were regressed to the equation

$$B'_i = (E_{i,j}^2 - A_i)/U_j^{c_i} = B_i(\cos^2\phi_{i,j} + k_i^2\sin^2\phi_{i,j})^{c_i/2}$$

where $i = 1,2$ and $j = 1,n$

via a least squares approach with the secant method to find the best new estimate for the yaw factor, k_i . A_i , B_i , c_i and k_i for both films are thus obtained. For the reduction algorithm used, k_i must be equal for both films and not a function of velocity. Providing that both films have a similar aspect ratio, then both k_i values should be of similar magnitude; hence, setting them equal does not introduce large errors. Once a value for k is specified then a least squares fit will determine the optimal values for B_i . Once the value of k was

determined for a specific probe, it was no longer necessary to perform further angle calibrations.

Given the calibration constants A_i , B_i , c_i and the equations

$$E_i^2 = A_i + B_i (V_{\text{eff},i})^{c_i}; \quad i = 1,2$$

where $V_{\text{eff},i} = V(\cos^2 \phi_i + k^2 \sin^2 \phi_i)^{1/2}; \quad i = 1,2$

$V_{\text{eff},i}$ = effective cooling velocity for film i , and

V = total velocity vector approaching sensor array.

To take measurements with this calibrated X-film probe both anemometer signals and the temperature signal were digitized and stored on a disk file within an IBM AT computer. These voltage time series were converted to u and v (or w) velocity time series using the following algorithm proposed by Brunn, 1974

$$u = (V_{\text{eff},1} + V_{\text{eff},2}) / [2(\cos^2 \alpha + k^2 \sin^2 \alpha)^{1/2}]$$

$$v \text{ (or } w) = (V_{\text{eff},1} - V_{\text{eff},2}) / [(\cos^2 \alpha + k^2 \sin^2 \alpha)^{1/2} A \tan \alpha]$$

where $A = \cos^2 \alpha (1 - k^2) / [\cos^2 \alpha (1 - k^2) + k^2]$

$$\alpha = 45^\circ$$

$$V_{\text{eff},i} = [(E_i^2 - A_i^*) / B_i^*]^{1/c_i}$$

$$A_i^* = A_i T_{\text{factor}}$$

$$B_i^* = B_i T_{\text{factor}}$$

$$T_{\text{factor}} = (T_{\text{sensor}} - T_{\text{environment}}) / (T_{\text{sensor}} - T_{\text{calibration}})$$

The accuracy of X-film velocity measurements and associated reduction algorithms can be estimated by directing different known mean velocity vectors at the probe. Tests at calibration temperature determined that the mean velocity magnitude is generally within ± 5 percent of the calibrators value. The error in angle calculations was approximately $\pm 2^\circ$ for angular deviations of 15° or less and somewhat larger than this for greater deviations. Considering the accumulative effect of calibrator, calibration curve fit and temperature correction errors, the model longitudinal velocity time series should be accurate to within ± 10 percent. The lateral or vertical model velocity time series errors are greater than those of the longitudinal components but should be accurate to within ± 20 percent.

Temperature Measurements

A copper-constant thermocouple with a bead diameter of 0.07 mm was mounted 2 mm to the side of the hot film probes. An Omega model DSS-199 digital thermometer connected to this thermocouple provided an analog signal directly proportional to temperature. This analog signal was digitized and recorded in an IBM AT computer. The absolute accuracy of the temperature measurement is stated by the manufacturer to be $\pm 1.3^\circ\text{C}$. The ability of this digital thermometer to measure temperature differences is better than this and is estimated to be $\sim \pm 0.4^\circ\text{C}$.

3.3 POWER PLANT MODEL

In order to reproduce the stack plume dispersion physics at the Savannah River site in the MWT two different model to field length scale ratios were used. Initial tests on a neutral plumes size were made on an existing 1:400 scale model of the L-reactor complex. The

majority of the test program used 1:1000 scale models of the L and P reactor complexes (Figures 3 and 4). These models were made from wood for the buildings and from brass tubing for the stacks.

To change the wind direction between the different tests, the model reactor complex was rotated inside the wind tunnel. To increase the turbulence levels within the stacks an 0.5 diameter orifice was placed 4 diameters below the stack exit.

The stack plume specific gravity was ~ 1.0 ; thus, a neutrally buoyant gas mixture of 90 percent air and 10 percent ethane (C_2H_6) was used as a stack simulant. This gas mixture was metered into the model power plant stack by a Matheson gas proportioning flowmeter. This method provided source gas tracer accuracies of ± 10 percent and overall source gas flow rate accuracies of ± 5 percent.

3.4 FLOW VISUALIZATION TECHNIQUES

A visible plume was produced by passing the simulant gas through an oil smoke generator (Fog/Smoke Machine manufactured by Roscolab, Ltd.). The visible plumes for each test were recorded on VHS video cassettes with a Panasonic camera/recorder system.

3.5 CONCENTRATION MEASUREMENTS

The experimental measurements of concentration were performed using a Hewlett Packard gas-chromatograph and sampling systems designed by Fluid Dynamics and Diffusion Laboratory staff.

3.5.1 Gas Chromatograph

A gas chromatograph (Hewlett-Packard Model 5710A) (GC) with flame ionization detector (FID) operates on the principle that the electrical conductivity of a gas is directly proportional to the concentration of charge particles within the gas. The ions in this case are formed by the burning a mixture of hydrogen and the sample

gas in the FID. The ions and electrons formed enter an electrode gap and decrease the gap resistance. The resulting voltage drop is amplified by an electrometer and fed to the HP 3390A integrator. When no effluent gas is flowing, a carrier gas (nitrogen) flows through the FID. Due to certain impurities in the carrier, some ions and electrons are formed creating a background voltage or zero shift. When the effluent gas enters the FID, the voltage increase above this zero shift is proportional to the degree of ionization or correspondingly the amount of tracer gas present. Since the chromatograph used in this study features a temperature control on the flame and electrometer, there is very low drift of the zero shift. In case of any zero drift, the HP 3390A, which integrates the effluent peak, also subtracts out the zero drift.

The lower limit of measurement is imposed by the instrument sensitivity and the background concentration of tracer within the air in the wind tunnel. Background concentrations were measured and subtracted from all data quoted herein.

3.5.2 Sampling System

The tracer gas sampling system consists of a series of fifty 30 cc syringes mounted between two circular aluminum plates. A variable-speed motor raises a third plate, which lifts the plunger on all 50 syringes, simultaneously. Computer controlled valves and tubing are connected such that airflow from each tunnel sampling point passes over the top of each designated syringe. When the syringe plunger is raised, a sample from the tunnel is drawn into the syringe container. The sampling procedure consists of flushing (taking and expending a sample) the syringe three times after which the test

sample is taken. The draw rate is variable and generally set to be approximately 6 cc/min.

The sampling was periodically calibrated to insure proper function of each of the valves and tubing assemblies. To calibrate the sampler each intake was connected to a manifold. The manifold, in turn, was connected to a gas cylinder having a known concentration of tracer gas. The gas was turned on, and a valve on the manifold was opened to release the pressure produced in the manifold. The manifold was allowed to flush for about one minute. Normal sampling procedures were carried out during calibration to insure exactly the same procedure is reproduced as when taking a sample from the tunnel. Each sample was then analyzed for tracer gas concentration. Percent error was calculated, and "bad" syringe/tube systems (error > 2 percent) were repaired.

3.5.3 Test Procedure

The test procedure consisted of: 1) setting the proper tunnel wind speed, 2) releasing the metered mixtures of source gas from the plant stack, 3) withdrawing samples of air from the tunnel designated locations, and 4) analyzing the samples with a FID. The samples were drawn into each syringe over a 300 s (approximate) time period and then consecutively injected into the GC.

The procedure for analyzing the samples from the tunnel is: 1) to introduce the sample into the GC which separates ethane tracer from other hydrocarbons, 2) the voltage output from the electrometer is sent to the Hewlett-Packard 3390A Integrator, 3) the 3390A communicates the measured ppm to an IBM computer for storage, 4) these values χ_{mea} , along with the response levels for the background χ_{bg} and

source x_{source} are converted into source normalized concentration by the equation

$$x_m = \frac{x_{\text{mea.}} - x_{\text{bg}}}{x_{\text{source}} - x_{\text{bg}}}$$

The background concentrations, x_{bg} , were accurate only to $\sim \pm 20$ percent due to background variations as the result of previous tests within the same area. The measured concentrations, $x_{\text{mea.}}$, were accurate to ± 2 percent. The source gas concentration, x_{source} , was accurate to ± 10 percent. Thus the source normalized concentration for $x_{\text{mea.}} \gg x_{\text{bg}}$ was accurate to approximately ± 10 percent. For low concentration values, $x_{\text{mea.}} \lesssim x_{\text{bg}}$, the errors are larger.

4.0 TEST PROGRAM AND DATA

A 1:400 reduced scale model of the Savannah River L-reactor complex and 1:1000 scale models of the L and P reactor complexes were constructed and placed in the Meteorological Wind Tunnel (MET) facility at Colorado State University. Three different simulated atmospheric stabilities were reproduced and tests were performed on different stack heights and wind directions. The velocity and temperature profiles measured upwind of the model area are described in Section 4.1. Simulant gases were released from the power plant stack. The downwind concentrations from the stack were measured at up to 144 spacial locations. The concentration measurement program and results are described in Section 4.2. The simulant gases were also tagged with smoke to make them visible, and video movies for each of the tests were obtained (see Section 4.3).

4.1 VELOCITY AND TEMPERATURE PROFILES

The techniques employed in the acquisition of upwind velocity and temperature information are discussed in Section 3.2. Scaling laboratory measurements up to those expected in the actual field situation are described in Section 3.3. All flow and concentration values reported in this report have been scaled to field conditions.

Figures 5, 6 and 7 display the longitudinal mean velocity and local turbulent intensity profiles for the neutral, stable, and unstable boundary layer respectively. Figures 8, 9 and 10 display the local turbulent intensity profiles for all three velocity components for neutral, stable, and unstable boundary layers respectively. Figure 11 displays the longitudinal-vertical Reynolds stress profiles for all three stability classes. Figures 12 and 13 display the potential temperature profiles for the stable and unstable boundary

layers. These velocity profiles demonstrate the effect that the temperature gradient has upon the transfer of momentum within the boundary layer. In the convective situation (unstable) the momentum of the free stream penetrates close to the ground due to the large vertical convective velocities generated by the thermal instability. In the stable situation, vertical motions are suppressed.

An analysis of selected neutral-stability mean wind profiles measured at the Savannah River T.V. Tower suggested that the appropriate value for the local roughness length, z_0 , is 0.4 meters. This value compares well with the neutral stability simulated boundary layer measurements. Tables 9, 10 and 11 display the numeric values of the pertinent wind field characteristics for neutral, stable, and unstable approach flows.

4.2 CONCENTRATION DATA RESULTS

Techniques employed to obtain the concentration data are discussed in Section 3.5. Tables 1 and 2 summarize the model and field test conditions respectively for which concentration data was obtained. There were two different model scales, three different stability classes, three different wind directions, two different reactor complexes, and three different stack heights tested. A total of 56 different test conditions were examined. For each test condition at least three runs of 48 sample positions each were obtained. Each run consisted of an array of positions in the y-z direction at a fixed downwind distance. The plant stack release rates of $51.9 \text{ m}^3/\text{s}$ remained constant for all tests.

Table 5-1 through 5-3 list the mean concentrations measured for the 1:1000 scale model neutral flow test series. Table 6-1 through 6-3 list the mean concentrations measured for the stable flow test

series. Tables 7-1 through 7-3 list the mean concentrations measured for the unstable flow test series. Table 8 lists the mean concentrations measured for the 1:400 scale model test series.

The origin of the right-handed coordinate system used in these tables to specify sample locations is at ground level at the center of the plant stack. The x direction is always in the mean wind direction, and z is the height above ground level.

4.3 VISUAL PLUME RESULTS

Techniques employed to obtain a visual plume are discussed in Section 3.4. VHS video motion pictures were taken during all test conditions. Table 3 lists the run conditions and tape index for the entire test series. The "comments on the downwash study" column in Table 3 are more fully explained below.

- Laminar - No turbulent trip was in the model stack.
- Turbulent - A one-half diameter orifice was placed four diameters down inside the model stack.
- Hat - A two diameter ring was placed one diameter down around the outside of the model stack.
- Nozzle - A 0.86 diameter nozzle was placed on top of the existing model stack, this increased the stack height by one diameter.
- Small Nozzle - A 0.63 diameter nozzle was placed on top of the existing model stack, this increased the stack height by one diameter.

5.0 DISCUSSION

Approach flow wind conditions are discussed in Section 5.1. Stack plume visual behavior is discussed in Section 5.2. Concentration distributions, vertical profiles, and surface isopleths are reviewed in Section 5.3.

5.1 APPROACH WIND CONDITIONS

As noted earlier in Section 2.1 the simulated atmospheric stratification is usually related quantitatively to prototype conditions through the Monin-Obukhov length or the Richardson number. Golder (1972) prepared a figure which relates Pasquill-Gifford stability categories A thru F to surface roughness, z_0 , and Monin-Obukhov length, L . Once the Monin-Obukhov length is specified the bulk Richardson number value can be calculated over a specific measurement height through equations for the dimensionless shear and temperature and the value of the relevant roughness length. The reference model velocity chosen can then be inserted into the definition of the Richardson number to calculate the desired temperature variation over the specified model measurement height.

Unfortunately, this temperature difference can only be a goal sought while setting the wind tunnel stratification conditions, because the temperature and velocity profiles are nonlinearly interactive! Once an operating condition is finally selected, the actual bulk Richardson number may be calculated using measured model velocity and temperature profiles. Relating these magnitudes to a specific Pasquill-Gifford category becomes the inverse of the earlier process. The report by Snyder (1981) summarizes the necessary equations and provides ranges of Richardson number for different Pasquill-Gifford categories.

The magnitudes of bulk Richardson number calculated for the model conditions studied herein are provided in Table 4. Note that Pasquill-Gifford category specified is a function of the height of the parameter evaluation. For a 5 m to 10 m data range the Richardson numbers calculated suggest unstable and stable stratifications modeled were mildly unstable Class C, and moderately stable Class E. For a 10 m to 61 m data range the Richardson numbers calculated suggest unstable and stable stratifications modeled were mildly unstable Class B and stable Class F. Temperature profiles indicate there were elevated inversions present at about 150 m during the unstable cases.

During the unstable cases in particular there is some uncertainty in relating Pasquill-Gifford categories and the Monin-Obukhov stability length. Recent wisdom suggests that most of the unstable convective boundary layer is governed by the convective velocity, w_* , and the inversion layer height, h , but no data is now available which relates these parameters to Pasquill-Gifford categories. An alternative approach was suggested by Gifford (1976), he noted that σ_θ took on values at a 10 meter height of 25, 20, 15, 10, 5 and 2.5 degrees for Pasquill-Gifford categories A, B, C, D, E, and F, respectively. Presuming a direct relationship between σ_θ and turbulence intensity, v'/U , then the Pasquill-Gifford categories simulated for the unstable, neutral and stable flows were B (18.7°), D (8.5°), and F (1.0°)

5.2 VISUALIZATION RESULTS

During the visualization experiments on the 1:400 scale model of the L-reactor complex it was observed that stack downwash was present. Several additional visual tests were performed on the 1:400 scale model to help define the extent of this problem. When the stack

height was increased, the downwash problem was intensified due to the increased wind velocities at greater elevations within the model boundary layer. Two different mitigation techniques were visually tested. The first was the placement of a circular rim of two stack diameters near the top of the stack exit. This technique produces no visual improvement in the extent of stack downwash. The second mitigation technique was to place different diameter nozzles over the stack exit. Reducing the stack exit area increased the stack exit velocity. It was shown that sufficient reduction of the stack exit eliminated the stack downwash problem.

The visual experiments of the 1:1000 scale models of the L and P reactor complexes demonstrated the following points.

1. There was no noticeable change in stack plume behavior for the different wind directions studied.
2. There was no noticeable change in stack plume behavior for the different reactor complexes studied; L and P.
3. At the 1:1000 model scale the stack plume appeared to be laminar at the exit even though an orifice was placed inside the model stack to trip the internal gases turbulent (the long range dispersion effect of this near source modeling distortion is felt to be minimal).
4. The approach flow stability had a pronounced effect on the visual appearance of the plume. In stable flow plume meandering was minimal and dispersion appeared to be small. In unstable flow the plume would take large vertical and lateral excursions and dispersion was rapid.
5. An increase in stack height increased the distance downwind to where the plume met the ground.
6. In the unstable flow case there was an elevated inversion at ~150 meters height. This cap to the unstable layer was observable in the tests where the model stack height was an equivalent of 152 meter high. This plume would experience larger downward excursions as compared to upward excursions.

5.3 CONCENTRATION RESULTS

Figures 14-17 display selected vertical concentration profiles. Figures 18-20 display the maximum ground level concentrations versus downwind distance for selected tests. Figures 21-1 to 21-27 display concentration contour plots at 1 km, 4 km, and 10 km for the L-reactor complexes three stack heights under conditions of neutral, stable, and unstable atmospheric stability.

The following insights are observed in these figures:

1. Figure 14 shows that for neutral flow (L-reactor at 0°) increasing the plant stack height has the most dramatic effect at 1 km downwind. The taller stacks peak concentrations are still elevated at 1 km downwind. This improvement in ground level peak concentrations is less significant at 4 km downwind. AT 10 km downwind all three plumes are nearly identical (10 km data not shown in Figure 14).
2. Figure 15 shows that for stable flow (L-reactor at 180°) the plume maximum concentration for all three stack heights remained above ground level at both 1 km and 4 km downwind. The concentration distribution remained so narrow as these stable plumes moved downwind that the model measurement grid was not able to resolve the peak concentrations as accurately as in the neutral and unstable flow tests. The top part of Figure 17 shows that at 10 km the peak concentrations of only the 26 m stack occur at ground level.
3. Figure 16 shows that for unstable flow (L-reactor at 0°) the 62 m and 107 m stacks yielded similar concentration distributions at both the 1 km and 4 km locations. The 152 m stack exit was near the bottom of the elevated inversion thus resulting in some persistence of concentration levels at the 1 km location. At 4 km and 10 km (see bottom of Figure 17) all three stacks yielded the same concentration distributions as would be expected in this highly convective situation.
4. The top part of Figure 18 shows that for neutral flow and a 62 m stack there is little difference in maximum ground level concentrations versus downwind distance for changes in the reactor (L or P) complex or wind direction (0° , 180° , 270°). At 1 km the ground level concentrations for the passive plume (Run No. 1; i.e. no stack, no buildings) are less than the others. This shows that stack downwash is causing slightly higher ground level concentrations in the near field.

5. The bottom part of Figure 18 again shows that for neutral flow the most dramatic effect of increasing the stack height is only at 1 km downwind.
6. The top part of Figure 19 shows that for stable flow and a 62 m stack that there appears to be a notable difference in maximum ground level concentrations versus downwind distance for changes in reactor complex (L or P) or wind direction (0° , 180° , 270°).
7. The bottom part of Figure 19 shows that for stable flow large improvements in lowering ground level concentrations are obtained by increasing plant stack heights above the present 62 m.
8. The top part of Figure 20 shows that for unstable flow and a 62 m stack there is little difference in maximum ground level concentrations versus downwind distance for changes in the reactor complex (L or P) or wind direction (0° , 180° , 270°).
9. The bottom part of Figure 20 shows that for unstable flow with an elevated inversion at 150 m the only improvement ground level concentration magnitudes was for the 152 m high stack in the near field (1 km).
10. Figures 21-1 through 21-9 (L-reactor at 0°) display concentration contours for stack heights of 62 m, 107 m, and 152 m in neutral flow at 1 km, 4 km and 10 km downwind. From these figures it is seen that by 4 km downwind even the 152 m stacks maximum concentrations were at ground level. A secondary flow in the wind tunnels boundary layer caused the drift of the plume away from centerline.
11. Figures 21-10 through 21-8 (L-reactor at 0°) display concentration contours for stack heights of 62 m, 107 m, and 152 m in stable flow at 1 km, 4 km, and 10 km downwind. From these figures it is seen that only the 62 m stack plume produces its maximum concentrations at ground level in the 10 km range studied. The 107 m and 152 m high stack plume are still lofting at 10 km.
12. Figure 21-19 through 21-27 (L-reactor at 0°) display concentration contours for stack heights of 62 m, 107 m, and 152 m in unstable flow at 1 km, 4 km and 10 km downwind. From these figures it is seen that by 4 km downwind all stack heights yielded maximum concentrations near ground level. A secondary flow in the wind tunnels boundary layer caused the plume to drift away from centerline.

REFERENCES

- Allwine, K. J., Meroney, R. N., and Peterka, J. A. (1978), "Rancho Seco Building Wake Effects on Atmospheric Diffusion: Simulation in a Meteorological Wind Tunnel," FDDL Report No. CER77-78KJA-RNM-JAP25, Colorado State University, Fort Collins, Colorado.
- Arya, S. P. S., and Plate, E. J. (1969), "Modeling of the Stably Stratified Atmospheric Boundary Layer," J. Atmos. Sci., Vol. 26, No. 4, pp. 656-665.
- Ayra, S. P. S. (1975), "Buoyancy Effects in a Horizontal Flat-Plate Boundary Layer," J. Fluid Mech., Vol. 68, Pt. 2, pp. 321-343.
- Barad, M. L., Ed. (1958), Project Prairie Grass: A Field Program in Diffusion, Geophysical Research Papers, No. 59, Vols. I and II, Report AFCRC-TR-58-235, Air Force Cambridge Research Center.
- Brunn, (1978), "Multi-Probes and Higher Moments," Proceedings of the Dynamic Flow Conference 1978, pp. 943-961.
- Cermak, J. E. (1975), "Applications of Fluid Mechanics to Wind Engineering--A Freeman Scholar Lecture," J. of Fluids Engineering, Vol. 97, pp. 9-38.
- Cermak, J. E., Shrivastava, P. K., and Poreh, M. (1983), "Wind-tunnel Research on the Mechanics of Plumes in the Atmospheric Surface Layer," Civil Engineering Department Report CER83-84JEC-PKS-MP12, Colorado State University, Fort Collins, CO, Annual Progress Report to U.S. Dept. of Army Contract DAAK11-82-K-0004, 140 pp.
- Chaudhry, F. H. and Meroney, R. N. (1973), "A Laboratory Study of Diffusion in Stably Stratified Flow," Atmos. Envir., Vol. 7, pp. 443-454.
- Chien, H. C., Meroney, R. N., and Sandborn, V. A. (1979), "Sites for Wind-Power Installations: Physical Modeling of the Wind Field Over Kahuku Point, Hawaii," FDDL Report No. CER79-80HCC-RNM-VAS25, Colorado State University, Fort Collins, Colorado.
- Counihan, J. (1975), "Adiabatic Atmospheric Boundary Layers: A Review and Analysis of Data from the Period 1880-1972," Atmos. Envir., Vol. 9, pp. 871-905.
- Fage, A. and Warsap, J. H. (1929), "Effects of Turbulence and Surface Roughness on Drag of Circular Cylinders," U.K., ARC R&M 1283.
- Farell, C., Carrasquel, S., Guven, O., and Patel, V. C. (1977), "Effect of Wind-Tunnel Walls on the Flow Past Circular Cylinders and Cooling Tower Models," J. of Fluids Engineering, Vol. 99, pp. 470-479.
- Gifford, F. A. (1976), Turbulent Diffusion-Typing Schemes: A Review, Nucl. Saf., Vol. 17, No. 1, pp. 72 ff.

- Golden, J. (1961), "Scale Model Techniques," M.S. Thesis, Dept. of Met. and Ocean., New York University, 42 pp.
- Golder, D. G. (1972), "Relations Among Stability Parameters in the Surface Layer," Boundary-Layer Meteorol., Vol. 3, No. 1, pp. 47-58.
- Halitsky, J., Golden, J., Halpern, P., and Wu, P. (1963), "Wind Tunnel Tests of Gas Diffusion from a Leak in the Shell of a Nuclear Power Reactor and from a Nearby Stack," N.Y.U. Meteorol. and Oceanog. Geophys. Sciences Lab. Report 63-2 (New York Univ., College of Engineering, New York).
- Halitsky, J. (1968), "Gas Diffusion Near Buildings," Meteorology and Atomic Energy, 1968, editor D. H. Slade, Atomic Energy Commission, Ch. 5-5, pp. 221-256.
- Hatcher, R. V. and Meroney, R. N. (1977), "Dispersion in the Wake of a Model Industrial Complex," Joint Conf. on Applications of Air Pollution Meteorology, Proceedings, Am. Meteorol. Soc., Salt Lake City, Utah, 29 November - 2 December, 1977, pp. 343-346.
- Haugen, D. A., Kaimal, J. C., and Bradley, E. F. (1971), "An Experimental Study of Reynolds Stress and Heat Flux in the Atmospheric Surface Layer," Quart. J. Roy. Meteorol. Soc., Vol. 97, pp. 168-180.
- Hinze, J. O. (1975), Turbulence, McGraw-Hill, New York, 2nd. edition, 790 pp.
- Horst, T. W. (1979), "Lagrangian Similarity Modeling of Vertical Diffusion from a Ground Level Source," J. Appl. Meteorol., Vol. 18, pp. 733-740.
- Hosker, R. P., Jr. (1984), "Flow and Diffusion Near Obstacles," Atmospheric Science and Power Production, DOE/TIC-27601, pp. 241-326.
- Hsi, G., and Cermak, J. E. (1965), "Meteorological-Tower Induced Wind Field Perturbations," Prepared under U.S. Army Research Grant DA-AMC-28-043-64-G-9, Fluid Mechanics Program Report No. CER65GH-JEC49, Colorado State University, Fort Collins, Colorado.
- Hunt, J. C. R. (1974), "Wakes Behind Buildings," presented at the Aeronautical Research Council's Atmospheric Environment Committee Meeting, Oct. 23, ARC Report 35601, Atmos. 229, Aeronautical Research Council of Great Britain, Her Majesty's Stationery Office, London.
- Hunt, J. C. R., Snyder, w. H., and Lawson, R. E., Jr. (1978), "Flow Structure and Turbulent Diffusion around a Three-Dimensional Hill: Fluid Modeling Study on Effects of Stratification: Part I: Flow Structure," Envir. Prot. Agcy. Report No. EPA 600/4-78-041, Research Triangle Park, NC, 84 pp.

- Islitzer, N. F. and Dumbauld, R. K. (1963), "Atmospheric Diffusion-Deposition Studies over Flat Terrain," Int. J. Air Water Pollut., Vol. 7 (11-12), pp. 999-1022.
- Kline, S. J. (1965), Similitude and Approximation Theory, McGraw-Hill Book Company, New York, 229 pp.
- Kothari, K. M., Meroney, R. N., Bouwmeester, (1981), "An Algorithm to Estimate Field Concentrations Under Nonsteady Meteorological Conditions from Wind Tunnel Experiments," Journal of Applied Meteorology, Vol. 30, pp. 92-101.
- Kothari, K. M., Meroney, R. N. and Peterka, J. A. (1979), "Nuclear Power Plant Building Works Effects on Atmosphere Diffusion," EPRI Report No. 1891, CER79-80KMK-RNM-JAP28, 109 pp.
- Lamb, R. G. (1982), "Diffusion in the Convective Boundary Layer," Chapter 5, Atmospheric Turbulence and Air Pollution Modeling, Nieuwstadt and van Dop, editors, D. Reidel Publishing Company, Dordrecht, Holland, pp. 159-230.
- Meroney, R. N. (1980), "Wind-Tunnel Simulations of the Flow Over Hills and Complex Terrain," J. of Industrial Aerodynamics, Vol. 5, pp. 297-321.
- Meroney, R. N. (1982), "Turbulent Diffusion Near Buildings," Engineering Meteorology, Chapter 11, pp. 481-521.
- Meroney, R. N., Cermak, J. E., and Garrison, J. A. (1975a), "Wind-Tunnel Study of Stack Gas Dispersal at Lansing Power Station, Units 1, 2, 3, and 4," FDDL Report No. CER74-75RNM-JEC-JAG28, Colorado State University, Fort Collins, Colorado.
- Meroney, R. N., Cermak, J. E., and Garrison, J. A. (1975b), "Wind-Tunnel Study of Stack Gas Dispersal at Lansing Power Station, Units 1, 2, 3, and 4," FDDL Report No. CER74-75RNM-JEC-JAG29, Colorado State University, Fort Collins, Colorado.
- Meroney, R. N., Sandborn, V. A., Bouwmeester, R. J. B., Chien, H. C., and Rider, M. (1978), "Sites for Wind-Power Installations: Physical Modeling of the Influence of Hills, Ridges and Complex Terrain - Part II: Executive Summary," Dept. of Energy Report RLO/2438-77/3, 90 pp.
- Niemann, H. J. and Ruhwedel, J. (1980), "Full-scale and Model Tests on Wind-induced, Static and Dynamic Stresses in Cooling Tower Shells," Eng. Struct., Vol. 2, pp. 81-89.
- Ogawa, Y., Diosey, P. G., Uehara, K., and Ueda, H. (1985), "Wind Tunnel Observation of Flow and Diffusion Under Stable Stratification," Atmos. Envir., Vol. 19, pp. 65-74.
- Peterka, J. A., Meroney, R. N. and Kothari, K. (1985), "Wind Flow Patterns About Buildings," J. of Wind Engineering and Industrial Aerodynamics, Vol. 21, pp. 21-38.

- Plate, E. J. and Cermak, J. E. (1963), "Micro-meteorological Wind-tunnel Facility," Fluid Dynamics and Diffusion Laboratory Report CER63EJP-JEC9, Colorado State University, Fort Collins, Colorado, 65 pp.
- Poreh, M. and Cermak, J. E. (1984), "Wind Tunnel Simulation of Diffusion in a Convective Boundary Layer," Boundary-Layer Meteorol., Vol. 30, pp. 431-455.
- Poreh, M. and Cermak, J. E. (1985), "Wind-tunnel Research on the Mechanics of Plumes in the Atmospheric Surface Layer, Part II," Annual Report to U.S. Dept. of Army, Chemical Systems Laboratory, Aberdeen Proving Ground, Maryland, Colorado State University Civil Engineering Department Report CER84-85MP-JEC47, 45 pp.
- Ranga Raju, K. G. and Singh, V. (1976), "Blockage Effects on Drag of Sharp Edged Bodies," J. of Industrial Aerodynamics, Vol. 1, pp. 301-309.
- Schlichting, H. (1968), Boundary Layer Theory, McGraw-Hill Book Company, New York, 774 pp.
- Schon, J. P. and Mery, P. (1971), "A Preliminary Study of the Simulation of Neutral Atmospheric Boundary Layer Using Air Injection in a Wind Tunnel," Atmos. Enviro., Vol. 5, No. 5, pp. 299-312.
- Sethurama, S., and Cermak, J. E. (1973), "Stratified Shear Flows Over a Simulated Three-Dimensional Urban Heat Island," Project Themis Technical Report No. 23, CER73-74SS-JEC4, Colorado State University, Fort Collins, Colorado.
- Snyder, W. H., Britter, R. E., and Hunt, J. C. R. (1979), "A Fluid Modeling Study of the Flow Structure and Plume Impingement on a Three-Dimensional Hill in Stably Stratified Flow," Proc. Fifth Int. Conf. on Wind Engr., Pergamon Press, NY, Vol. 1, pp. 319-329.
- Snyder, W. H. (1981), "Guidelines for Fluid Modeling of Atmospheric Diffusion," EPA Report EPA-600/8-81-009, 185 pp.
- Szechenyi, E. (1975), "Supercritical Reynolds Number Simulation for Two-dimensional Flow over Circular Cylinders," J. Fluid Mech., Vol. 70, pp. 529-542.
- Teunissen, H. W. (1975), "Simulation of the Planetary Boundary Layer in a Multiple Jet Wind Tunnel," Atmos. Envir., Vol. 9, pp. 145-174.
- Willis, G. E. and Deardorff, J. W. (1974), "A Laboratory Model of the Unstable Planetary Boundary Layer," J. Atmos. Sci., Vol. 31, pp. 1297-1307.
- Willis, G. E. and Deardorff, J. W. (1976), "A Laboratory Model of Diffusion into the Convective Planetary Boundary Layer," Quart. J. Roy. Meteorol. Soc., Vol. 102, pp. 427-445.

Willis, G. E. and Deardorff, J. W. (1978), "A Laboratory Study of Dispersion from an Elevated Source Within a Modeled Convective Planetary Boundary Layer," Atmos. Envir., Vol. 12, pp. 1305-1311.

Yamada, T. and Meroney, R. N. (1971), "Numerical and Wind-Tunnel Simulation of Response of Stratified Shear Layers to Nonhomogeneous Surface Features," CER7071TY-RNM62, Colorado State University, also (AD-730-953).

Table 1. Model Test Conditions

Test Number	Wind Speed @ H ref. (cm/s)	Stability PG cat.	Wind Dir from CL (degree)	Reactor Complex	Stack Height (cm)	Stack Flow Rate (ccs)
1A	150	D	0	NONE	15.5	96.7
2A	150	D	0	1:400 L	15.5	96.7
1	150	D	0	NONE	6.2	15.6
2	150	D	0	NONE	10.7	15.6
3	150	D	0	NONE	15.2	15.6
4	150	D	0	1:1000 L	6.2	15.6
5	150	D	0	1:1000 L	10.7	15.6
6	150	D	0	1:1000 L	15.2	15.6
7	150	D	0	1:1000 P	6.2	15.6
8	150	D	0	1:1000 P	15.2	15.6
9	150	D	180	1:1000 L	6.2	15.6
10	150	D	180	1:1000 L	10.7	15.6
11	150	D	180	1:1000 L	15.2	15.6
12	150	D	180	1:1000 P	6.2	15.6
13	150	D	180	1:1000 P	15.2	15.6
14	150	D	270	1:1000 L	6.2	15.6
15	150	D	270	1:1000 L	10.7	15.6
16	150	D	270	1:1000 L	15.2	15.6
17	69	E-F	0	NONE	6.2	11.9
18	69	E-F	0	NONE	10.7	11.9
19	69	E-F	0	NONE	15.2	11.9
20	69	E-F	0	1:1000 L	6.2	11.9
21	69	E-F	0	1:1000 L	10.7	11.9
22	69	E-F	0	1:1000 L	15.2	11.9
23	69	E-F	0	1:1000 P	6.2	11.9
24	69	E-F	0	1:1000 P	15.2	11.9
25	69	E-F	180	1:1000 L	6.2	11.9
26	69	E-F	180	1:1000 L	10.7	11.9
27	69	E-F	180	1:1000 L	15.2	11.9
28	69	E-F	180	1:1000 P	6.2	11.9
29	69	E-F	180	1:1000 P	15.2	11.9
30	69	E-F	270	1:1000 L	6.2	11.9
31	69	E-F	270	1:1000 L	10.7	11.9
32	69	E-F	270	1:1000 L	15.2	11.9
33	45	B-C	0	NONE	6.2	11.9
34	45	B-C	0	NONE	10.7	11.9
35	45	B-C	0	NONE	15.2	11.9
36	45	B-C	0	1:1000 L	6.2	11.9
37	45	B-C	0	1:1000 L	10.7	11.9
38	45	B-C	0	1:1000 L	15.2	11.9
39	45	B-C	0	1:1000 P	6.2	11.9
40	45	B-C	0	1:1000 P	15.2	11.9
41	45	B-C	180	1:1000 L	6.2	11.9
42	45	B-C	180	1:1000 L	10.7	11.9
43	45	B-C	180	1:1000 L	15.2	11.9
44	45	B-C	180	1:1000 P	6.2	11.9
45	45	B-C	180	1:1000 P	15.2	11.9
46	45	B-C	270	1:1000 L	6.2	11.9
47	45	B-C	270	1:1000 L	10.7	11.9
48	45	B-C	270	1:1000 L	15.2	11.9

Table 2. Field Test Conditions

Test Number	Wind Speed @ 62 m (m/s)	Stability PG cat.	Wind Dir from CL (degree)	Reactor Complex	Stack Height (m)	Stack Flow Rate (cu. m/s)
1A	5	D	0	NONE	62	51.9
2A	5	D	0	L	62	51.9
1	5	D	0	NONE	62	51.9
2	5	D	0	NONE	107	51.9
3	5	D	0	NONE	152	51.9
4	5	D	0	L	62	51.9
5	5	D	0	L	107	51.9
6	5	D	0	L	152	51.9
7	5	D	0	P	62	51.9
8	5	D	0	P	152	51.9
9	5	D	180	L	62	51.9
10	5	D	180	L	107	51.9
11	5	D	180	L	152	51.9
12	5	D	180	P	62	51.9
13	5	D	180	P	152	51.9
14	5	D	270	L	62	51.9
15	5	D	270	L	107	51.9
16	5	D	270	L	152	51.9
17	3	E-F	0	NONE	62	51.9
18	3	E-F	0	NONE	107	51.9
19	3	E-F	0	NONE	152	51.9
20	3	E-F	0	L	62	51.9
21	3	E-F	0	L	107	51.9
22	3	E-F	0	L	152	51.9
23	3	E-F	0	P	62	51.9
24	3	E-F	0	P	152	51.9
25	3	E-F	180	L	62	51.9
26	3	E-F	180	L	107	51.9
27	3	E-F	180	L	152	51.9
28	3	E-F	180	P	62	51.9
29	3	E-F	180	P	152	51.9
30	3	E-F	270	L	62	51.9
31	3	E-F	270	L	107	51.9
32	3	E-F	270	L	152	51.9
33	2	B-C	0	NONE	62	51.9
34	2	B-C	0	NONE	107	51.9
35	2	B-C	0	NONE	152	51.9
36	2	B-C	0	L	62	51.9
37	2	B-C	0	L	107	51.9
38	2	B-C	0	L	152	51.9
39	2	B-C	0	P	62	51.9
40	2	B-C	0	P	152	51.9
41	2	B-C	180	L	62	51.9
42	2	B-C	180	L	107	51.9
43	2	B-C	180	L	152	51.9
44	2	B-C	180	P	62	51.9
45	2	B-C	180	P	152	51.9
46	2	B-C	270	L	62	51.9
47	2	B-C	270	L	107	51.9
48	2	B-C	270	L	152	51.9

Table 3. Visualization Test Log

Video Run Title	Conc Test Number	Wind Speed @ 62 m (cm/s)	Stability PG cat.	Wind Dir from CL (degree)	Reactor Complex	Stack Height (m)	Stack Flow Rate (cu. m/s)	Time Factor	Video Tape Index	Comments on Downwash Study
2*	2A	5	D	0	L	62	51.9	120	283	
1*	-	5	D	0	L	62	51.9	120	0950 & 2251	Laminar
2*	-	5	D	0	L	62	51.9	120	1062 & 2312	Turbulent
3*	-	5	D	0	L	62	51.9	120	1135 & 2358	Hat
4*	-	5	D	0	L	62	51.9	120	1224 & 2399	Nozzle
5*	-	5	D	0	L	62	51.9	120	1324 & 2435	Small Nozzle
1	1	5	D	0	NONE	62	51.9	300	1428	
2	2	5	D	0	NONE	107	51.9	300	1473 & 2083	
3	3	5	D	0	NONE	152	51.9	300	1515	
4	4	5	D	0	L	62	51.9	300	1550 & 2120	
5	5	5	D	0	L	107	51.9	300	1597 & 2161	
6	6	5	D	0	L	152	51.9	300	1639 & 2193	
7	7	5	D	0	P	62	51.9	300	1687	
8	8	5	D	0	P	152	51.9	300	1722	
9	9	5	D	180	L	62	51.9	300	1768	
10	10	5	D	180	L	107	51.9	300	1813	
11	11	5	D	180	L	152	51.9	300	1858	
12	12	5	D	180	P	62	51.9	300	1903	
13	13	5	D	180	P	152	51.9	300	1943	
14	14	5	D	270	L	62	51.9	300	1982	
15	15	5	D	270	L	107	51.9	300	2015	
16	16	5	D	270	L	152	51.9	300	2053	
17	17	3	E-F	0	NONE	62	51.9	230	3067	
18	18	3	E-F	0	NONE	107	51.9	230	3099	
19	19	3	E-F	0	NONE	152	51.9	230	3130	
20	20	3	E-F	0	L	62	51.9	230	2540	
21	21	3	E-F	0	L	107	51.9	230	2602	
22	22	3	E-F	0	L	152	51.9	230	2664	
23	23	3	E-F	0	P	62	51.9	230	2999	
24	24	3	E-F	0	P	152	51.9	230	3030	
25	25	3	E-F	180	L	62	51.9	230	2833	
26	26	3	E-F	180	L	107	51.9	230	2866	
27	27	3	E-F	180	L	152	51.9	230	2901	
28	28	3	E-F	180	P	62	51.9	230	2936	
29	29	3	E-F	180	P	152	51.9	230	2969	
30	30	3	E-F	270	L	62	51.9	230	2713	
31	31	3	E-F	270	L	107	51.9	230	2754	
32	32	3	E-F	270	L	152	51.9	230	2800	
33	33	2	B-C	0	NONE	62	51.9	225	3236	
34	34	2	B-C	0	NONE	107	51.9	225	3261	
35	35	2	B-C	0	NONE	152	51.9	225	3291	
36	36	2	B-C	0	L	62	51.9	225	3320	
37	37	2	B-C	0	L	107	51.9	225	3341	
38	38	2	B-C	0	L	152	51.9	225	3369	
39	39	2	B-C	0	P	62	51.9	225	3395	
40	40	2	B-C	0	P	152	51.9	225	3411	
41	41	2	B-C	180	L	62	51.9	225	3431	
42	42	2	B-C	180	L	107	51.9	225	3452	
43	43	2	B-C	180	L	152	51.9	225	3473	
44	44	2	B-C	180	P	62	51.9	225	3494	
45	45	2	B-C	180	P	152	51.9	225	3516	
46	46	2	B-C	270	L	62	51.9	225	3535	
47	47	2	B-C	270	L	107	51.9	225	3553	
48	48	2	B-C	270	L	152	51.9	225	3579	

* Note : These tests were performed on 1:400 scale model

Table 4. Bulk Richardson Number Calculations

MODEL CONDITIONS									
CONDITION	HEIGHT		VELOCITY (cm/sec)	TEMPERATURE (oC)	RiB (model)	RiB range field meas **	Pasquil- Gifford Category**	RiB range field meas ***	Pasquil- Gifford Category*
	Model (cm)	Field (m)							
Unstable	0.50	5.00	49.70	49.00		B: -.039 to -.009	C		
	1.00	10.00	57.10	45.00	-0.0037	C: -.009 to -.001	inversion	B: -.188 to -.046	B
	3.00	30.00	59.10	40.00		D: -.001 to +.002		C: -.046 to -.008	inversion
	5.00	50.00	57.90	38.00				D: -.008 to +.014	
	6.20	62.00	54.40	36.00	-0.0582				
Stable	1.00	10.00	31.00	12.50		D: -.001 TO +.002			
	2.00	20.00	41.20	16.00		E: +.002 TO +.012		D: -.008 to +.014	
	3.00	30.00	49.40	19.50		F: +.012 TO +.047		E: +.014 to +.059	E
	4.00	40.00	55.30	21.50				F: +.059 to +.129	
	5.00	50.00	62.40	24.00					
	6.20	62.00	69.00	26.00	0.0442				

** For assumed heights of H = 10 m and B = 5 m, Zo = 50 cm

*** For assumed heights of H = 61 m and B = 10 m, Zo = 50 cm

Table 7-2. Concentration Measurement Results (Unstable, 1:1000 scale)

POSITION			CONCENTRATION (ppm) for RUN NUMBER															
X (m)	Y (m)	Z (m)	33	34	35	36	37	38	39	40	41	42	43	44	45	46	47	48
4000	-600	0	39	34	30	34	34	41	36	38	34	36	34	33	50	26	32	34
4000	-600	100	38	34	29	31	33	38	32	39	32	32	33	32	52	25	31	37
4000	-600	200	34	30	26	26	31	37	25	39	34	27	32	29	45	27	28	36
4000	-600	300	16	16	12	13	12	18	12	17	17	12	13	13	20	18	16	23
4000	-600	400	7	10	6	7	5	9	6	8	12	5	5	5	8	16	9	14
4000	-600	550	1	2	4	1	1	1	0	1	3	0	0	2	1	5	2	2
4000	-400	0	93	85	85	79	69	85	78	93	84	80	85	80	105	71	73	83
4000	-400	100	98	94	86	89	77	95	86	99	93	86	89	82	106	87	82	97
4000	-400	200	91	90	88	88	80	92	80	92	92	84	86	83	107	92	91	104
4000	-400	300	68	67	63	63	65	75	60	70	77	67	68	64	79	77	78	91
4000	-400	400	37	39	36	37	33	45	36	42	55	38	39	34	50	56	53	61
4000	-400	550	7	8	8	8	5	7	5	6	19	4	5	7	12	20	15	15
4000	-400	700	0	1	0	0	0	0	0	1	2	0	0	1	1	1	1	0
4000	-200	0	135	129	129	138	132	130	138	136	132	136	131	136	117	125	136	131
4000	-200	100	136	134	135	140	136	135	142	141	137	139	140	137	124	132	141	138
4000	-200	200	124	125	127	131	129	136	135	137	134	129	135	132	128	126	134	133
4000	-200	300	100	99	100	101	106	108	104	106	114	103	114	104	103	107	106	110
4000	-200	400	53	53	52	53	54	61	56	48	68	54	60	51	57	67	63	72
4000	-200	550	6	7	7	4	5	5	2	5	12	4	5	5	7	12	10	10
4000	-200	700	0	1	0	0	0	0	0	1	1	0	0	1	0	0	0	1
4000	0	0	88	83	92	101	99	76	95	92	94	86	83	100	63	96	94	91
4000	0	100	77	73	79	80	85	68	82	73	79	75	78	81	53	75	76	74
4000	0	200	67	64	71	67	76	58	64	58	68	70	71	73	47	56	57	60
4000	0	300	48	48	55	51	56	44	47	45	52	56	55	59	33	40	44	48
4000	0	400	21	26	28	24	25	23	23	18	27	27	25	21	12	20	17	22
4000	0	550	1	2	2	2	2	1	1	1	4	1	1	1	1	2	2	2
4000	0	700	0	0	0	0	0	0	0	0	1	0	0	1	0	0	0	0
4000	200	0	15	14	18	18	16	9	23	17	29	17	12	20	7	28	19	21
4000	200	100	21	19	23	23	24	13	24	19	27	21	17	25	10	29	23	22
4000	200	200	22	22	26	27	28	15	26	22	25	23	18	28	11	28	24	20
4000	200	300	18	18	20	25	22	13	20	16	21	18	16	21	9	22	19	16
4000	200	400	8	8	8	10	8	6	9	7	10	7	7	8	3	12	9	7
4000	200	550	0	1	0	0	1	0	0	0	2	0	0	1	0	1	0	0
4000	200	700	0	0	0	0	0	0	0	3	1	0	0	1	0	0	0	0
4000	400	0	1	2	2	2	2	0	2	1	2	1	1	3	0	2	1	1
4000	400	100	1	2	3	3	2	1	3	2	4	2	2	4	1	4	3	2
4000	400	200	2	2	3	4	3	2	5	5	6	2	2	4	1	7	4	4
4000	400	300	1	1	1	3	2	2	3	2	5	1	2	3	1	7	3	4
4000	400	400	0	1	0	1	1	1	1	3	4	0	0	1	0	4	1	2
4000	400	550	0	0	0	0	0	0	0	0	1	0	0	1	0	1	0	0
4000	400	700	0	0	0	0	0	0	0	0	1	0	0	1	0	0	0	0
4000	600	0	0	0	0	0	0	0	0	0	0	0	0	1	0	0	0	0
4000	600	100	0	0	0	0	0	0	0	0	0	0	0	0	0	0	0	0
4000	600	200	0	0	0	0	0	0	0	0	1	0	0	0	0	0	0	0
4000	600	300	0	0	0	0	0	0	0	0	1	0	0	0	0	0	0	0
4000	600	400	0	0	0	0	0	0	0	0	1	0	0	0	0	0	0	0
4000	600	550	0	0	0	0	0	0	0	0	1	0	0	1	0	0	0	0
4000	600	700	0	0	0	0	0	0	0	0	1	0	0	1	0	0	0	0

Table 7-3. Concentration Measurement Results (Unstable, 1:1000 scale)

POSITION			CONCENTRATION (ppm) for RUN NUMBER															
X (m)	Y (m)	Z (m)	33	34	35	36	37	38	39	40	41	42	43	44	45	46	47	48
10000	-600	0	26	25	23	25	26	26	25	26	28	25	22	28	26	24	26	27
10000	-600	100	28	29	26	29	28	30	27	27	28	26	24	26	26	26	29	28
10000	-600	200	27	29	26	29	28	28	27	26	28	24	24	26	26	24	27	28
10000	-600	300	27	30	26	30	29	30	27	25	27	22	25	25	25	24	26	26
10000	-600	400	26	28	26	27	28	29	24	23	25	20	22	22	23	22	22	25
10000	-600	550	26	31	27	27	27	28	22	19	24	21	24	23	22	23	21	20
10000	-400	0	27	27	26	30	28	29	28	30	30	30	29	29	28	28	29	28
10000	-400	100	32	33	32	32	32	33	28	29	31	33	32	31	29	30	29	29
10000	-400	200	32	34	33	33	32	33	28	27	30	31	30	30	25	29	27	27
10000	-400	300	31	34	33	31	32	32	26	25	28	28	29	28	23	25	25	24
10000	-400	400	30	33	31	29	30	30	23	25	26	25	26	27	21	23	22	20
10000	-400	550	27	30	29	25	27	27	21	17	22	22	22	21	17	20	19	16
10000	-400	700	20	22	26	10	5	11	9	5	7	18	15	10	6	10	9	6
10000	-200	0	31	29	32	33	30	31	29	29	31	32	33	30	30	30	30	28
10000	-200	100	32	31	33	33	29	31	28	26	29	29	31	28	27	28	27	27
10000	-200	200	30	31	31	29	27	26	23	22	24	27	27	23	22	24	21	23
10000	-200	300	26	28	29	24	24	22	19	17	20	23	24	19	17	18	18	18
10000	-200	400	24	26	26	19	20	20	14	13	16	19	19	15	13	14	14	12
10000	-200	550	19	21	21	11	12	13	9	7	9	13	12	9	7	8	8	6
10000	-200	700	4	5	7	2	1	1	1	0	1	4	2	1	1	1	1	0
10000	0	0	29	25	29	28	24	27	27	23	23	28	30	27	27	28	29	23
10000	0	100	26	25	27	28	23	25	24	22	22	28	28	23	23	26	25	23
10000	0	200	21	21	24	22	18	19	19	15	16	23	22	16	16	20	18	17
10000	0	300	18	17	21	16	14	13	12	10	11	16	15	11	11	14	12	12
10000	0	400	13	13	15	9	8	8	6	6	6	10	9	6	6	7	6	6
10000	0	550	8	9	9	4	3	3	3	2	3	5	4	3	2	3	3	2
10000	0	700	0	1	1	0	0	0	0	0	1	0	0	0	0	0	0	0
10000	200	0	16	15	19	18	16	19	17	16	14	20	20	18	17	19	17	14
10000	200	100	17	13	16	17	14	17	15	12	13	19	19	13	13	16	15	12
10000	200	200	9	10	13	11	9	12	10	8	9	12	12	8	7	11	11	7
10000	200	300	7	7	9	7	6	6	4	4	5	7	7	5	4	5	7	4
10000	200	400	8	5	6	4	3	4	2	2	3	4	3	2	2	3	5	1
10000	200	550	5	3	3	1	1	1	1	0	1	2	1	1	0	1	1	0
10000	200	700	0	0	0	0	0	0	0	0	1	0	0	0	0	0	1	0
10000	400	0	6	6	6	8	7	10	7	7	6	8	9	7	7	8	7	4
10000	400	100	5	5	5	6	7	8	6	5	5	7	7	7	4	6	4	4
10000	400	200	4	3	3	3	4	4	3	3	4	3	4	2	2	3	3	2
10000	400	300	2	2	3	1	2	2	1	1	2	2	2	1	1	1	1	1
10000	400	400	2	3	2	1	1	1	1	0	1	1	1	0	1	0	1	0
10000	400	550	1	1	4	0	0	0	0	0	1	1	0	0	0	0	0	0
10000	400	700	0	0	0	0	0	0	0	0	1	0	0	0	0	0	3	0
10000	600	0	2	1	1	1	2	4	2	2	2	2	2	1	1	2	2	1
10000	600	100	1	1	1	1	3	2	5	1	2	1	2	1	1	1	1	1
10000	600	200	1	1	1	1	1	1	1	0	1	1	1	0	1	0	1	0
10000	600	300	1	1	0	0	1	0	0	0	1	1	1	0	0	0	0	0
10000	600	400	1	1	1	0	1	0	0	0	1	0	0	0	0	0	0	0
10000	600	550	0	0	0	0	0	0	0	0	1	0	0	0	0	0	0	0
10000	600	700	0	0	0	0	0	0	0	0	0	0	2	3	0	0	0	0

Table 8. Concentration Measurement Results (1:400 scale)

POSITION		CONCENTRATION (ppm) for RUN NUMBER				POSITION		CONCENTRATION (ppm) for RUN NUMBER			
Y	Z	1A	1A	2A	2A	Y	Z	1A	1A	2A	2A
(m)	(m)	X=600 m	X=1200 m	X=600 m	X=1200 m	(m)	(m)	X=2400 m	X=4000 m	X=2400 m	X=4000 m
183	0	5	7	7	12	244	0	16		20	40
183	61	5	11	7	23	244	80	20	33	22	39
183	122	5	11	6	17	244	160	10	19	10	19
183	183	5	5	7	7	244	244	5	9	5	8
183	244	5	5	7	7	244	324	4	7	4	6
183	305	5	5	6	7	244	404	4	6	4	5
183	366	5	5	5	5	244	484	3	5	3	4
122	0	5	67	16	147	160	0	62	60	72	85
122	61	28	114	28	173	160	80	88	85	95	102
122	122	6	69	9	84	160	160	43	54	39	57
122	183	4	10	6	15	160	244	8	14	7	13
122	244	5	4	6	6	160	324	5	7	5	6
122	305	5	4	6	6	160	404	4	6	3	4
122	366	3	4	4	4	160	484	3	5	3	4
61	0	62	343	361	539	80	0	286	153	274	198
61	61	354	376	548	439	80	80	219	154	226	175
61	122	89	194	101	202	80	160	88	102	93	96
61	183	5	34	6	33	80	244	9	21	11	18
61	244	3	5	5	5	80	324	3	5	3	4
61	305	3	3	4	4	80	404	1	3	1	1
61	366	1	0	2	2	80	484	2	3	1	1
0	0	273	514	719	675	0	0	346	212	369	237
0	61	1331	550	1228	535	0	80	259	182	256	181
0	122	296	294	167	211	0	160	103	120	93	94
0	183	3	44	4	25	0	244	13	29	8	14
0	244	2	4	3	3	0	324	3	3	1	2
0	305	4	3	3	2	0	404	0	0	0	0
0	366	0	0	1	1	0	484	0	0	0	1
-61	0	77	330	248	415	-80	0	244	169	236	189
-61	61	319	298	327	285	-80	80	156	137	148	134
-61	122	48	120	27	82	-80	160	41	66	32	51
-61	183	1	1	2	8	-80	244	3	12	2	5
-61	244	0	0	2	1	-80	324	0	2	1	0
-61	305	0	0	2	1	-80	404	0	0	0	0
-61	366	0	0	1	1	-80	484	0	0	0	0
-122	0	0	81	7	125	-160	0	81	90	90	90
-122	61	1	69	6	76	-160	80	49	69	49	68
-122	122	0	23	1	16	-160	160	8	23	6	21
-122	183	0	0	1	1	-160	244	0	1	0	0
-122	244	0	0	1	1	-160	324	0	0	0	0
-122	305	0	0	0	0	-160	404	0	0	0	0
-122	366	0	0	0	0	-160	484	0	0	0	0
-183	0	0	0	0	7	-244	0	10	31	9	33
-183	61	0	2	0	6	-244	80	6	20	5	21
-183	122	0	0	0	1	-244	160	0	4	0	3
-183	183	0	0	0	0	-244	244	0	0	0	0
-183	244	0	0	0	0	-244	324	0	0	0	0
-183	305	0	0	0	0	-244	404	0	0	0	0

Table 9. Neutral Wind Profile Data

RECORD NO.	HEIGHT	MEAN VELOCITY	TURBULENT INTENSITY			REY STRESS UW	POTENTIAL TEMP. (C)
			U-COMP %	V-COMP %	W-COMP %		
1	.13	.57	23.60	8.52	6.66	.00172	.00
2	.25	.70	22.57	8.46	7.38	.00047	.00
3	.32	.75	21.82	8.64	7.03	.00136	.00
4	.47	.85	20.48	7.85	6.33	.00084	.00
5	.66	.95	17.20	7.07	5.70	.00063	.00
6	.80	.98	17.84	7.30	5.98	.00051	.00
7	1.22	1.10	12.64	6.03	5.61	.00093	.00
8	1.61	1.12	12.94	6.16	5.32	.00114	.00
9	2.43	1.25	10.98	5.95	5.48	.00049	.00
10	3.22	1.34	9.49	4.85	4.89	.00164	.00
11	4.86	1.48	7.91	3.90	4.16	.00202	.00
12	6.46	1.58	4.20	2.45	2.89	.00075	.00
13	8.08	1.63	2.38	1.55	2.01	.00015	.00
14	12.08	1.70	1.49	.97	1.07	-.00006	.00
15	16.11	1.71	1.87	1.08	1.07	-.00016	.00

REF. HEIGHT= 62 m REF. VELOCITY= 5.0 m/s
 NEUTRAL PROFILE
 TURBULENT INTENSITY IS LOCAL
 REY STRESS IS NORMALIZED BY REF. VELOCITY SQUARED

Table 10. Stable Wind Profile Data

RECORD NO.	HEIGHT	MEAN VELOCITY	TURBULENT INTENSITY			REY STRESS UW	POTENTIAL TEMP. (C)
			U-COMP %	V-COMP %	W-COMP %		
1	.16	.37	6.70	1.20	2.61	.00004	-.32
2	.32	.58	7.36	1.75	2.41	.00006	-.20
3	.48	.70	7.34	2.03	2.41	.00006	-.13
4	.65	.80	7.68	2.29	2.36	.00002	-.09
5	.81	.89	7.57	2.37	2.23	.00005	-.06
6	1.00	1.00	6.09	2.16	1.99	.00000	.00
7	1.21	1.11	5.30	2.05	1.89	-.00005	.03
8	1.61	1.26	4.86	2.00	1.71	.00010	.08
9	2.42	1.48	3.86	1.79	1.66	.00020	.15
10	3.23	1.62	4.14	1.88	1.60	.00031	.18
11	4.84	1.88	3.16	1.69	1.38	.00041	.22
12	6.45	2.01	1.85	.90	.99	.00014	.26
13	12.10	2.16	1.78	.80	.80	.00016	.33
14	16.13	2.20	1.51	.90	.77	.00028	.35

REF. HEIGHT= 62 m REF. VELOCITY= 3.0 m/s
 STABLE PROFILE
 TURBULENT INTENSITY IS LOCAL
 REY STRESS IS NORMALIZED BY REF. VELOCITY SQUARED

Table 11. Unstable Wind Profile Data

RECORD NO.	HEIGHT	MEAN VELOCITY	TURBULENT INTENSITY			REY STRESS UW	POTENTIAL TEMP. (C)
			U-COMP %	V-COMP %	W-COMP %		
1	.16	.89	23.15	18.60	24.10	.00163	.16
2	.21	.98	20.76	16.84	24.26	.00191	.09
3	.29	.93	17.77	17.94	25.98	.00084	.03
4	.46	.91	16.15	16.04	19.67	.00565	-.05
5	.64	.93	14.86	18.37	18.55	.00673	-.05
6	.78	1.00	14.24	18.70	19.37	.00189	.00
7	1.19	1.00	12.83	17.98	16.88	.00325	.00
8	1.58	1.00	11.61	19.79	15.80	.00212	.01
9	2.39	.90	11.60	16.90	16.51	.00100	-.01
10	3.21	.86	9.48	11.40	10.65	.00002	.05
11	4.86	.91	3.45	5.02	4.86	-.00006	.10
12	6.44	.87	2.94	2.81	5.32	.00039	.13
13	8.04	.87	1.95	2.24	3.16	.00011	.13
14	12.08	.89	2.51	2.49	2.90	.00020	.15
15	16.14	.89	3.47	2.47	4.56	.00023	.16

REF. HEIGHT= 62 m REF. VELOCITY= 2.0 m/s
 UNSTABLE PROFILE
 TURBULENT INTENSITY IS LOCAL
 REY STRESS IS NORMALIZED BY REF. VELOCITY SQUARED

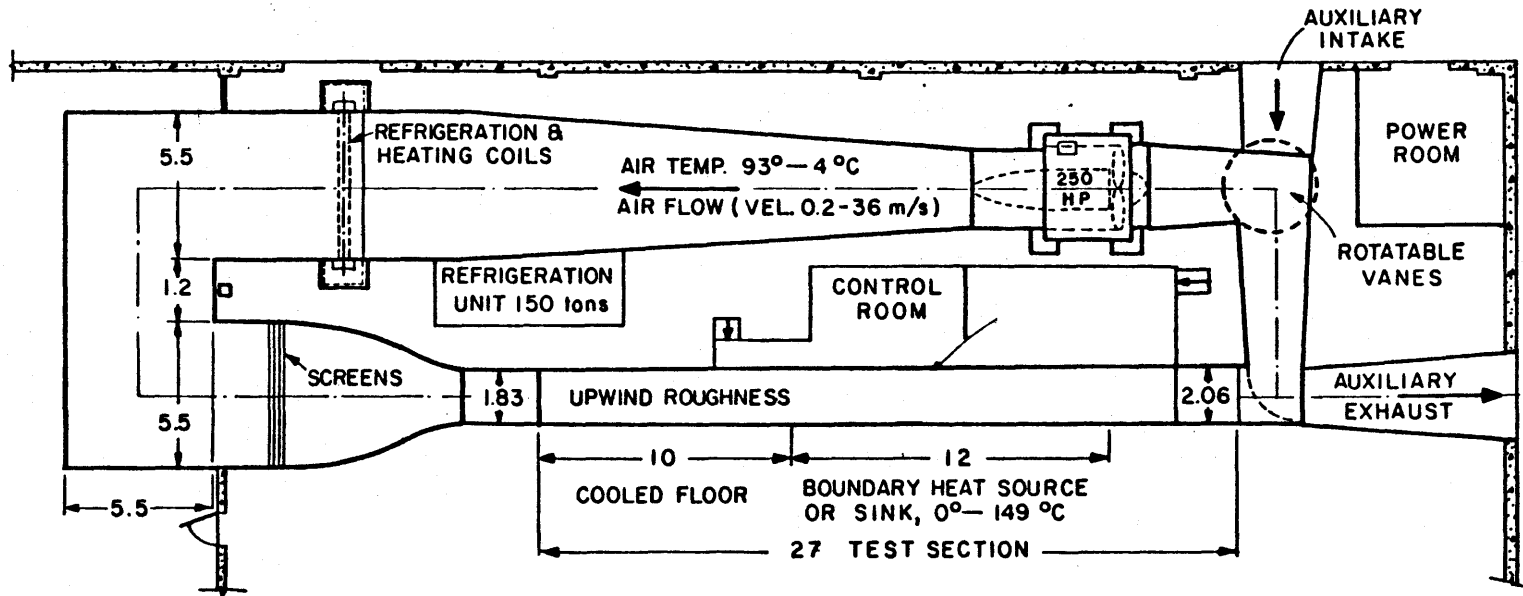


Figure 1. Meteorological Wind Tunnel

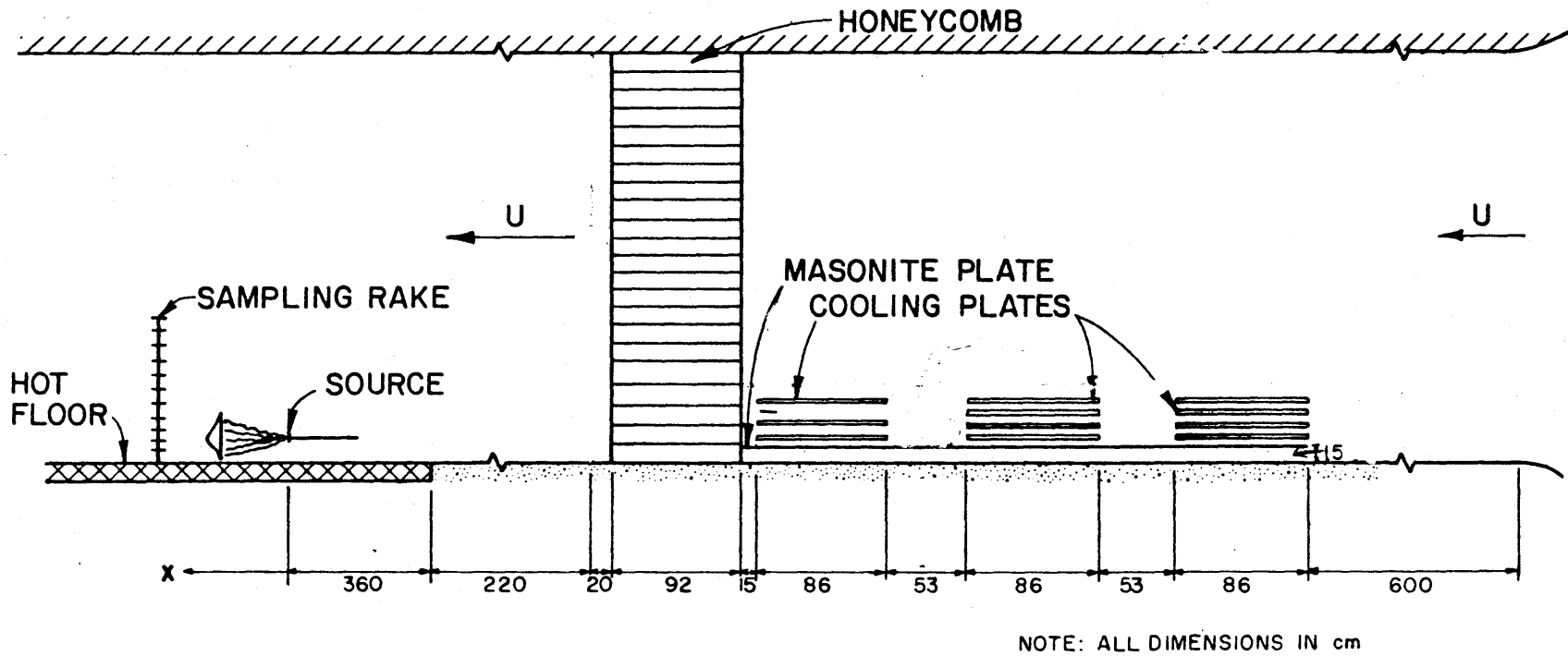


Figure 2. Wind Tunnel Configuration for Unstable Flow

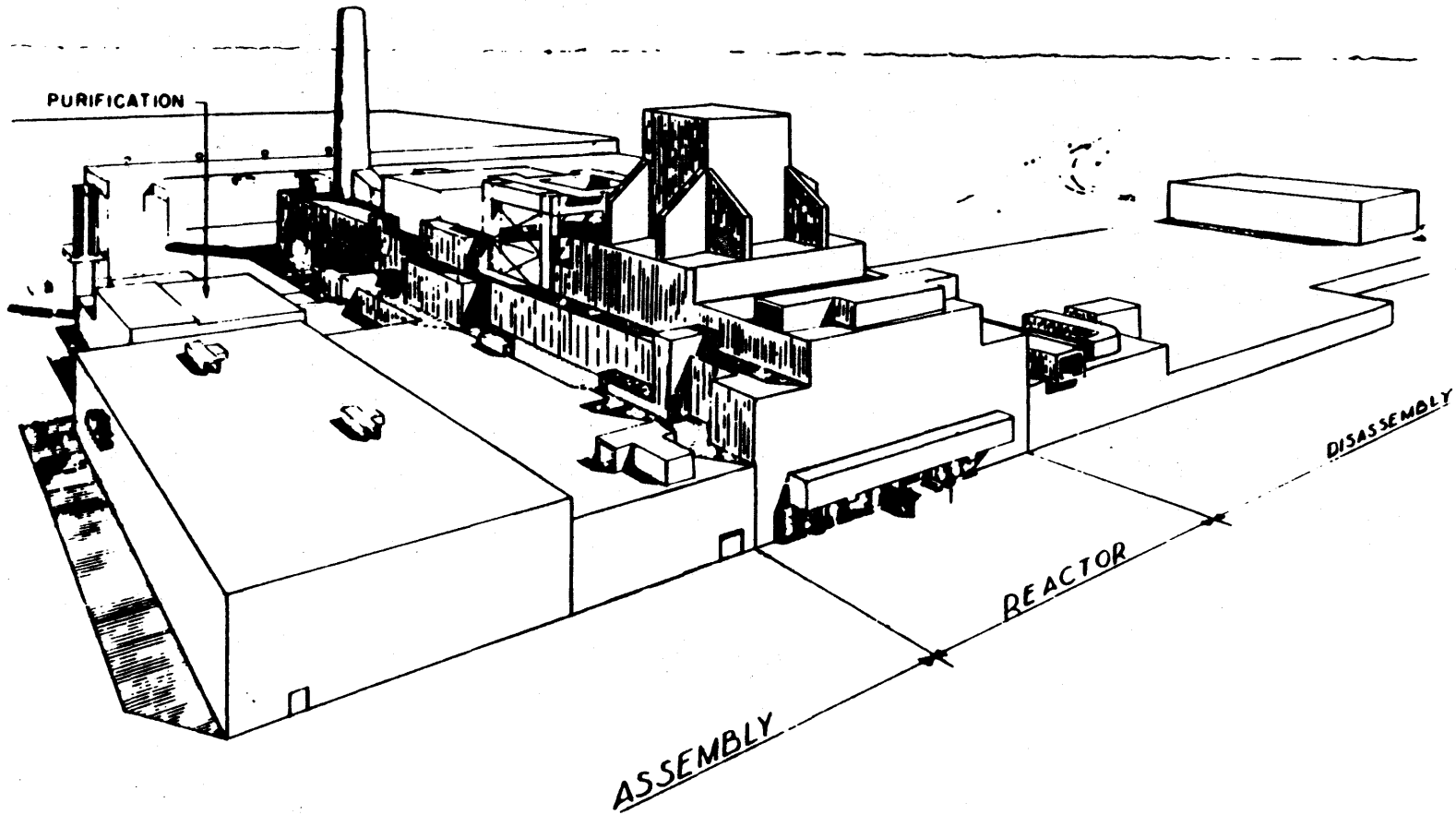
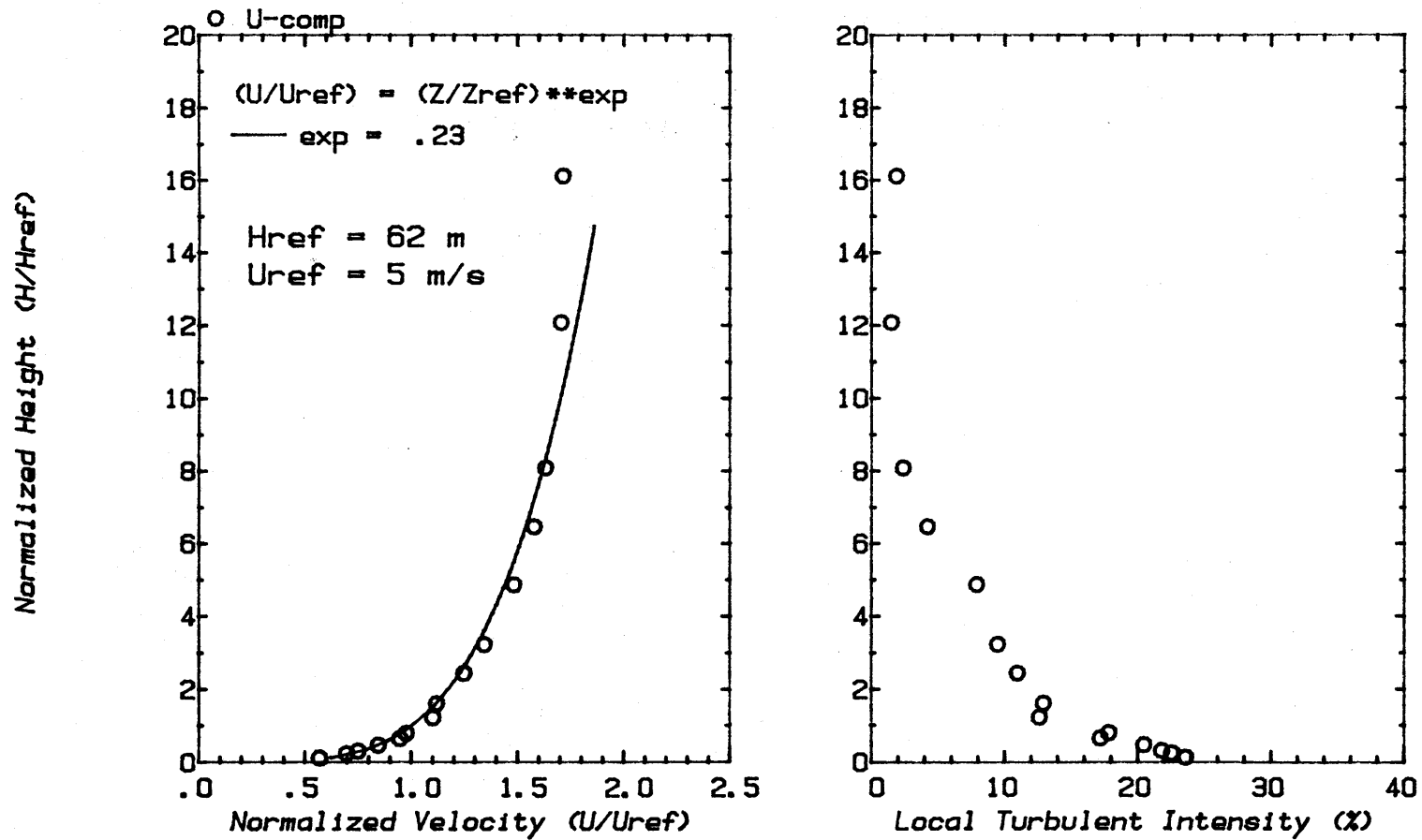
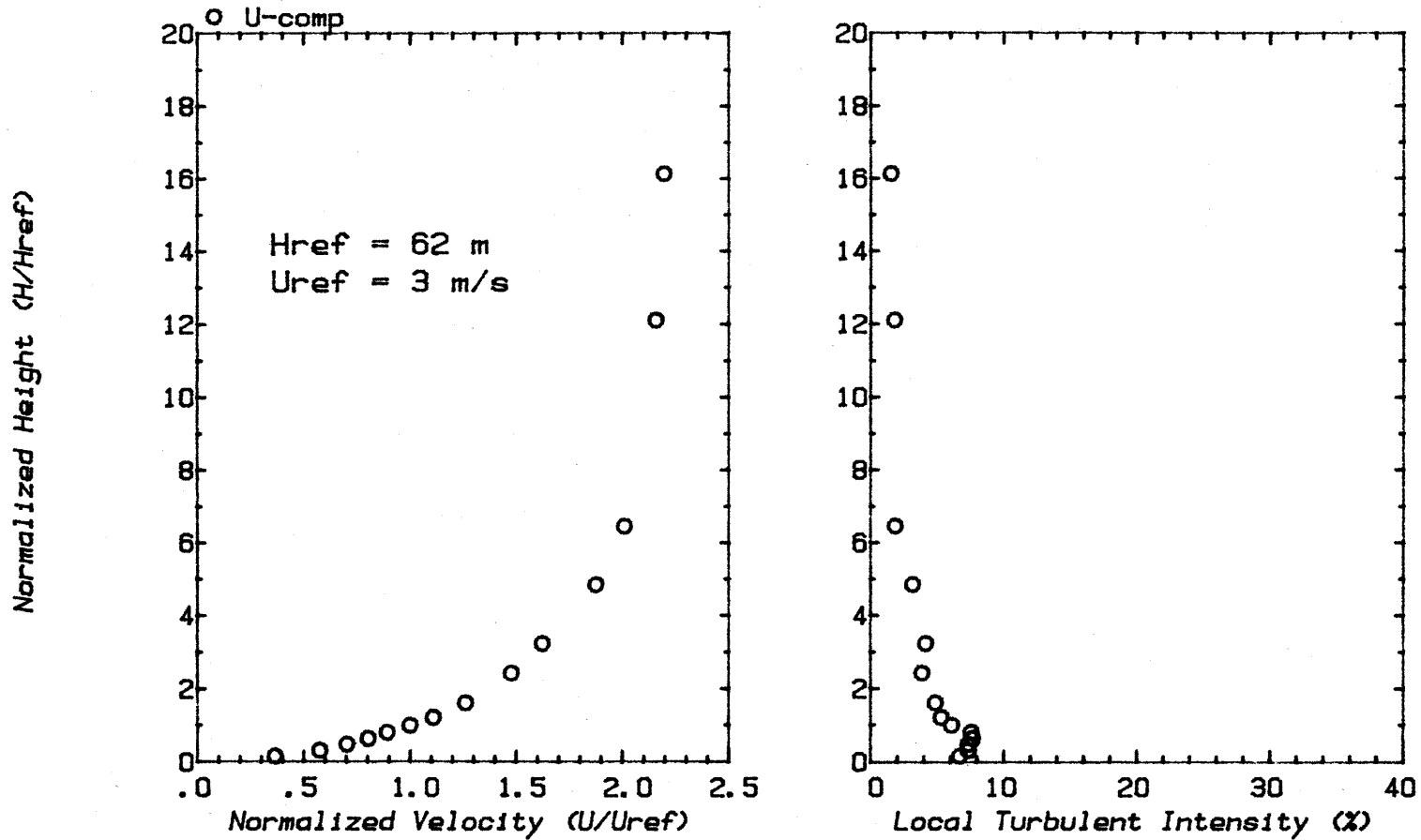


Figure 3. Savannah River Power Plant (P-reactor)



Neutral Stability
Longitudinal Velocity and Turbulence Profiles

Figure 5. Longitudinal Velocity and Turbulent Intensity Profiles (Neutral Stability)



Stable Stability
 Longitudinal Velocity and Turbulence Profiles

Figure 6. Longitudinal Velocity and Turbulent Intensity Profiles (Stable Stability)

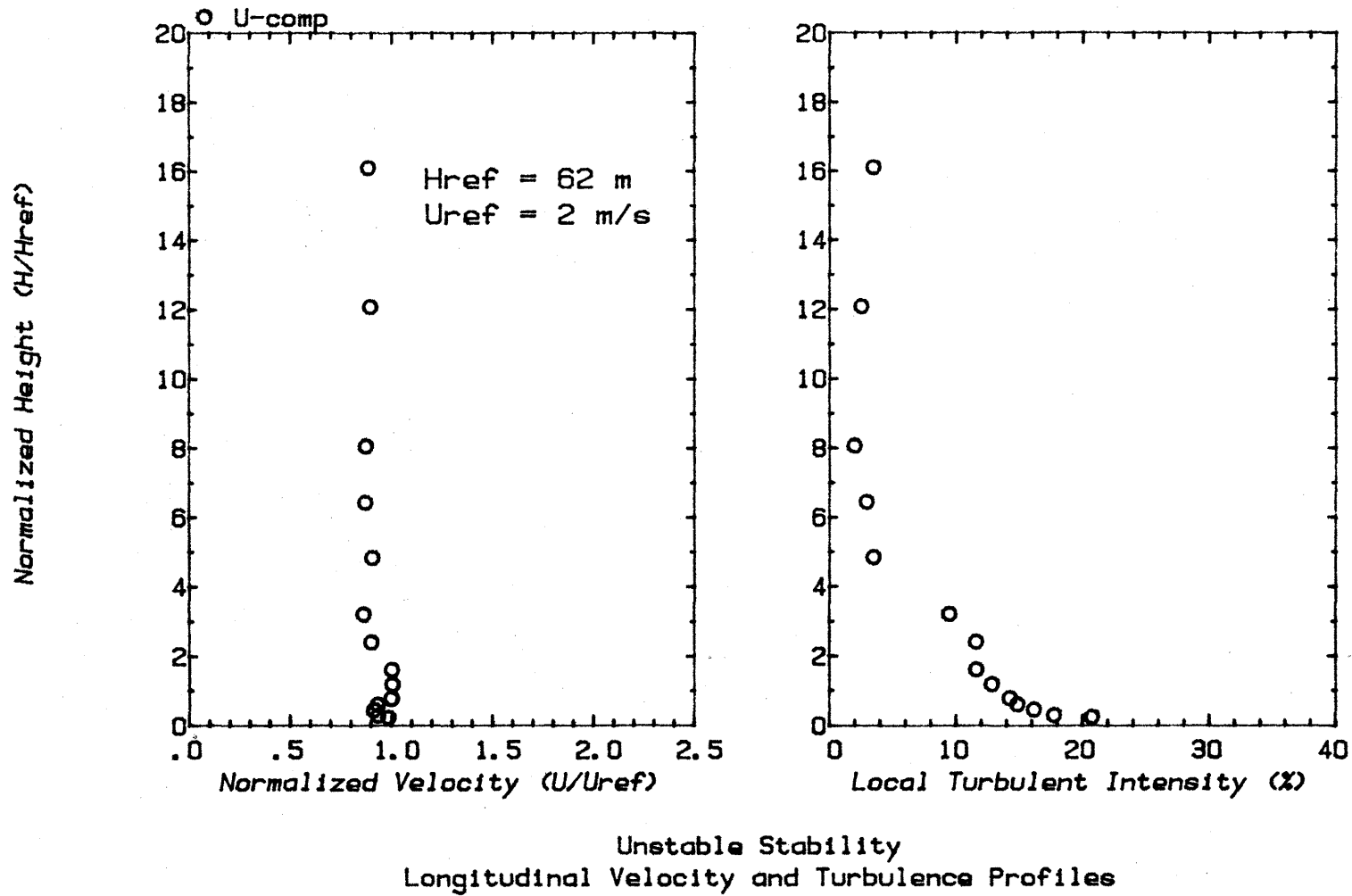


Figure 7. Longitudinal Velocity and Turbulence Intensity Profiles (Unstable Stability)

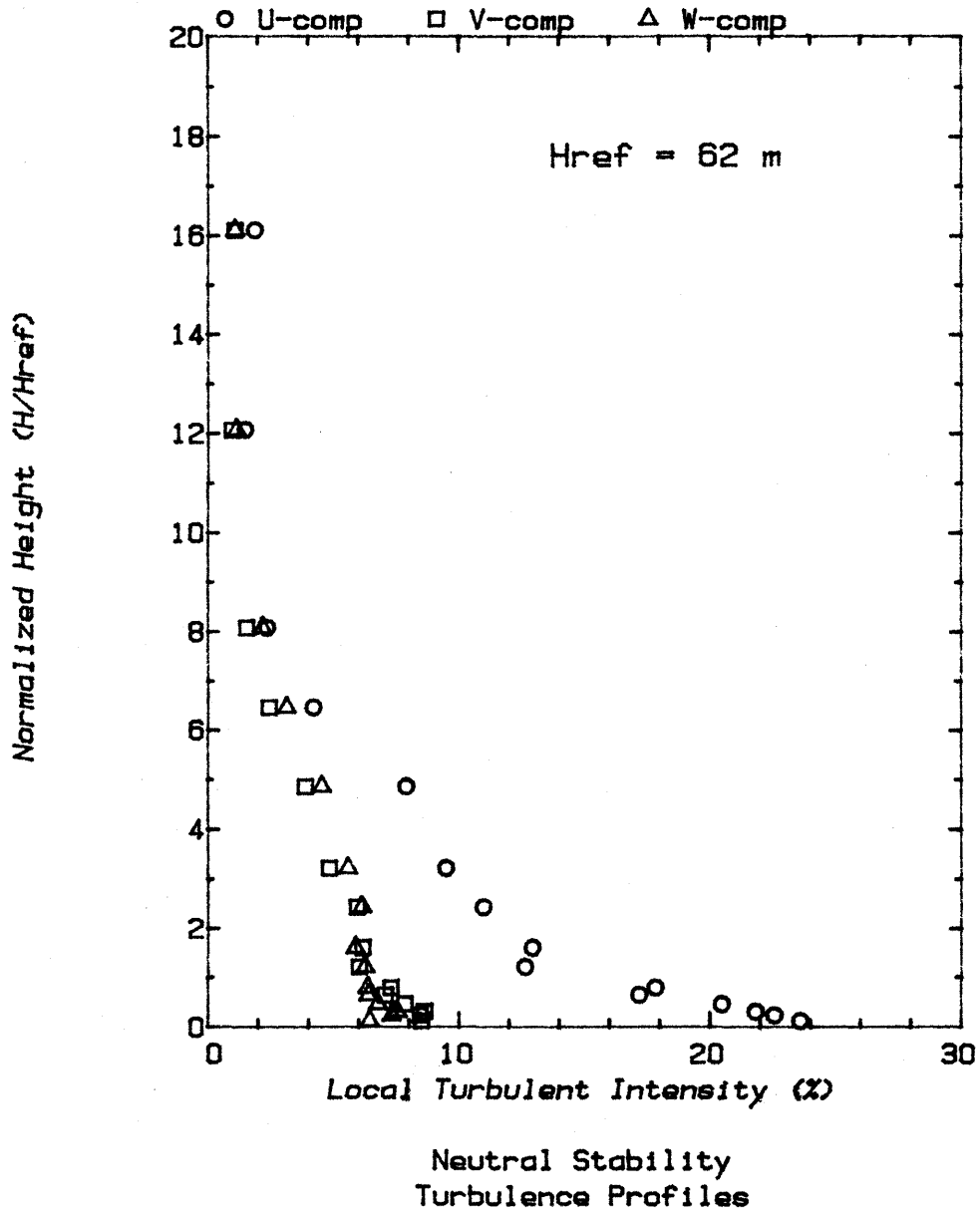


Figure 8. Turbulence Intensity Profiles (Neutral Stability)

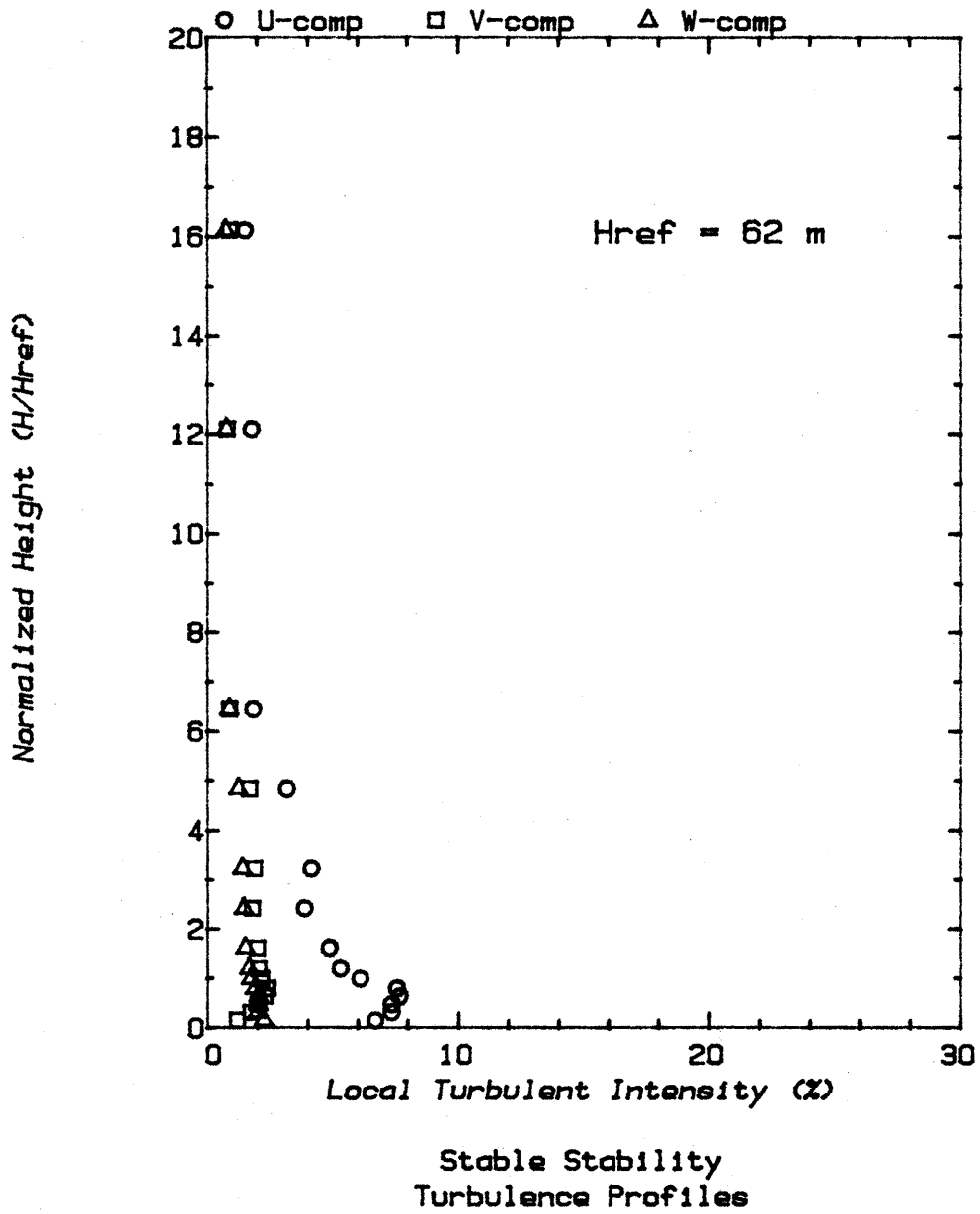


Figure 9. Turbulence Intensity Profiles (Stable Stability)

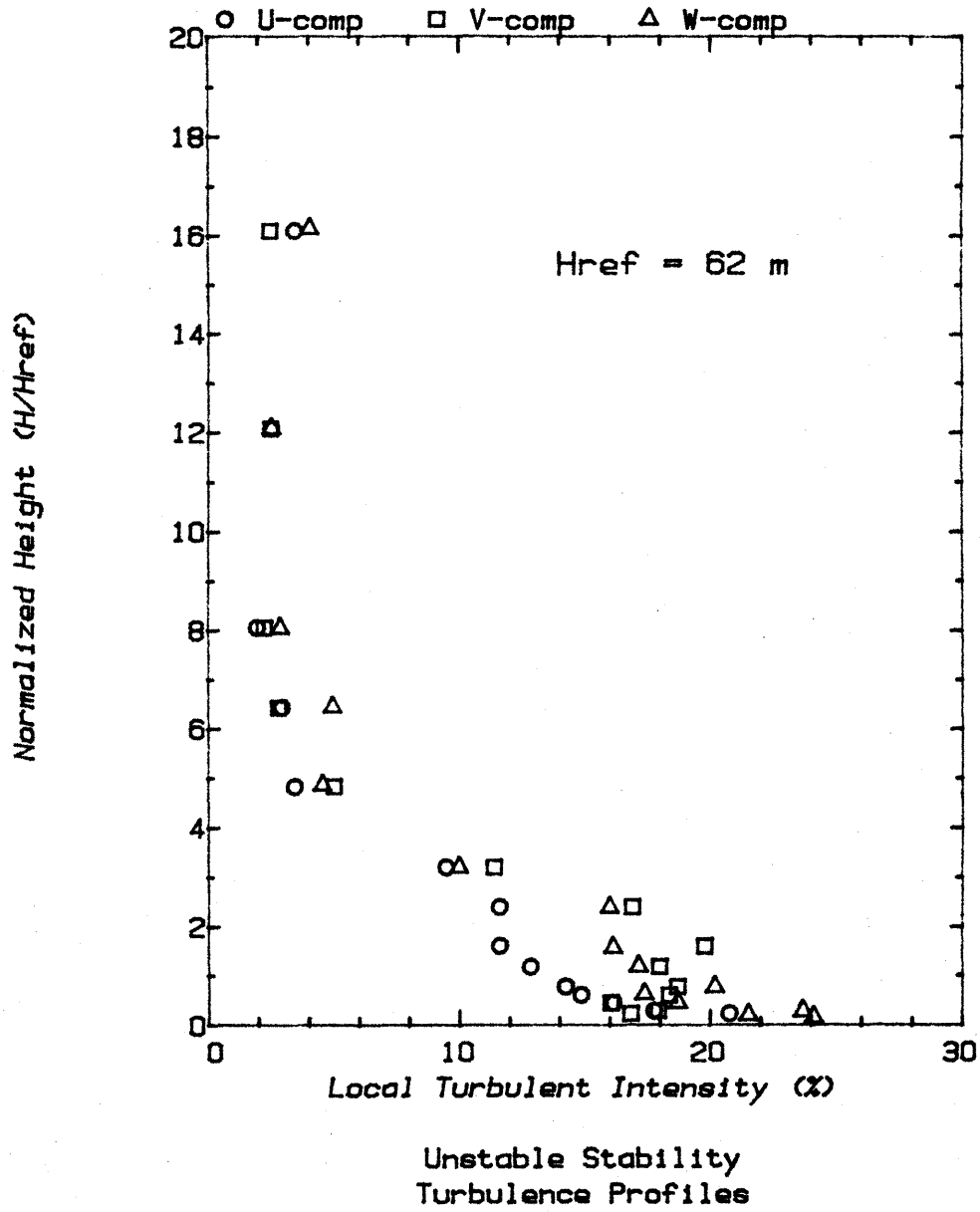


Figure 10. Turbulence Intensity Profiles (Unstable Stability)

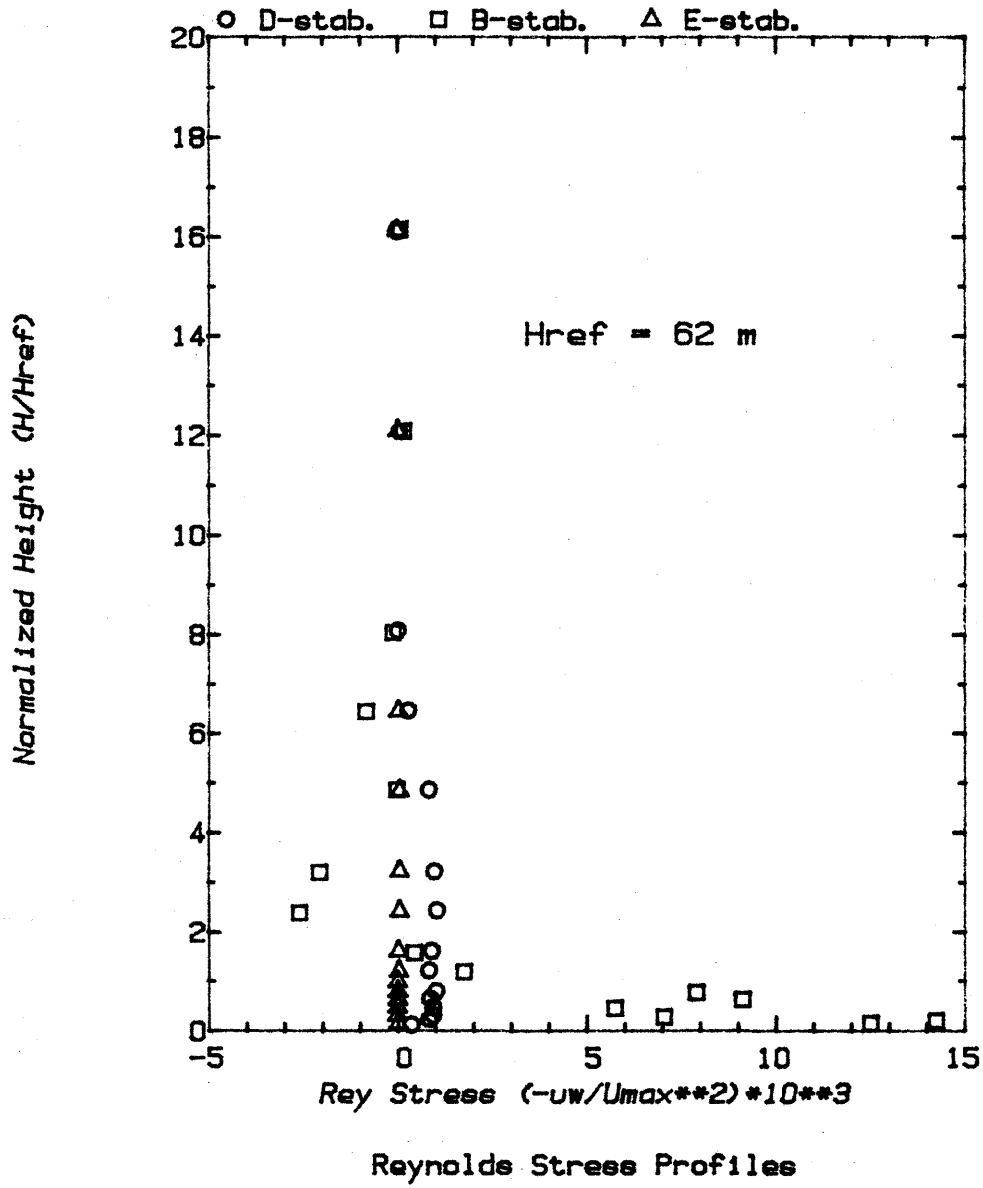


Figure 11. Reynolds Stress Profiles

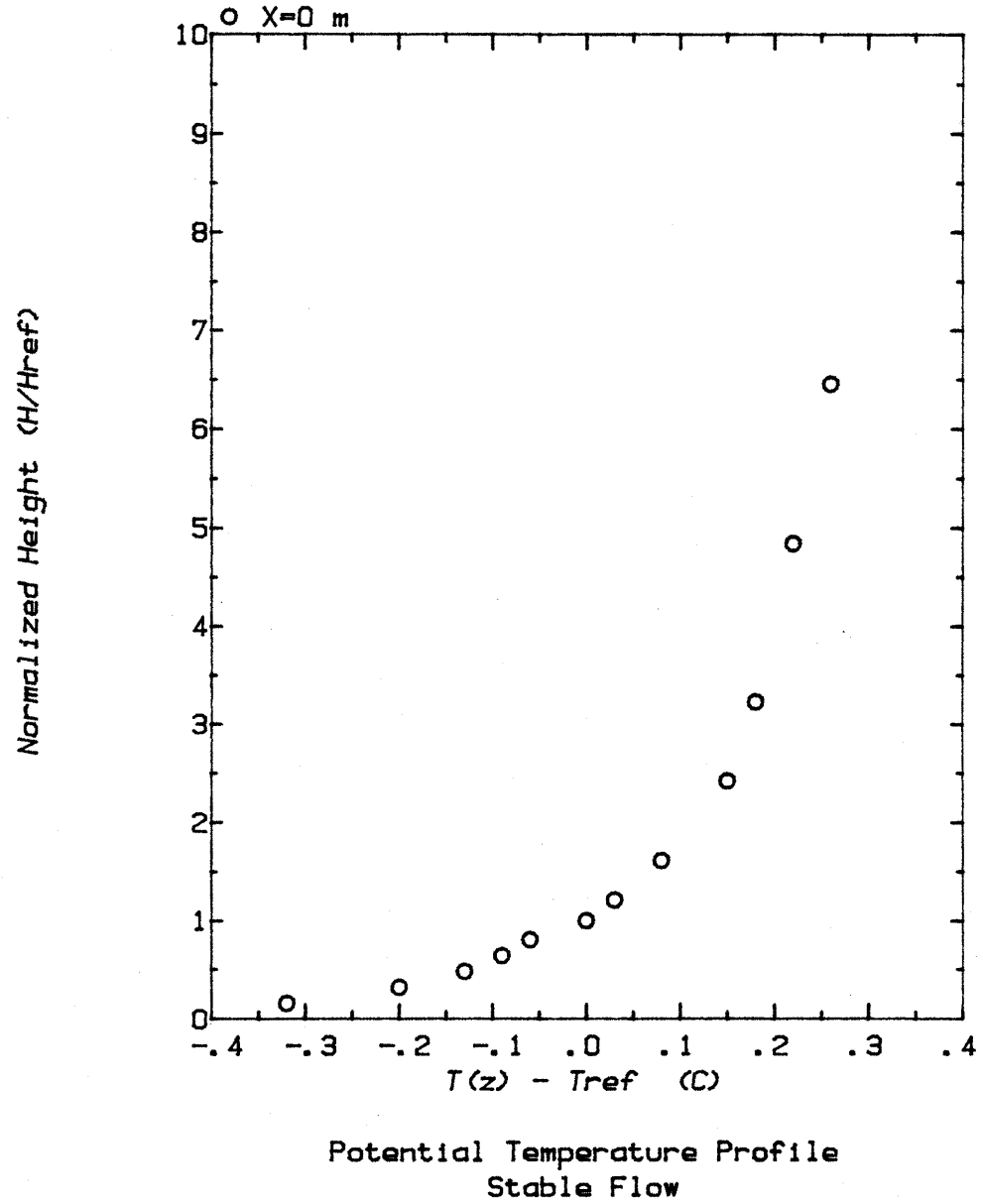


Figure 12. Temperature Profile (Stable Stability)

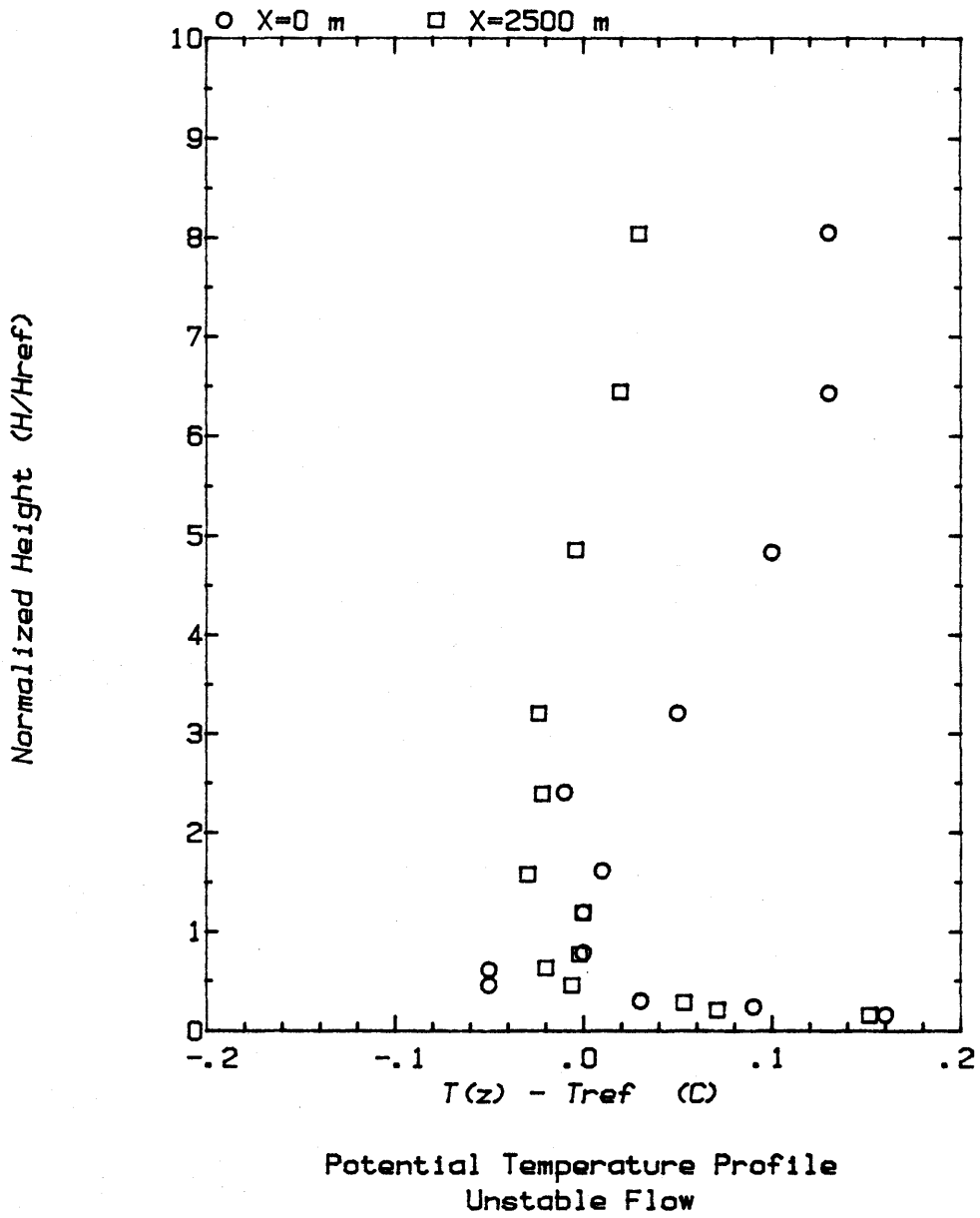
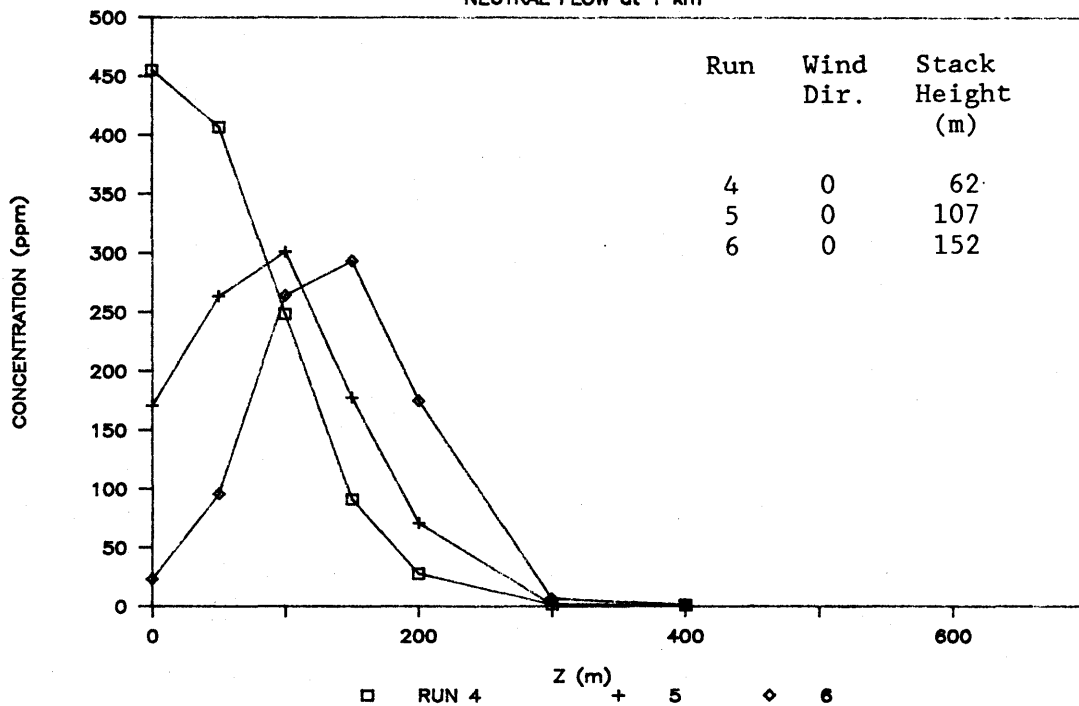


Figure 13. Temperature Profile (Unstable Stability)

VERTICAL CONCENTRATION PROFILES

NEUTRAL FLOW at 1 km



VERTICAL CONCENTRATION PROFILES

NEUTRAL FLOW at 4 km

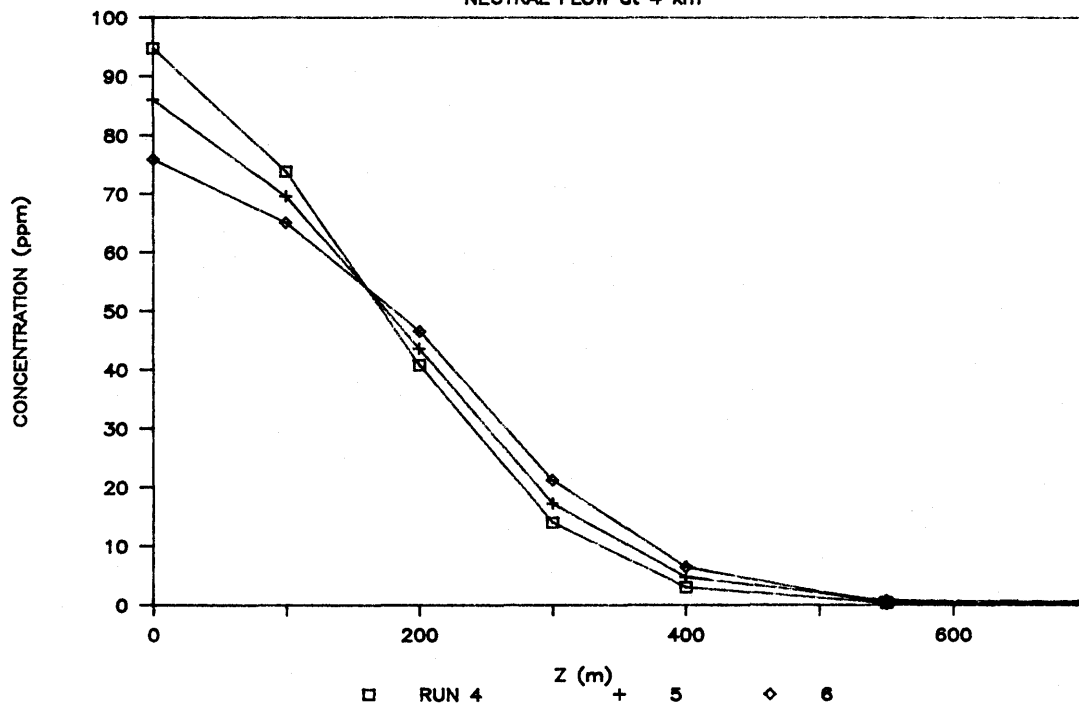
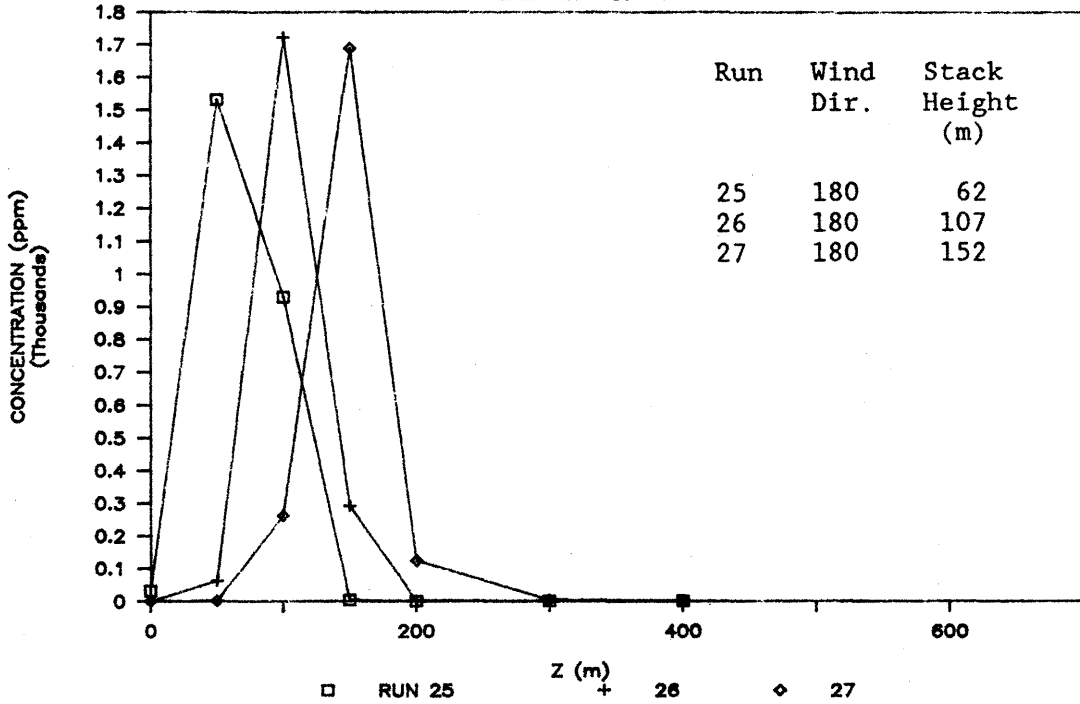


Figure 14. Vertical Concentration Profiles of Neutral Flow at 1 and 4 km (Runs 4, 5,6)

VERTICAL CONCENTRATION PROFILES

STABLE FLOW at 1 km



VERTICAL CONCENTRATION PROFILES

STABLE FLOW at 4 km

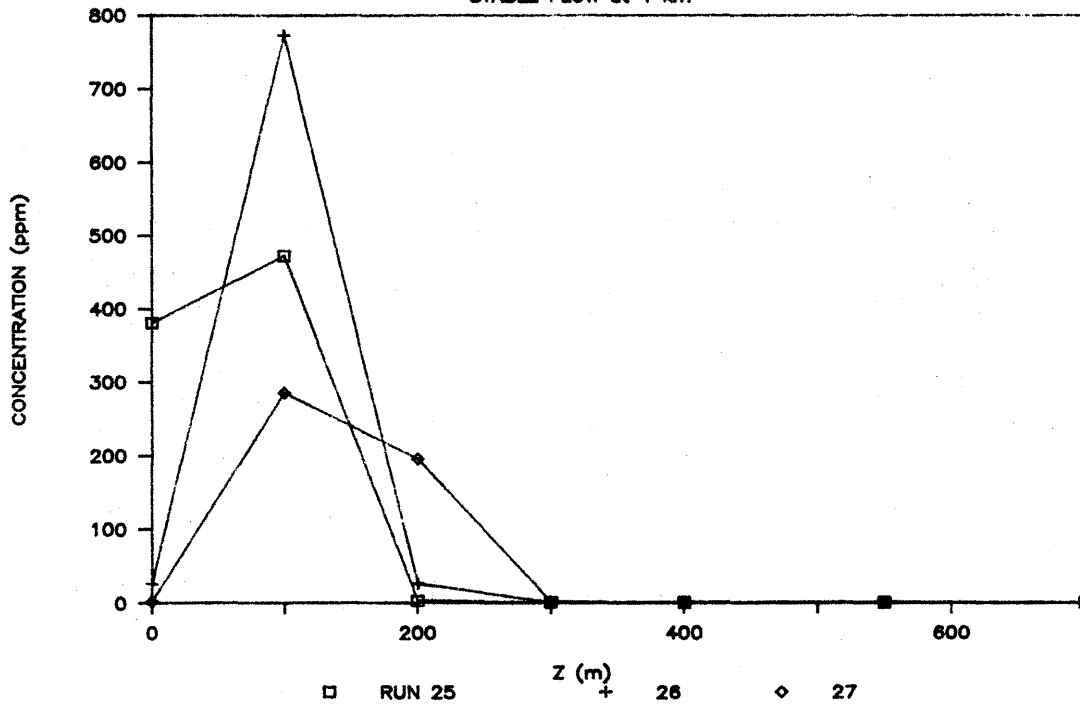
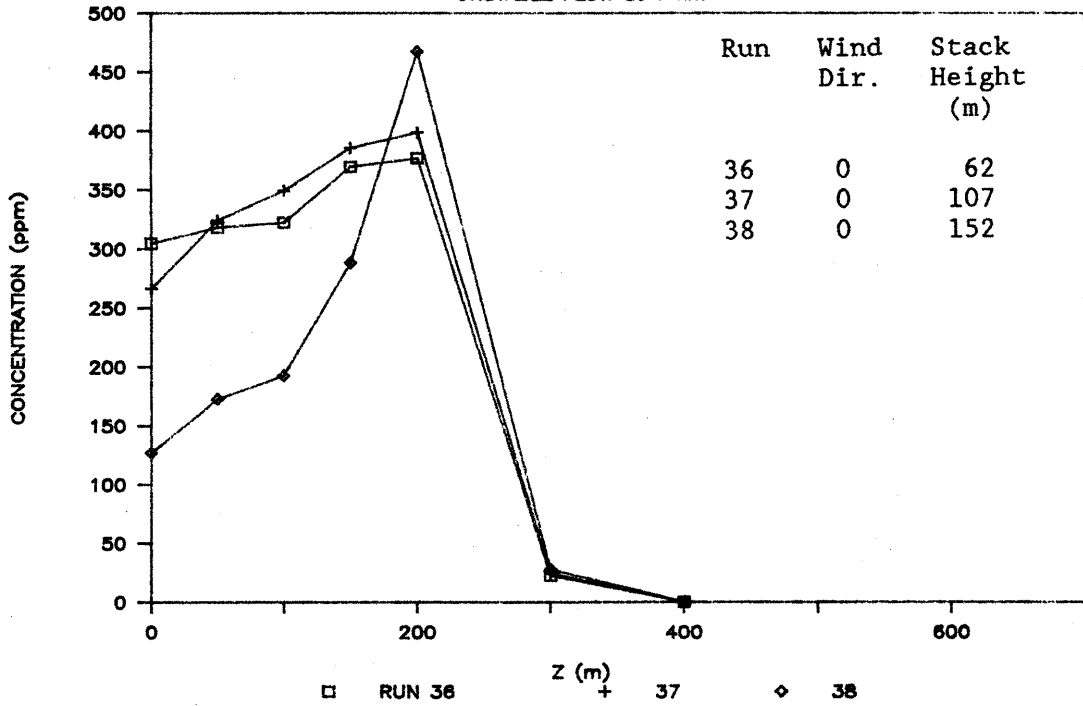


Figure 15. Vertical Concentration Profiles of Stable Flow at 1 and 4 km (Runs 25, 26, 27)

VERTICAL CONCENTRATION PROFILES

UNSTABLE FLOW at 1 km



VERTICAL CONCENTRATION PROFILES

UNSTABLE FLOW at 4 km

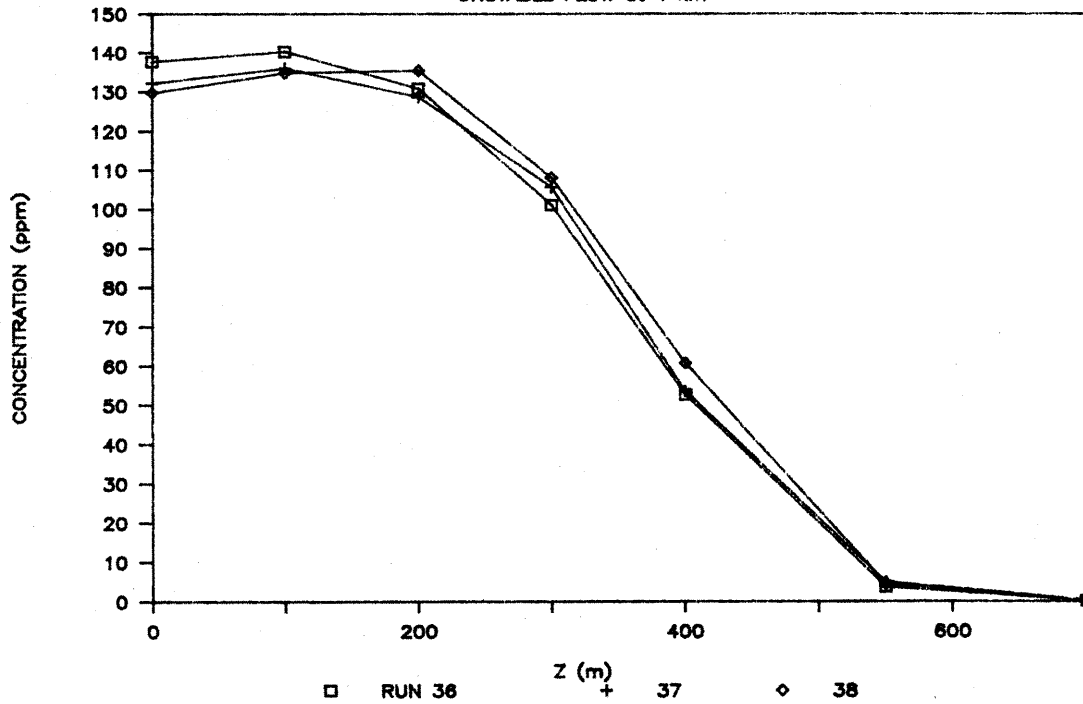
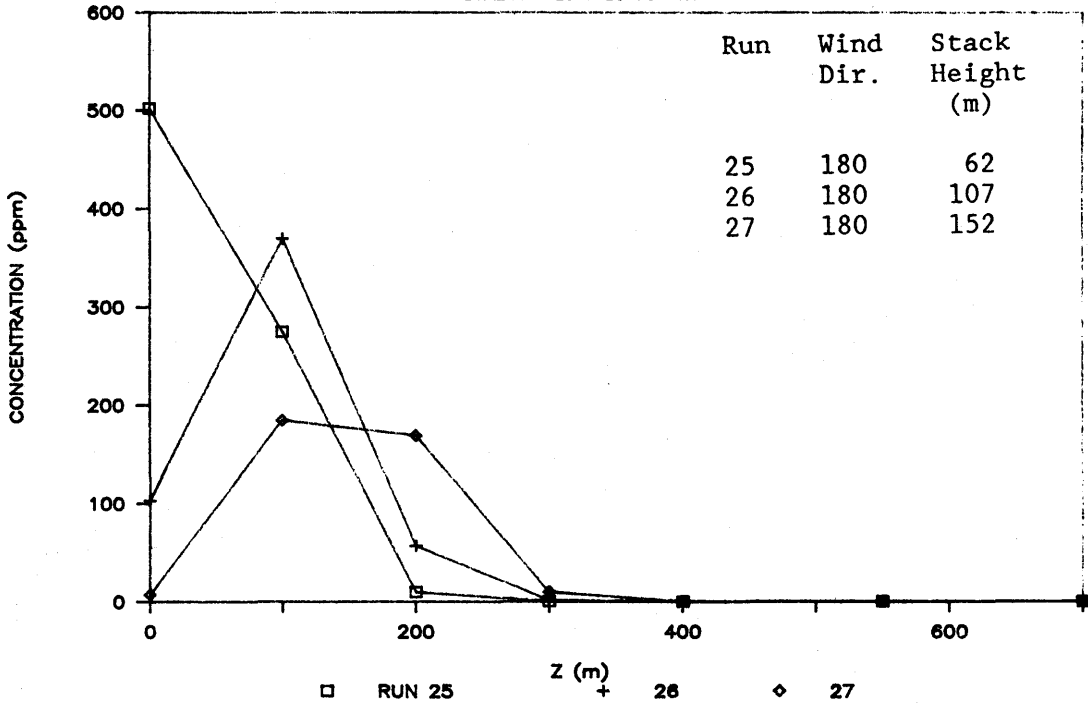


Figure 16. Vertical Concentration Profiles at Unstable Flow at 1 and 4 km (Runs 36, 37, 38)

VERTICAL CONCENTRATION PROFILES

STABLE FLOW at 10 km



VERTICAL CONCENTRATION PROFILES

UNSTABLE FLOW at 10 km

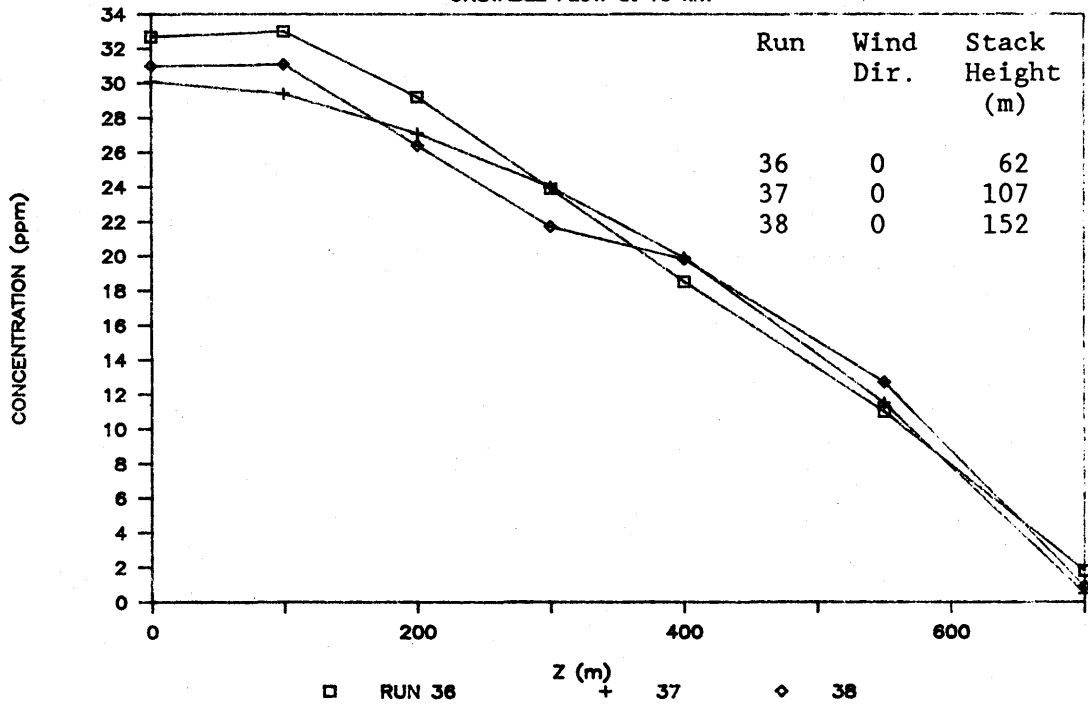
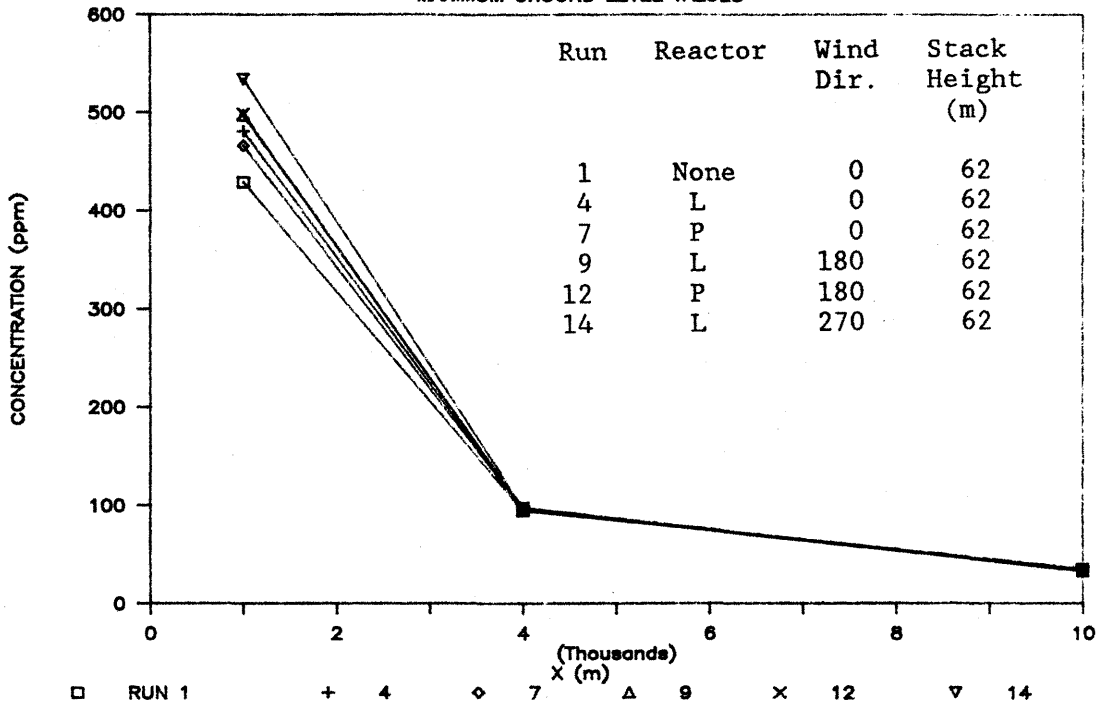


Figure 17. Vertical Concentration Profiles of Stable and Unstable Flow at 10 km (Runs 25, 26, 27 and 36, 37, 38)

LONGITUDINAL CONCENTRATION PROFILES

MAXIMUM GROUND LEVEL VALUES



LONGITUDINAL CONCENTRATION PROFILES

MAXIMUM GROUND LEVEL VALUES

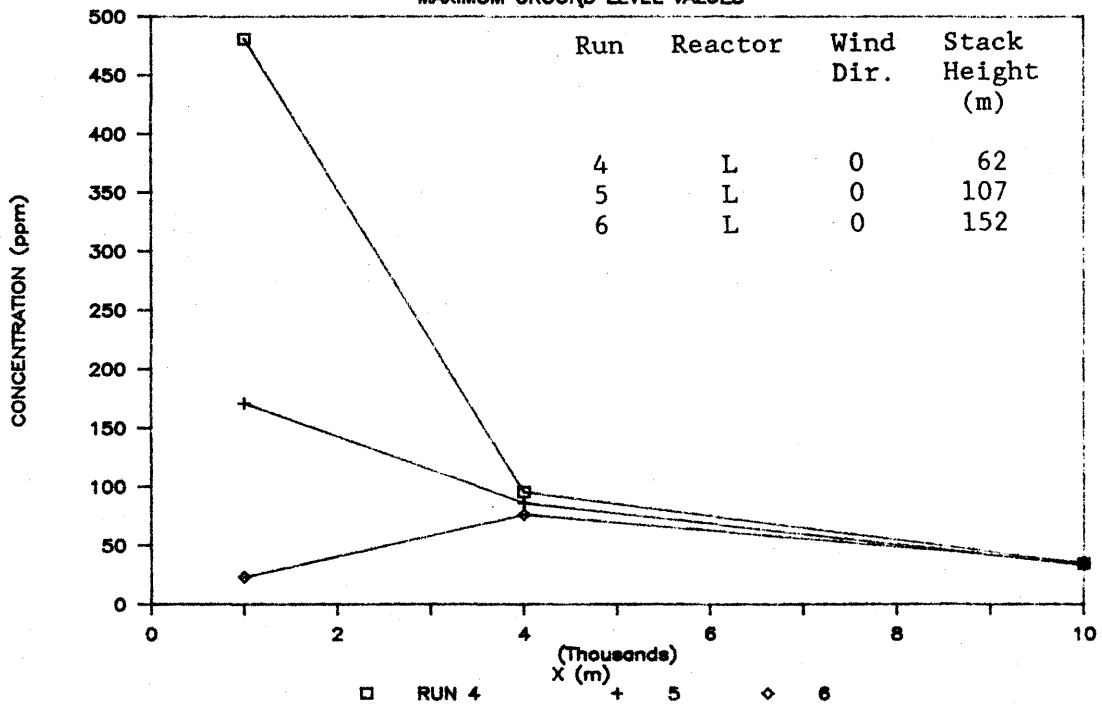
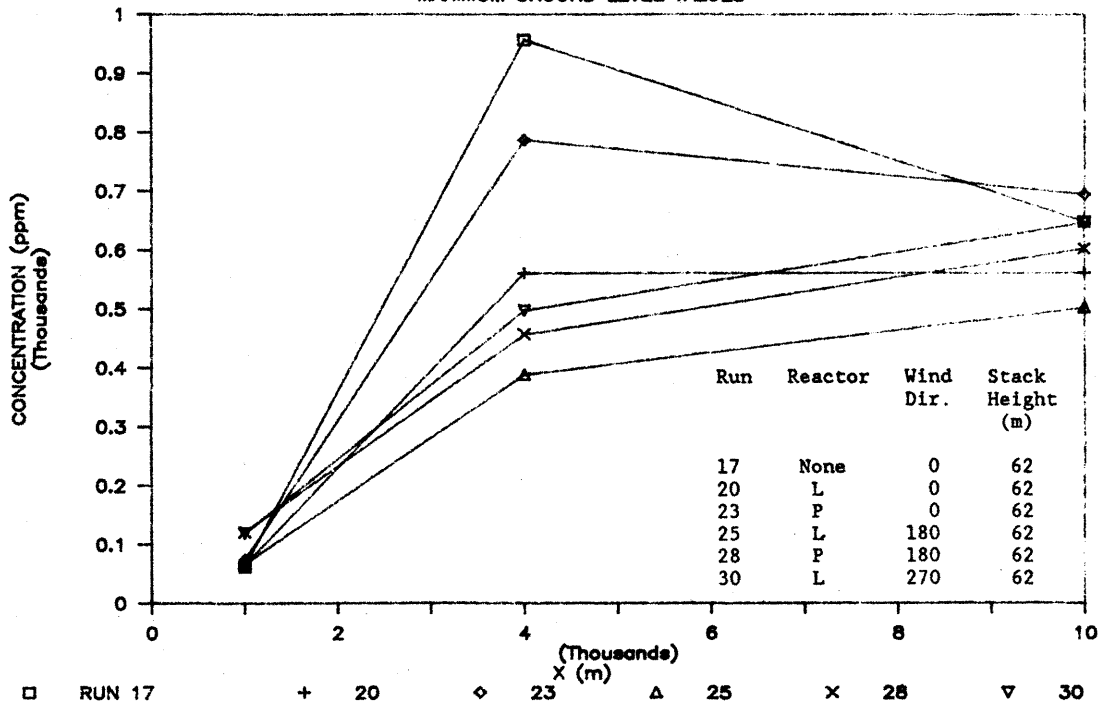


Figure 18. Longitudinal Concentration Profiles, Neutral Flows Maximum Ground Level Values (Runs 1, 4, 7, 9, 12, 14 and 4, 5, 6)

LONGITUDINAL CONCENTRATION PROFILES

MAXIMUM GROUND LEVEL VALUES



LONGITUDINAL CONCENTRATION PROFILES

MAXIMUM GROUND LEVEL VALUES

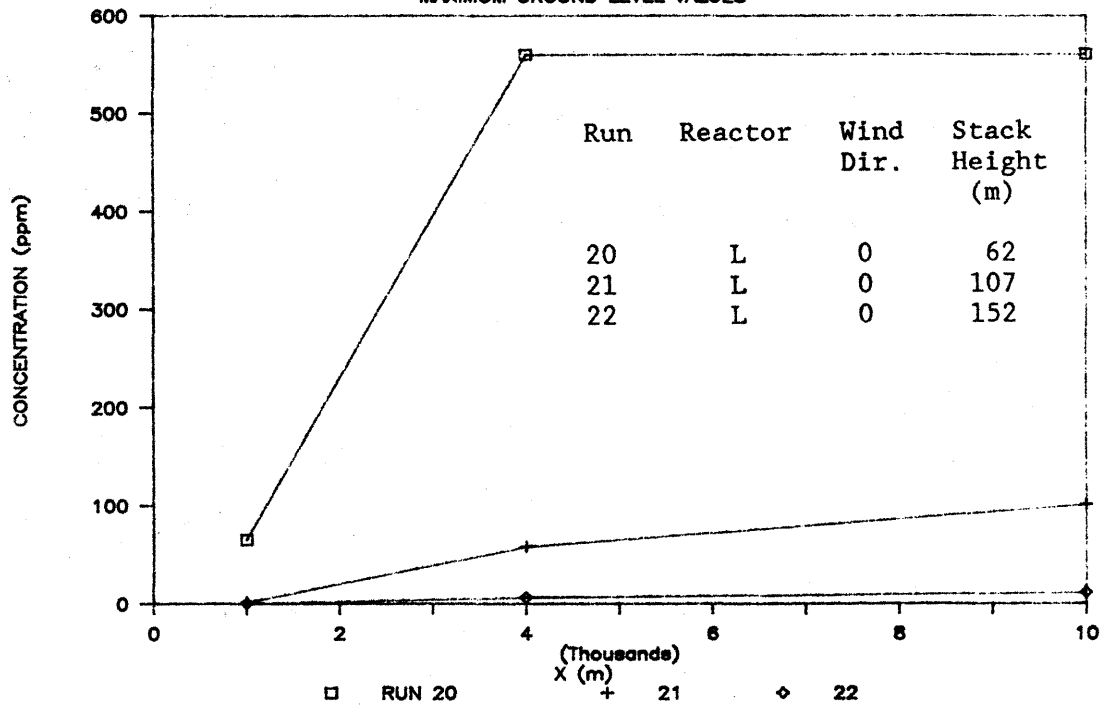
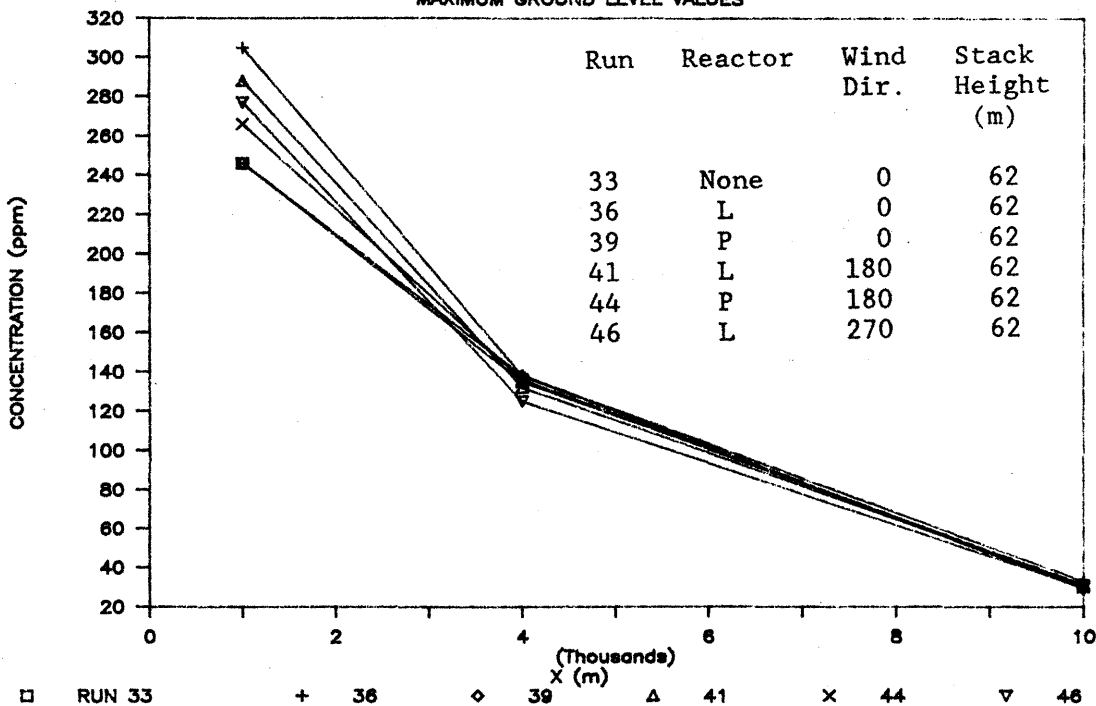


Figure 19. Longitudinal Concentration Profiles, Stable Flows Maximum Ground Level Values (Runs 17, 20, 23, 25, 28, 30 and 20, 21, 22)

LONGITUDINAL CONCENTRATION PROFILES

MAXIMUM GROUND LEVEL VALUES



LONGITUDINAL CONCENTRATION PROFILES

MAXIMUM GROUND LEVEL VALUES

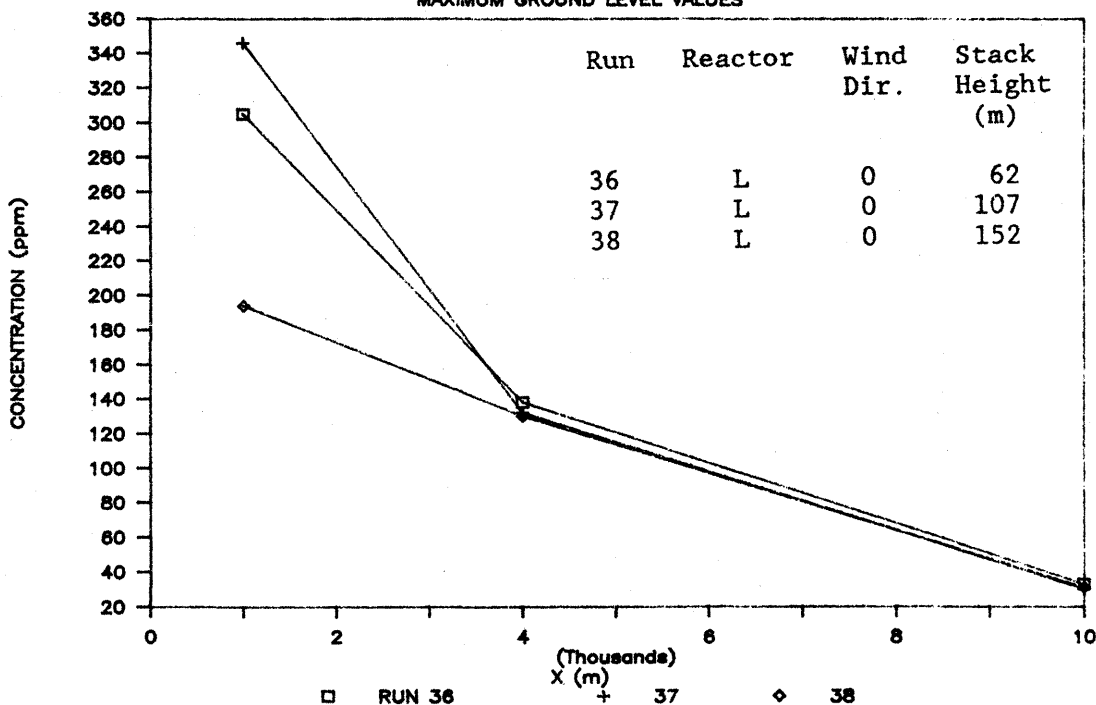


Figure 20. Longitudinal Concentration Profiles, Unstable Flows Maximum Ground Level Values (Runs 33, 36, 39, 41, 44, 46 and 36, 37, 38)

Run 4
Flow Neutral
Stack Height 62 m
Downwind Distance 1 km

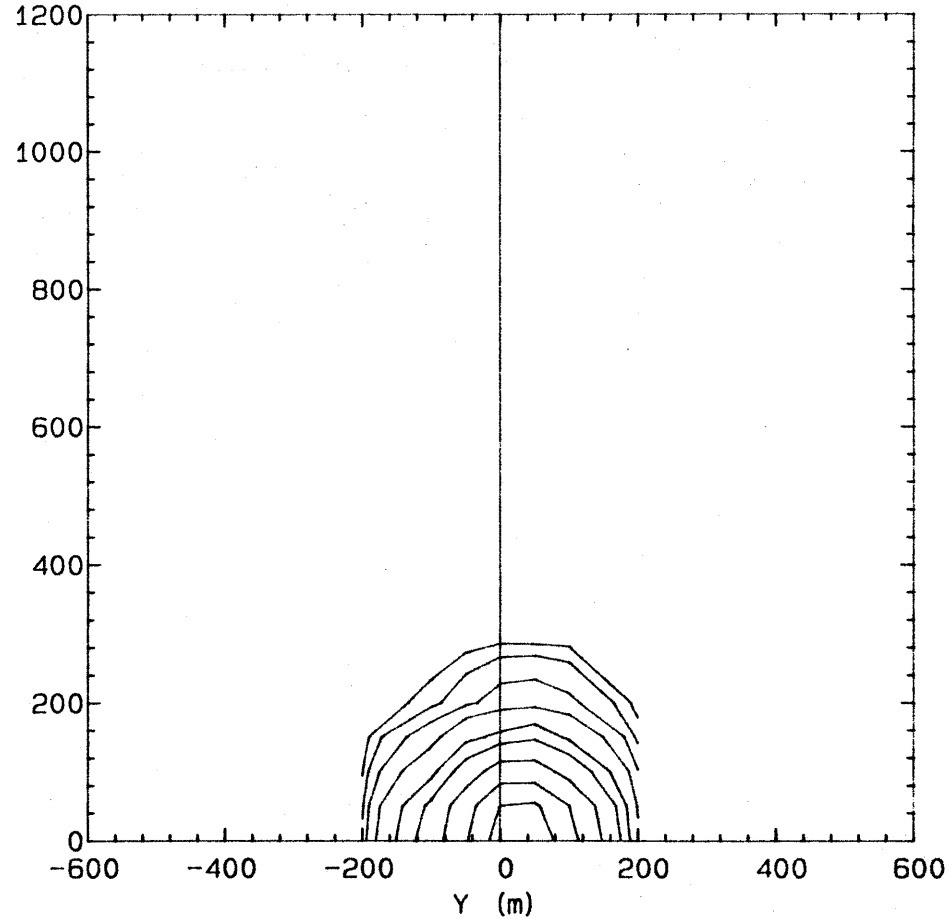
4
Neutral
62 m
1 km

Z (m)

C4-1.GC

CONTOUR LEVELS

- 5.0
- 10.0
- 20.0
- 40.0
- 80.0
- 120.0
- 200.0
- 300.0
- 400.0



CONCENTRATION CONTOURS
(ppm)

Figure 21-1. Concentration Contour Plots

Run
Flow
Stack Height
Downwind Distance

4
Neutral
62 m
4 km

C4-4.GC

CONTOUR LEVELS

5.0
10.0
20.0
40.0
80.0

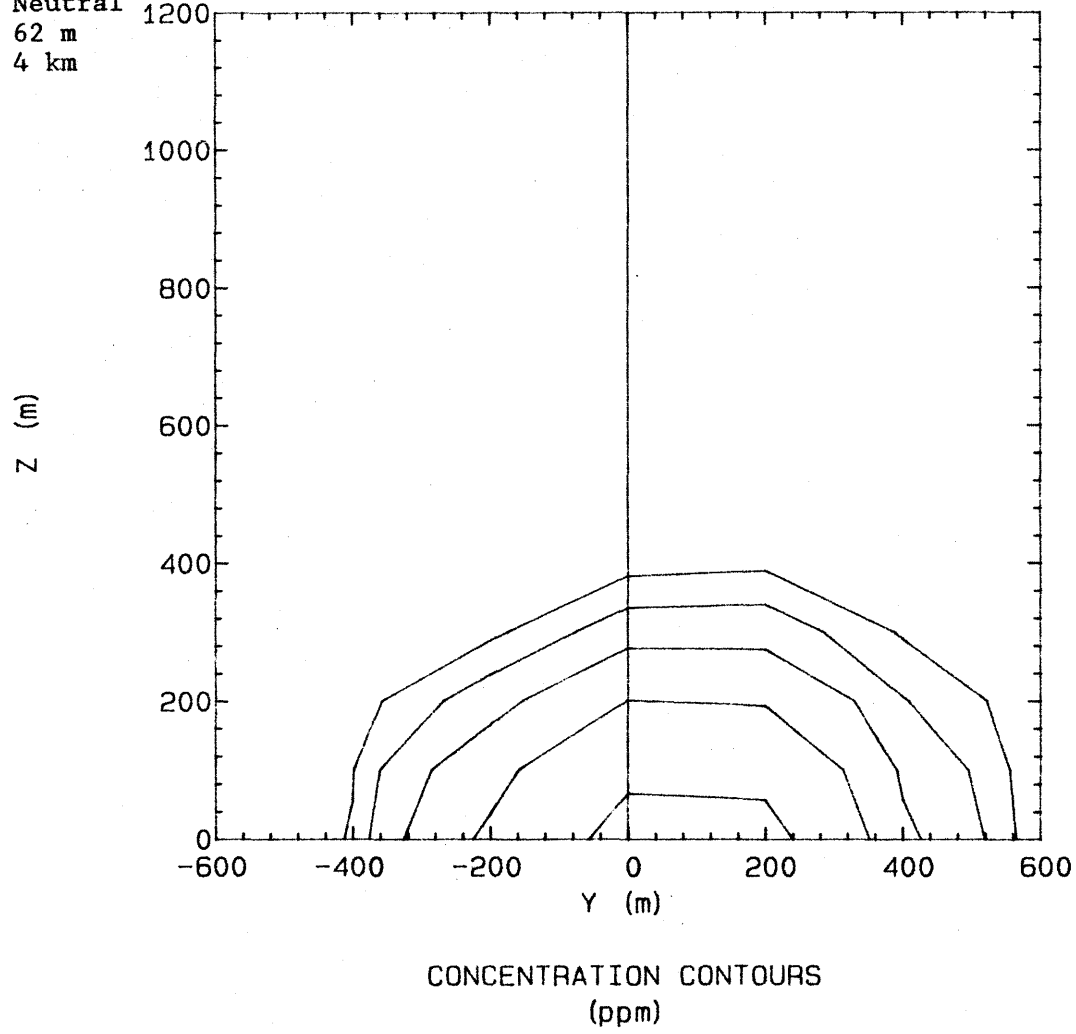


Figure 21-2. Concentration Contour Plots

Run 4
Flow Neutral
Stack Height 62 m
Downwind Distance 10 km

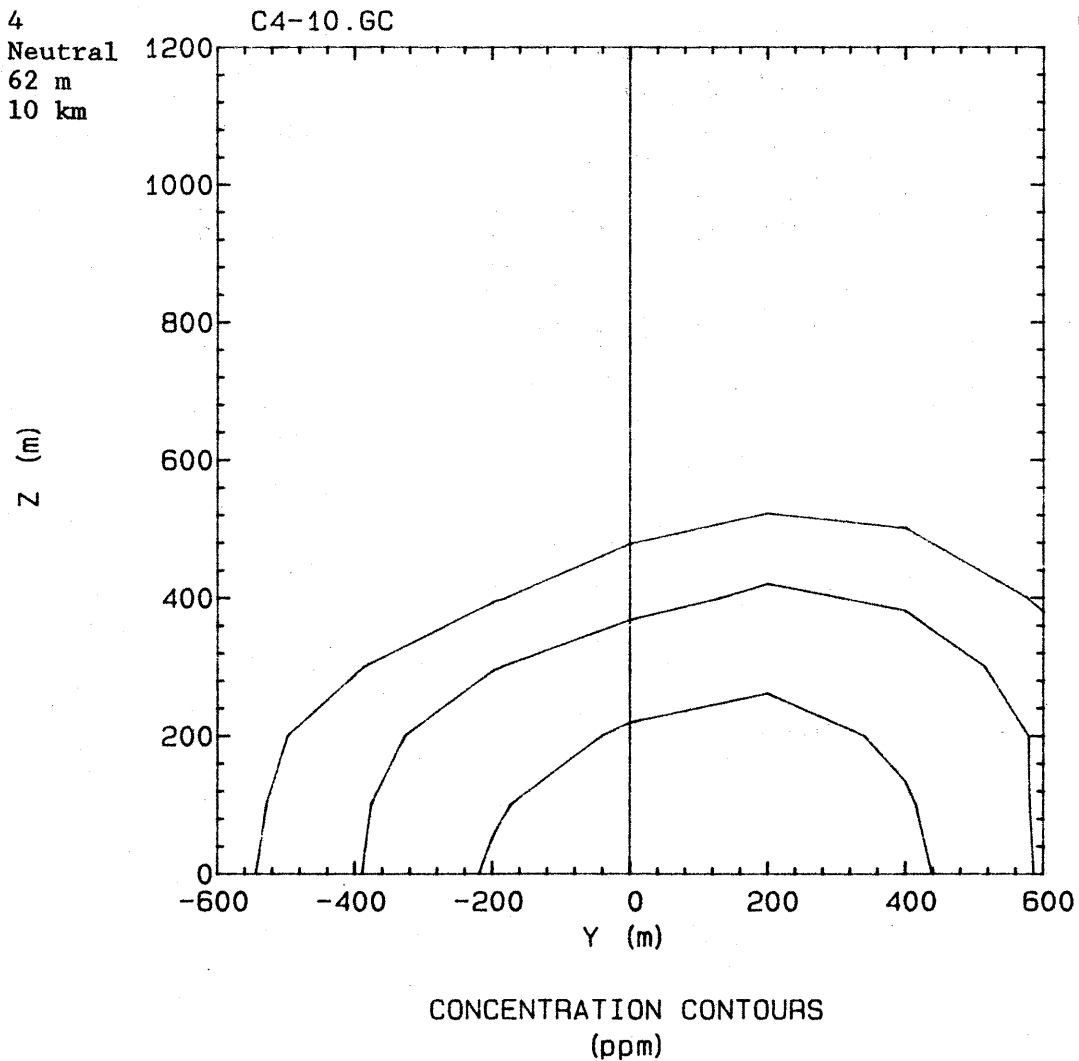
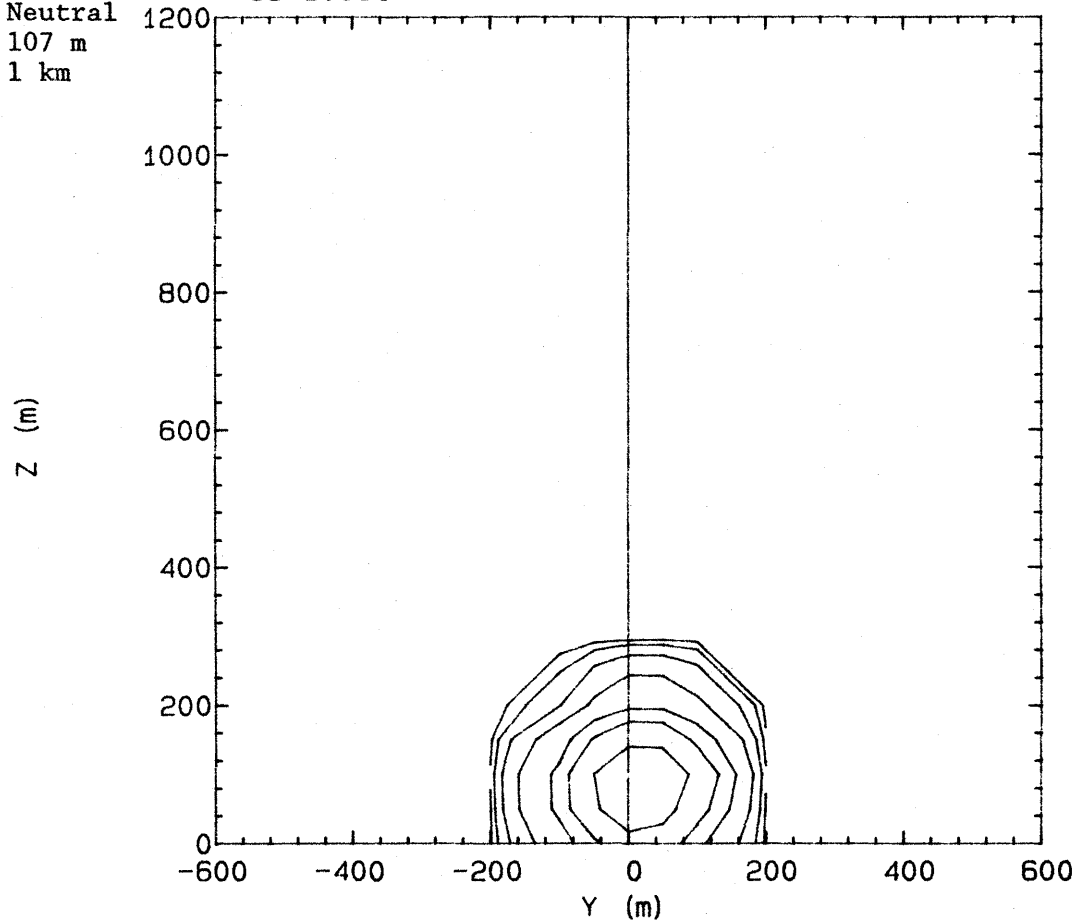


Figure 21-3. Concentration Contour Plots

Run 5
Flow Neutral
Stack Height 107 m
Downwind Distance 1 km

C5-1.GCC

CONTOUR LEVELS



CONCENTRATION CONTOURS
(ppm)

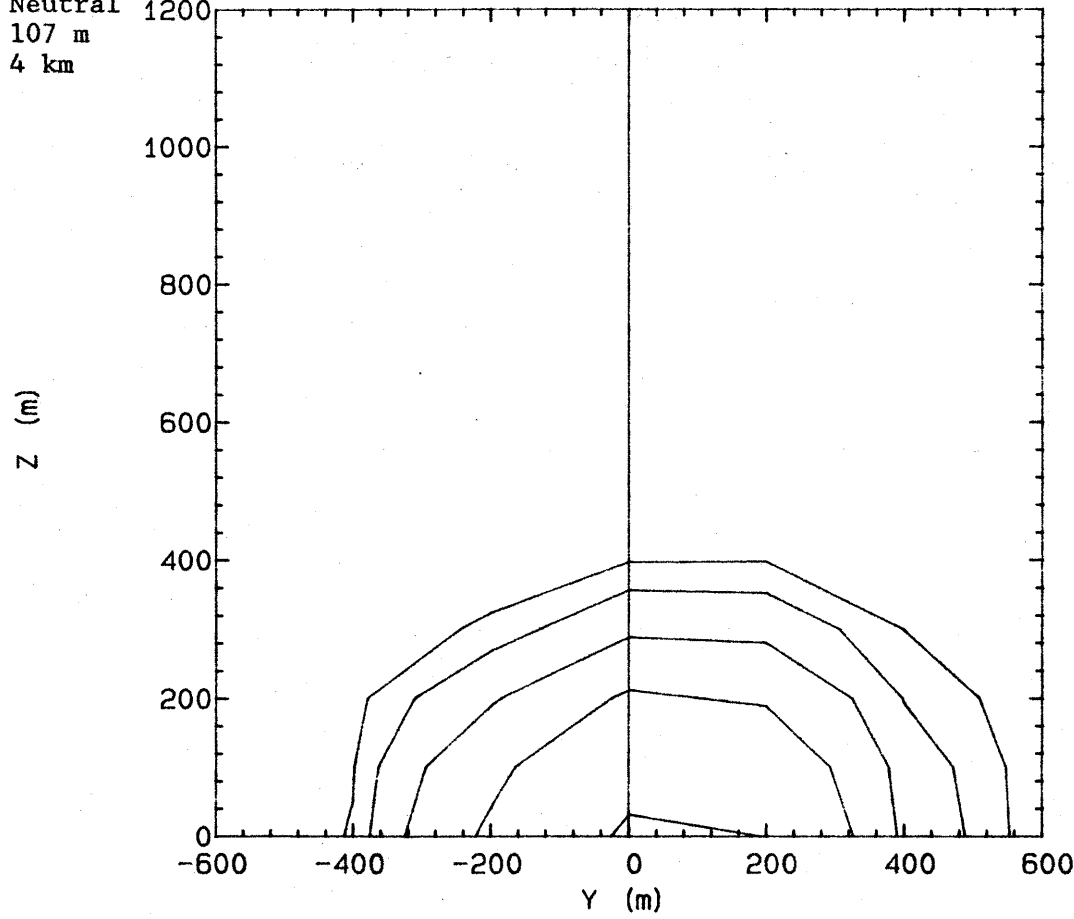
Figure 21-4. Concentration Contour Plots

Run
Flow
Stack Height
Downwind Distance

5
Neutral
107 m
4 km

C5-4.GCC

CONTOUR LEVELS



CONCENTRATION CONTOURS
(ppm)

Figure 21-5. Concentration Contour Plots

Run 5
Flow Neutral
Stack Height 107 m
Downwind Distance 10 km

C5-10.GC

CONTOUR LEVELS

5.0
10.0
20.0

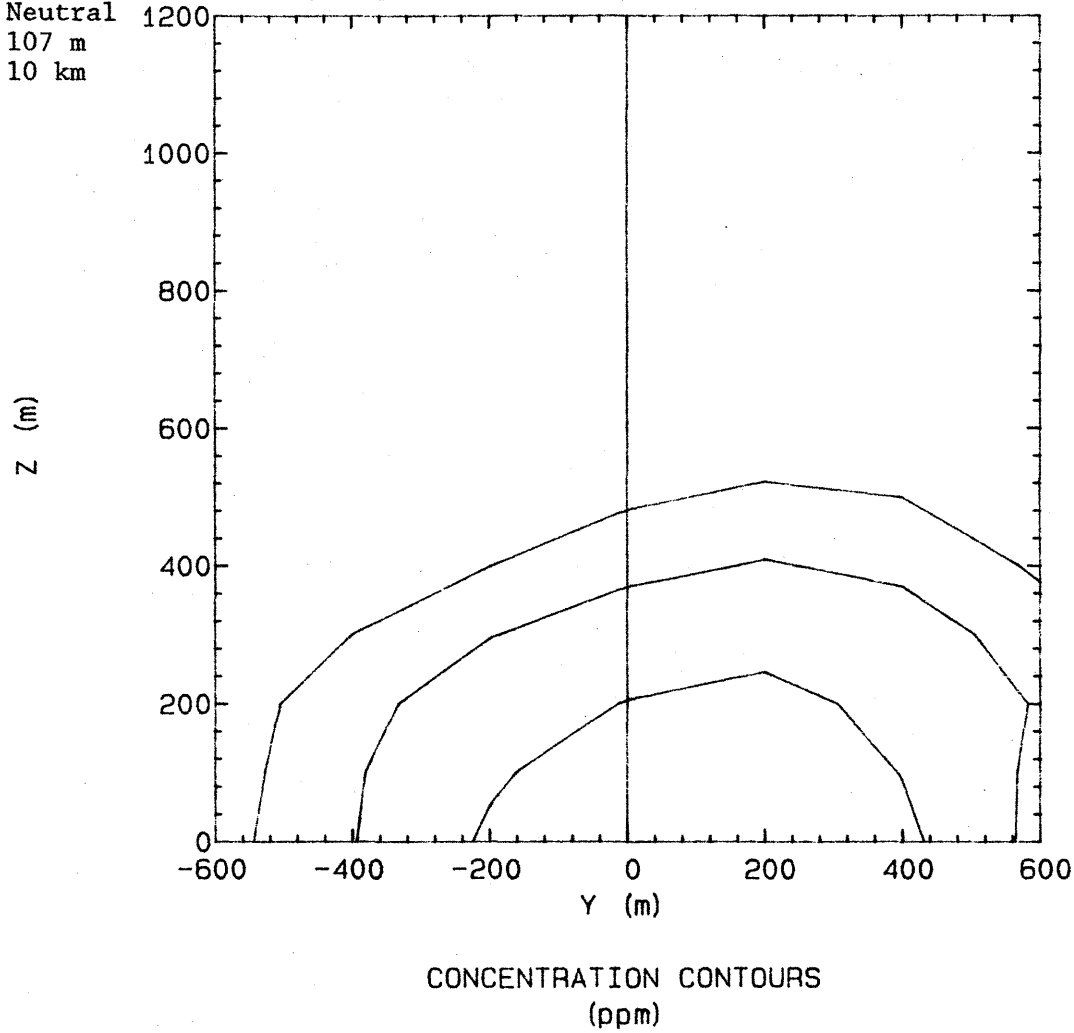


Figure 21-6. Concentration Contour Plots

Run 6
Flow Neutral
Stack Height 152 m
Downwind Distance 1 km

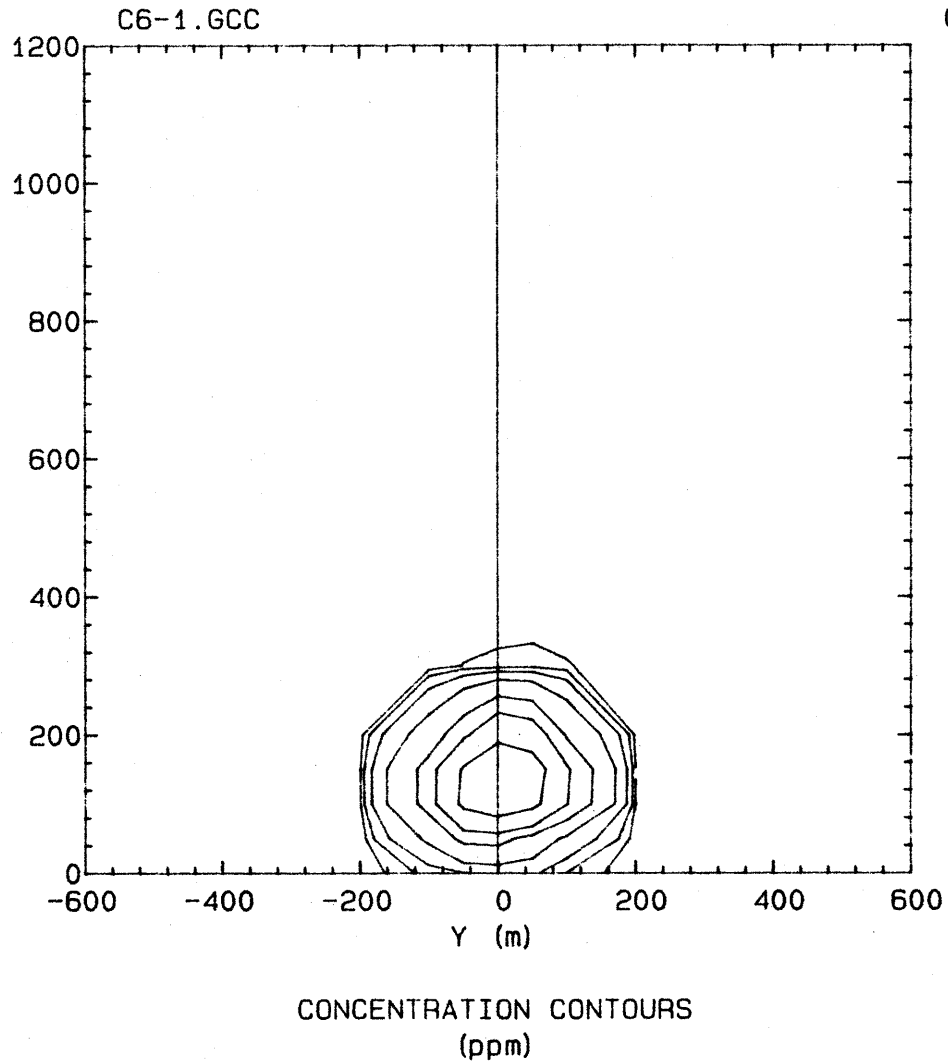


Figure 21-7. Concentration Contour Plots

Run 6
Flow Neutral
Stack Height 152 m
Downwind Distance 4 km

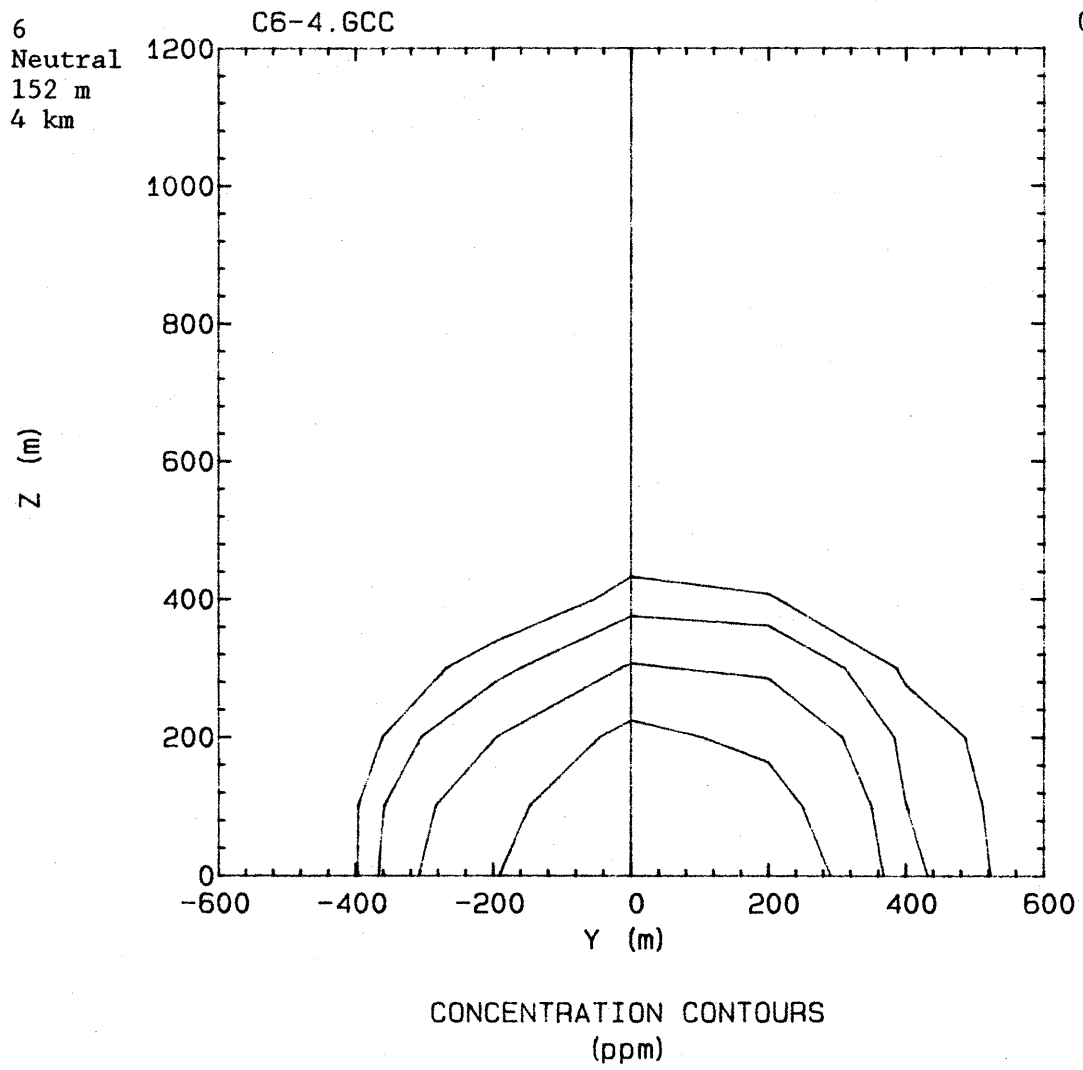


Figure 21-8. Concentration Contour Plots

Run 6
Flow Neutral
Stack Height 152 m
Downwind Distance 10 km

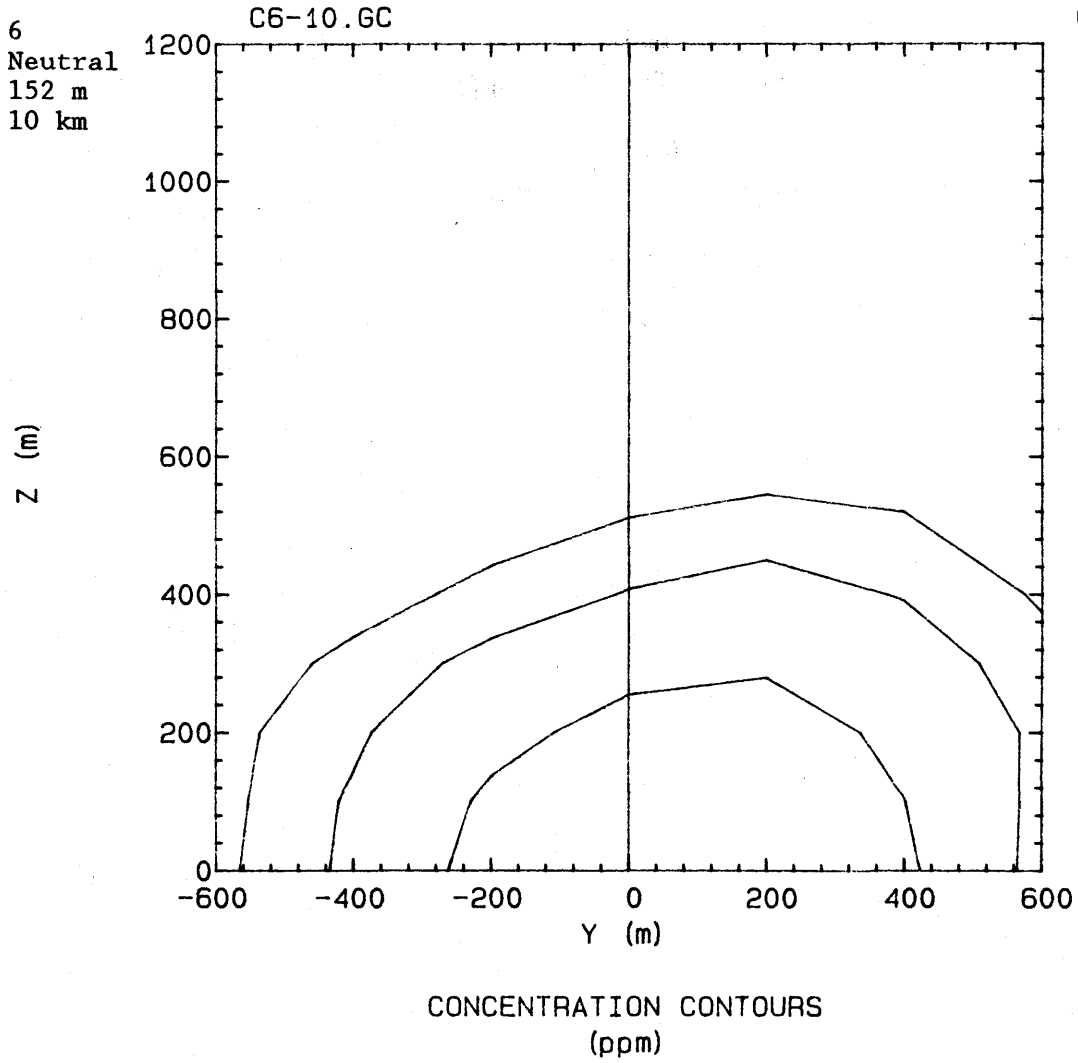
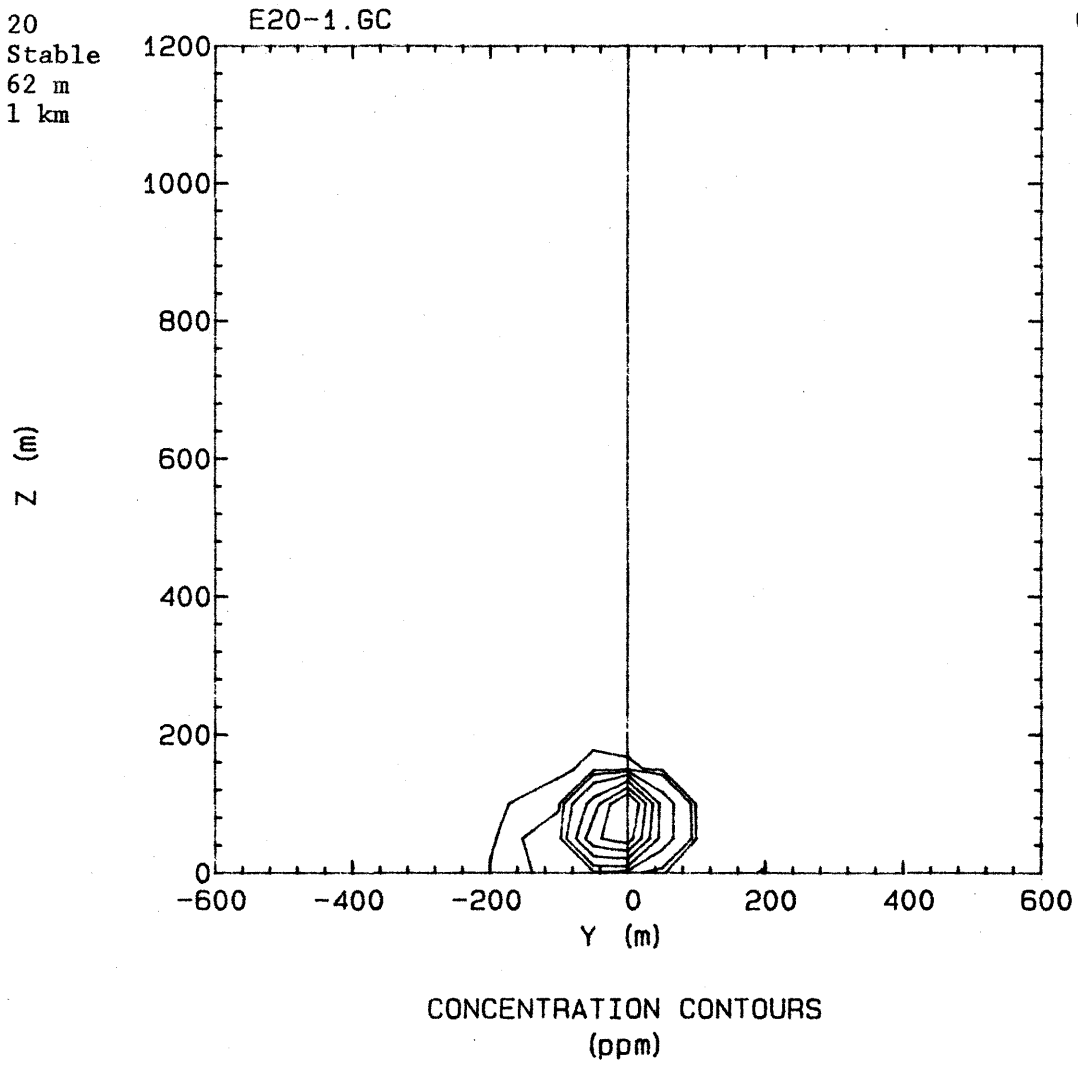


Figure 21-9. Concentration Contour Plots

Run 20
Flow Stable
Stack Height 62 m
Downwind Distance 1 km



CONTOUR LEVELS
5.0
5.0
25.0
100.0
250.0
500.0
750.0
1000.0

Figure 21-10. Concentration Contour Plots

Run 20
Flow Stable
Stack Height 62 m
Downwind Distance 4 km

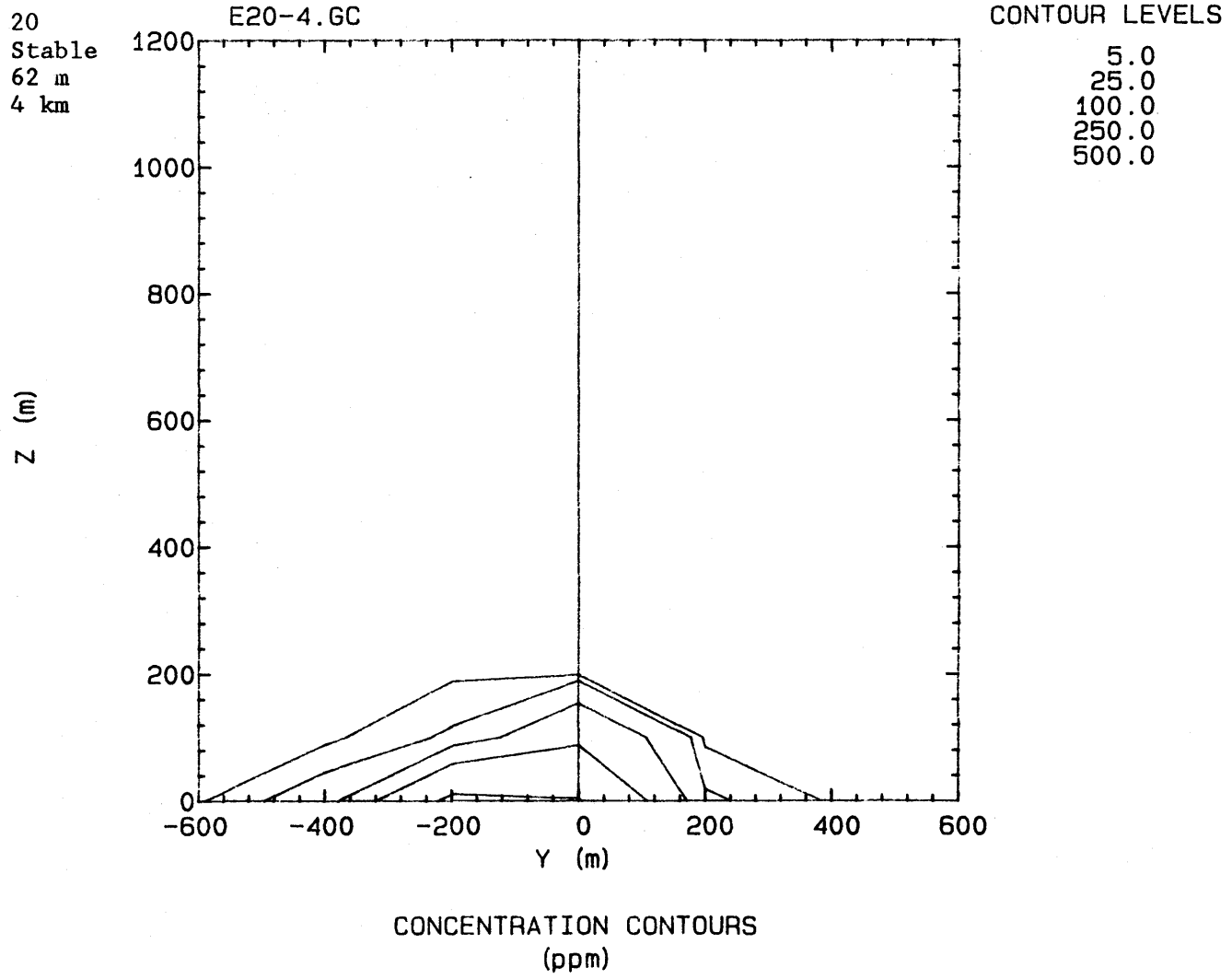
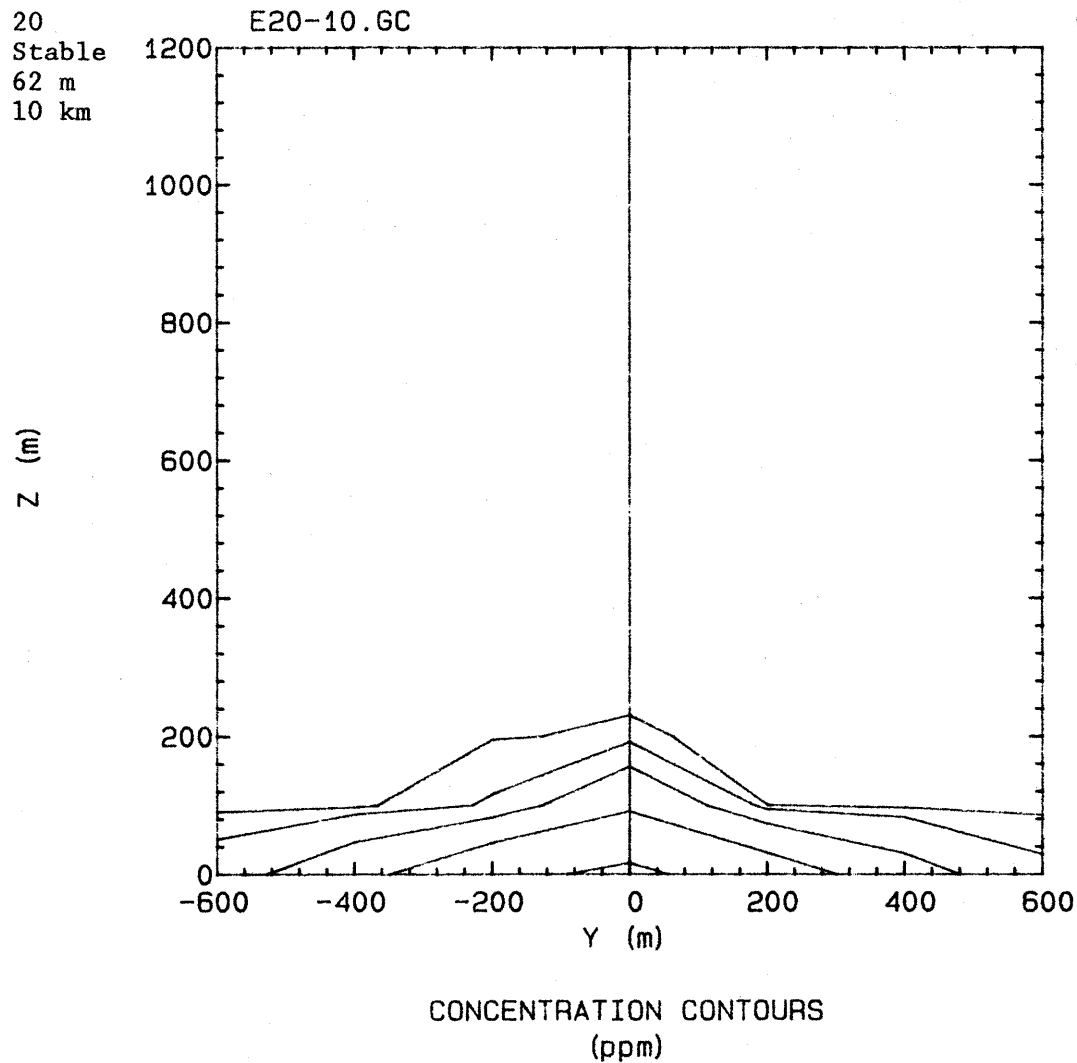


Figure 21-11. Concentration Contour Plots

Run 20
Flow Stable
Stack Height 62 m
Downwind Distance 10 km



CONTOUR LEVELS
5.0
25.0
100.0
250.0
500.0

Figure 21-12. Concentration Contour Plots

Run 21
Flow Stable
Stack Height 107 m
Downwind Distance 1 km

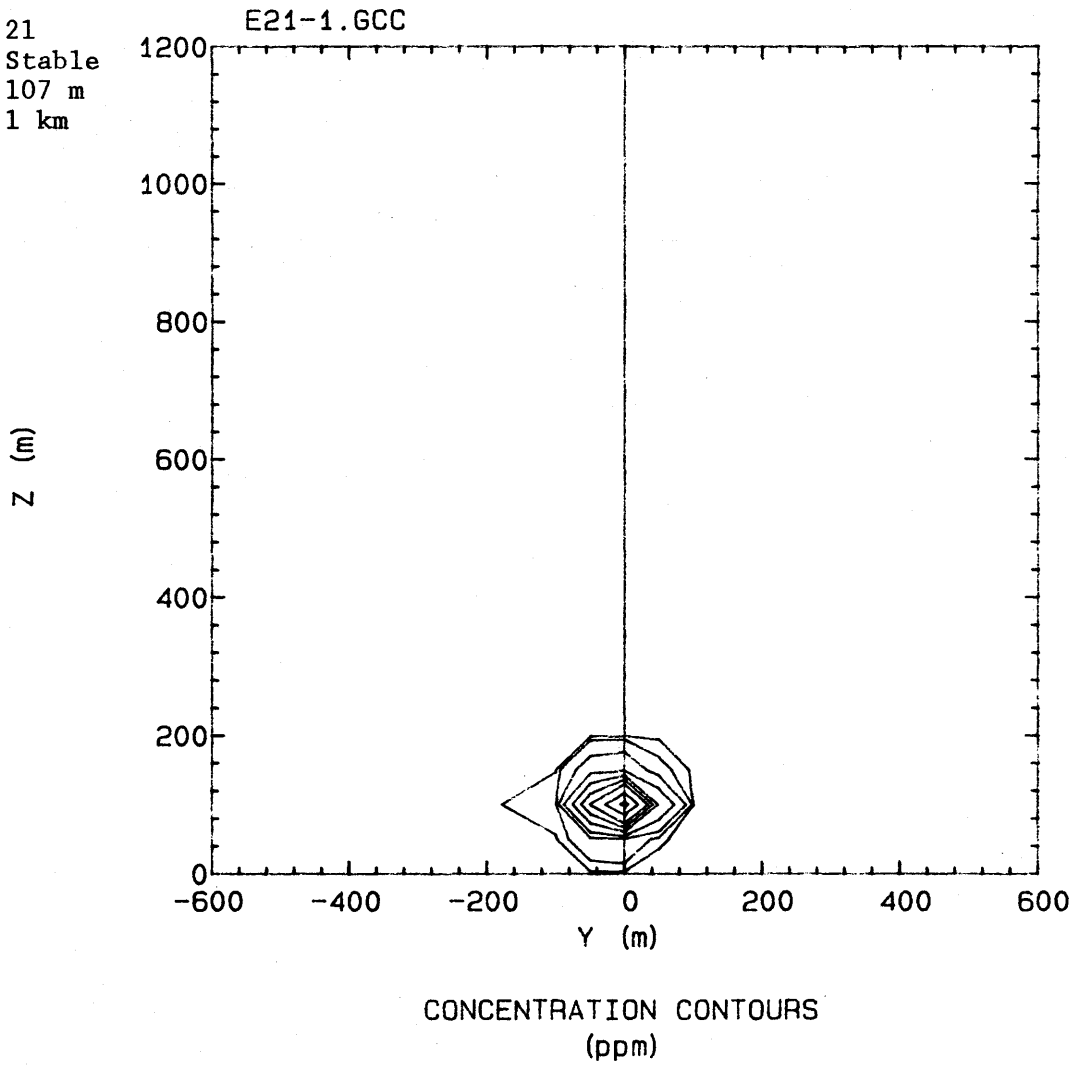


Figure 21-13. Concentration Contour Plots

Run 21
Flow Stable
Stack Height 107 m
Downwind Distance 4 km

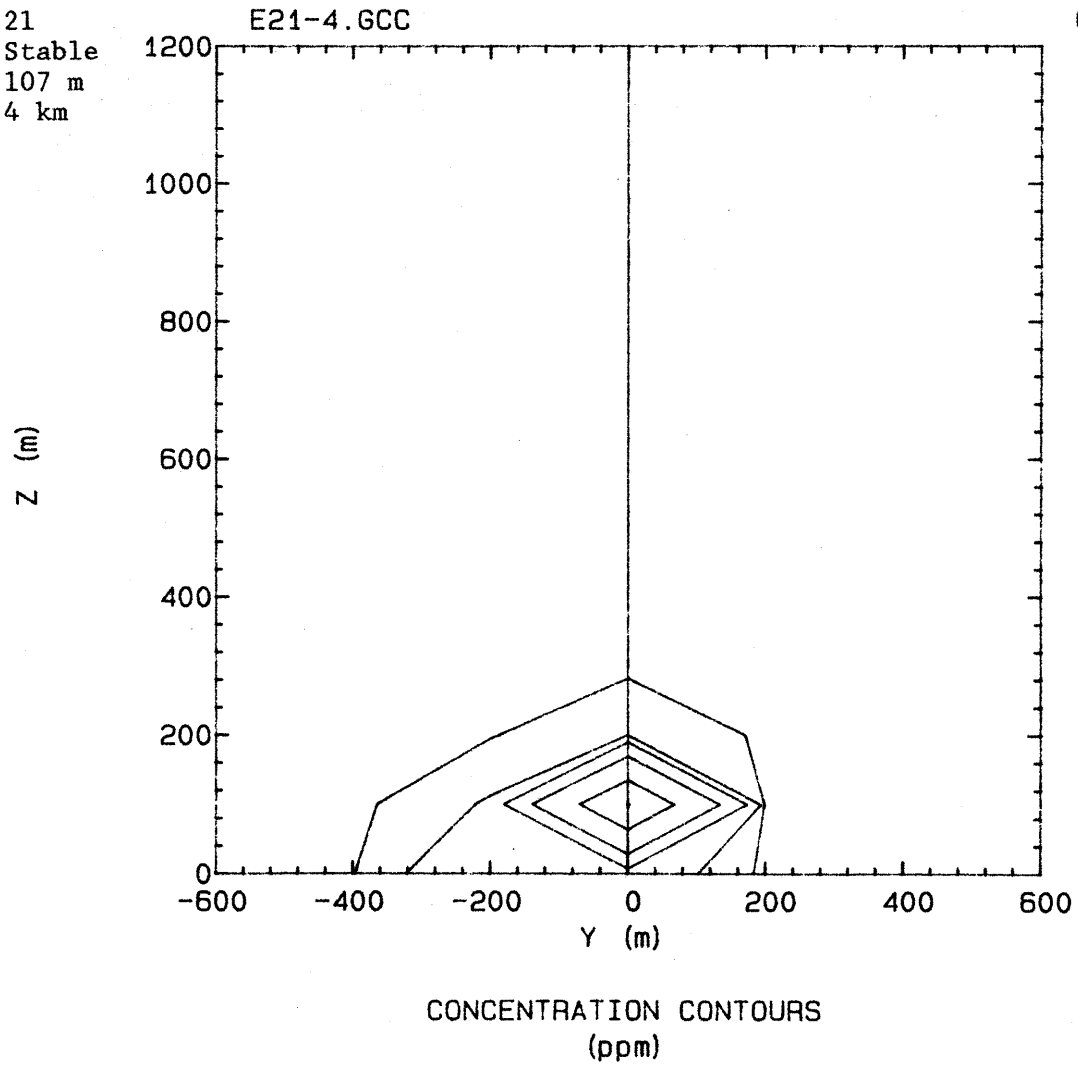


Figure 21-14. Concentration Contour Plots

Run 21
Flow Stable
Stack Height 107 m
Downwind Distance 10 km

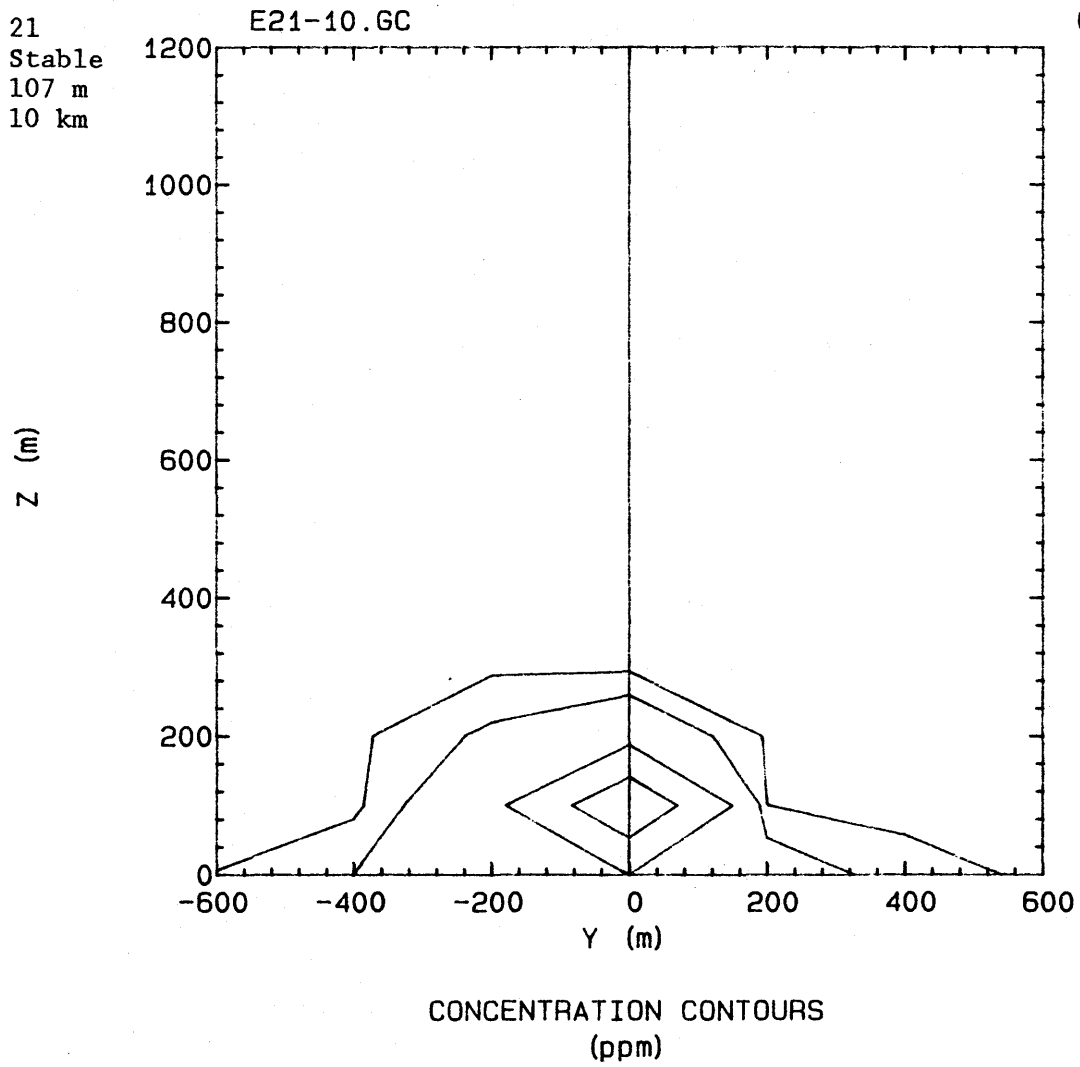
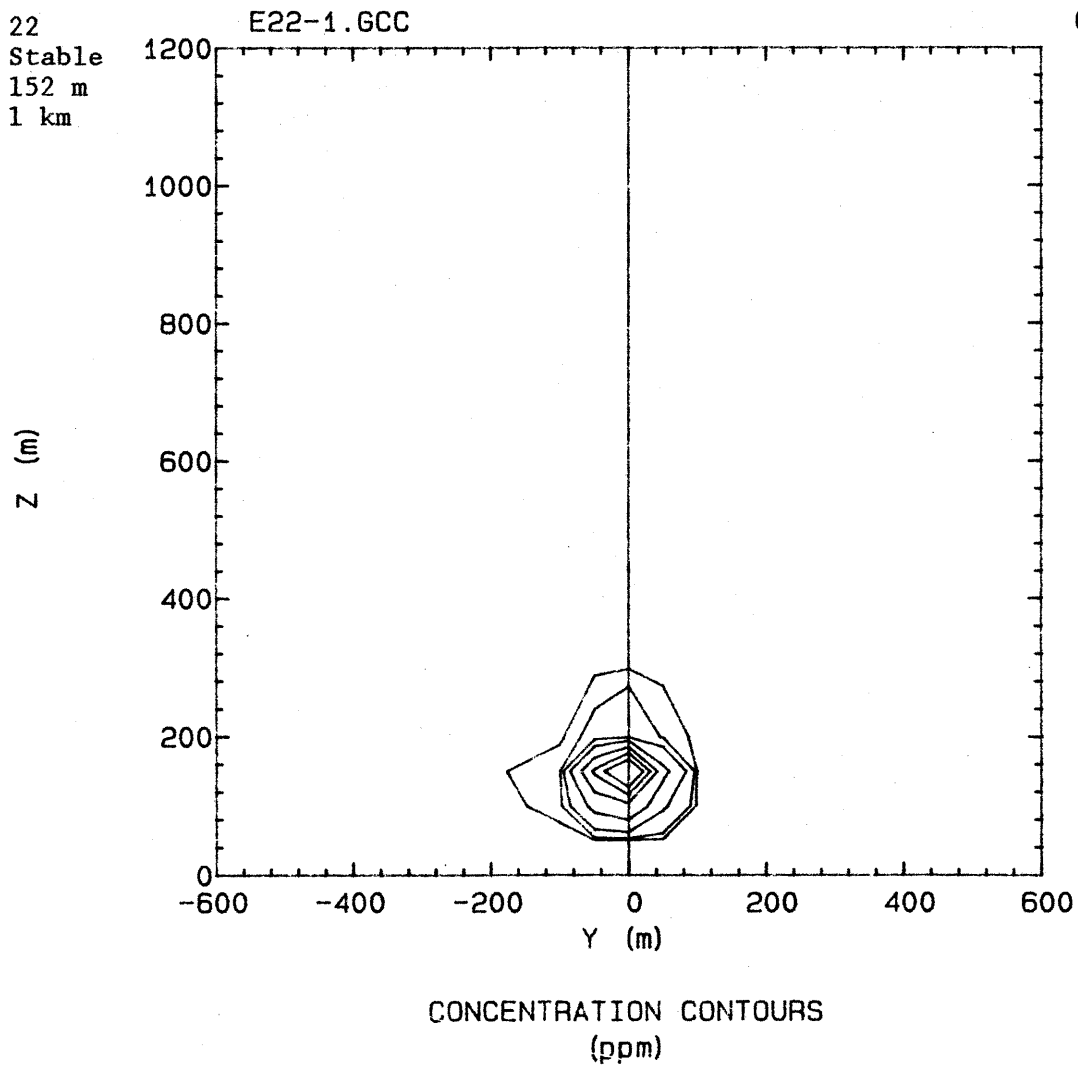


Figure 21-15. Concentration Contour Plots

Run 22
Flow Stable
Stack Height 152 m
Downwind Distance 1 km



CONTOUR LEVELS

5.0
25.0
100.0
250.0
500.0
750.0
1000.0

Figure 21-16. Concentration Contour Plots

Run 22
Flow Stable
Stack Height 152 m
Downwind Distance 4 km

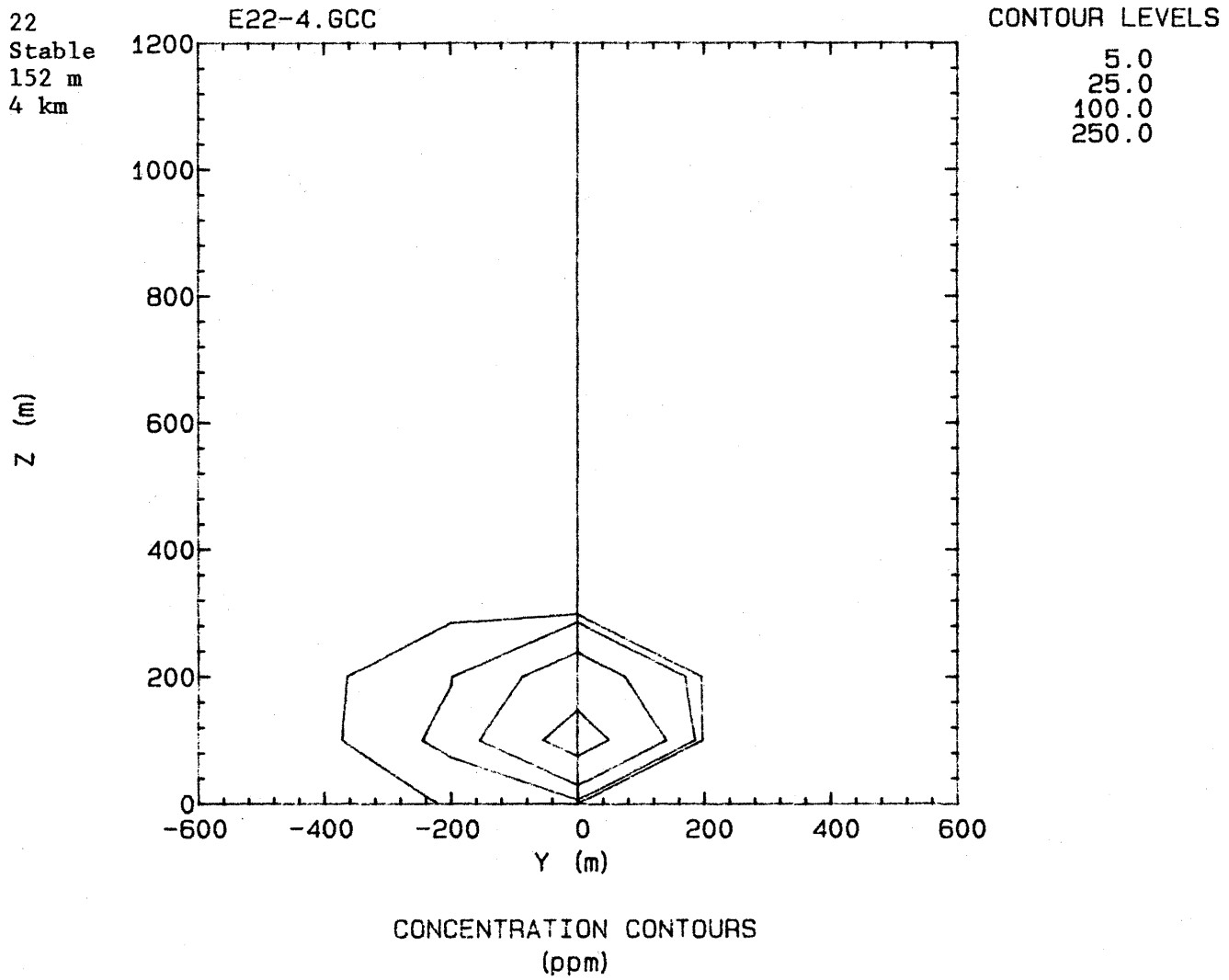


Figure 21-17. Concentration Contour Plots

Run 22
Flow Stable
Stack Height 152 m
Downwind Distance 10 km

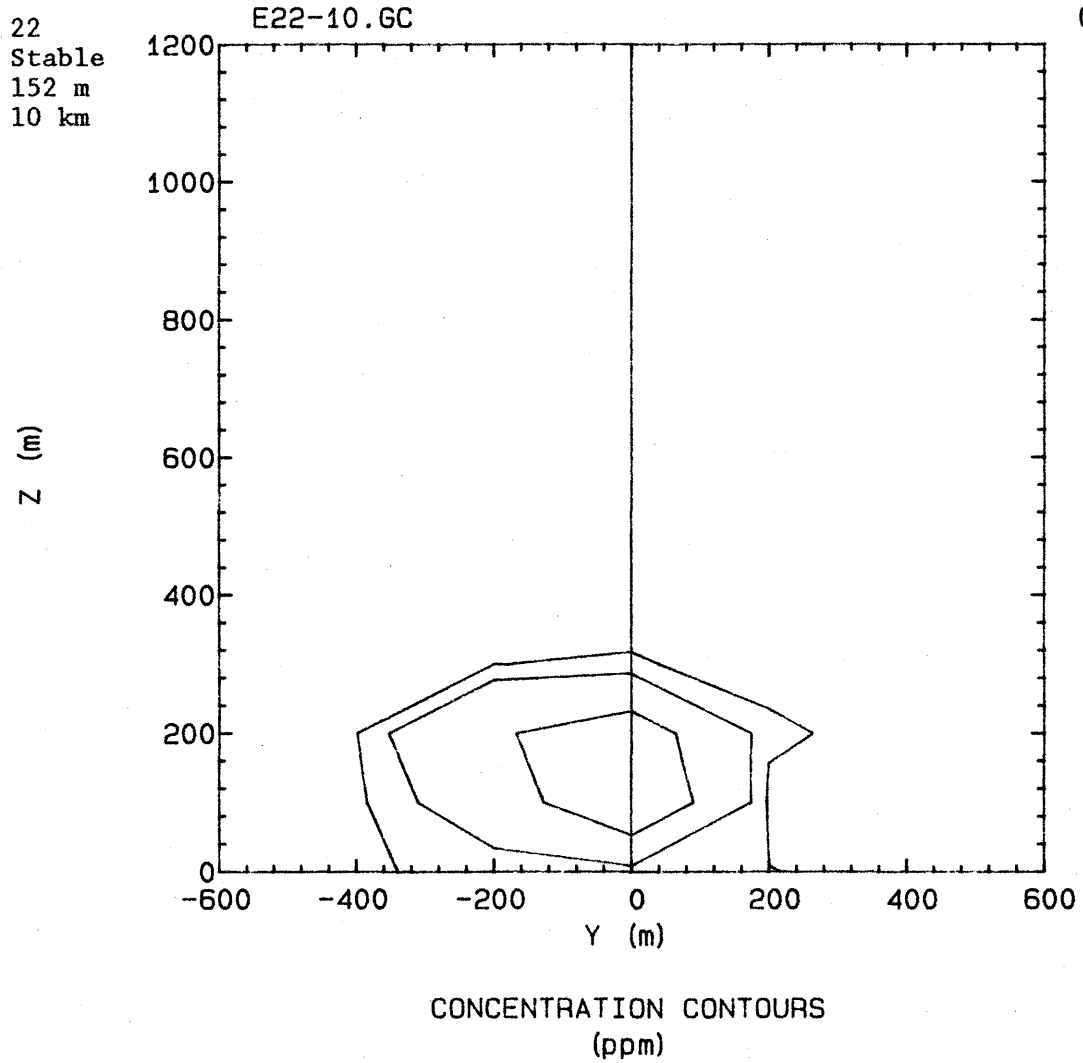


Figure 21-18. Concentration Contour Plots

Run 36
Flow Unstable
Stack Height 62 m
Downwind Distance 1 km

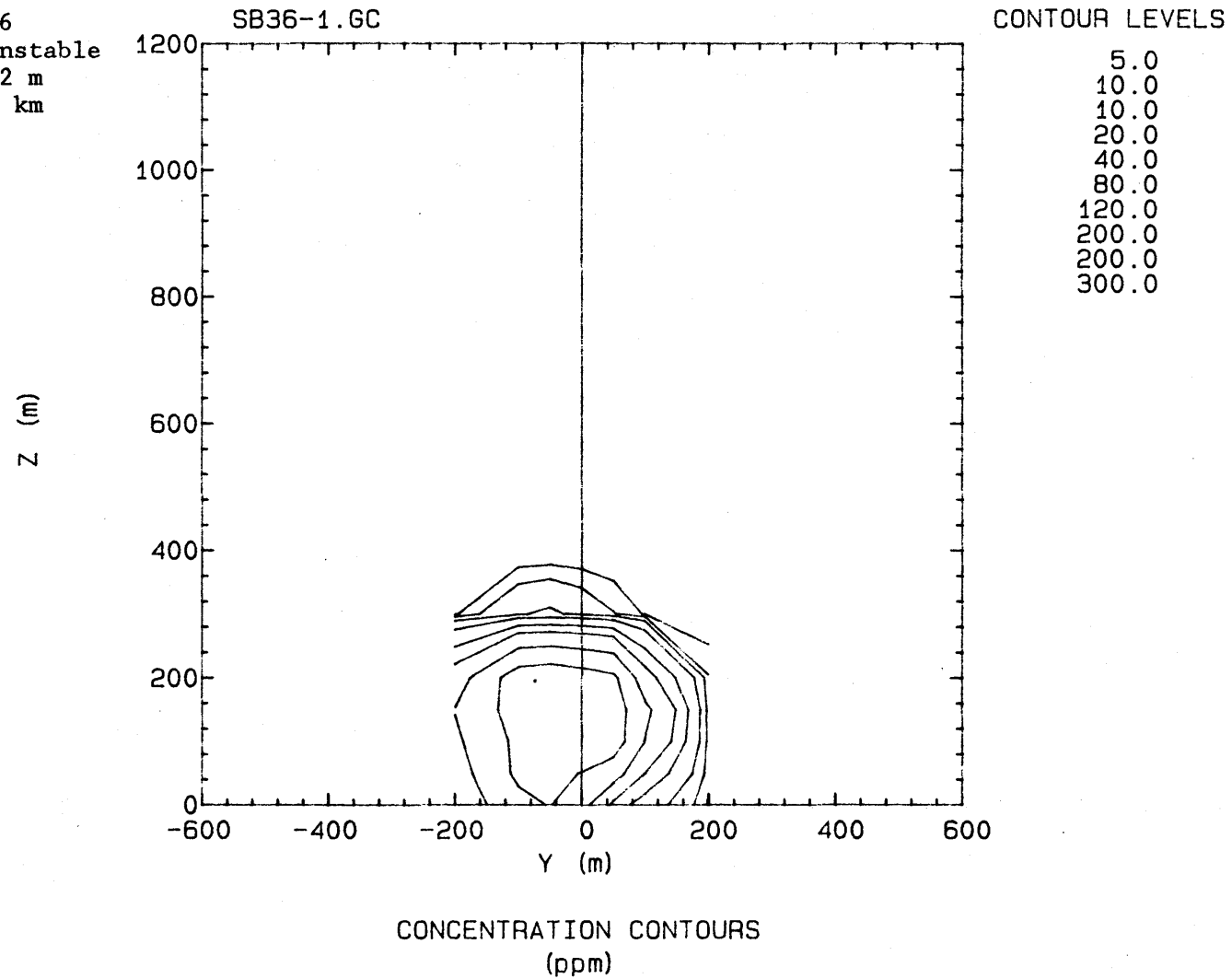
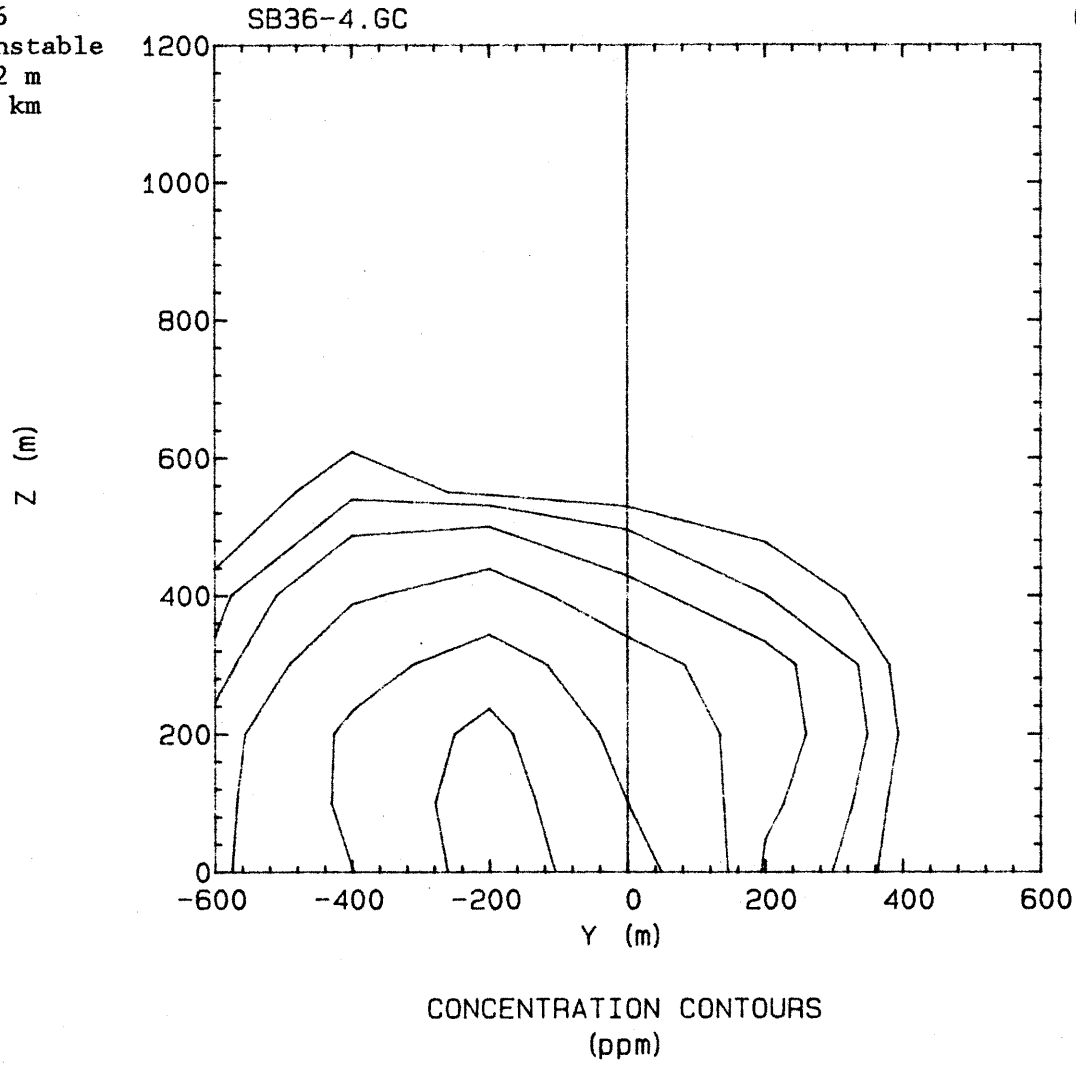


Figure 21-19. Concentration Contour Plots

Run 36
Flow Unstable
Stack Height 62 m
Downwind Distance 4 km



F-40

Figure 21-20. Concentration Contour Plots

Run 36
Flow Unstable
Stack Height 62 m
Downwind Distance 10 km

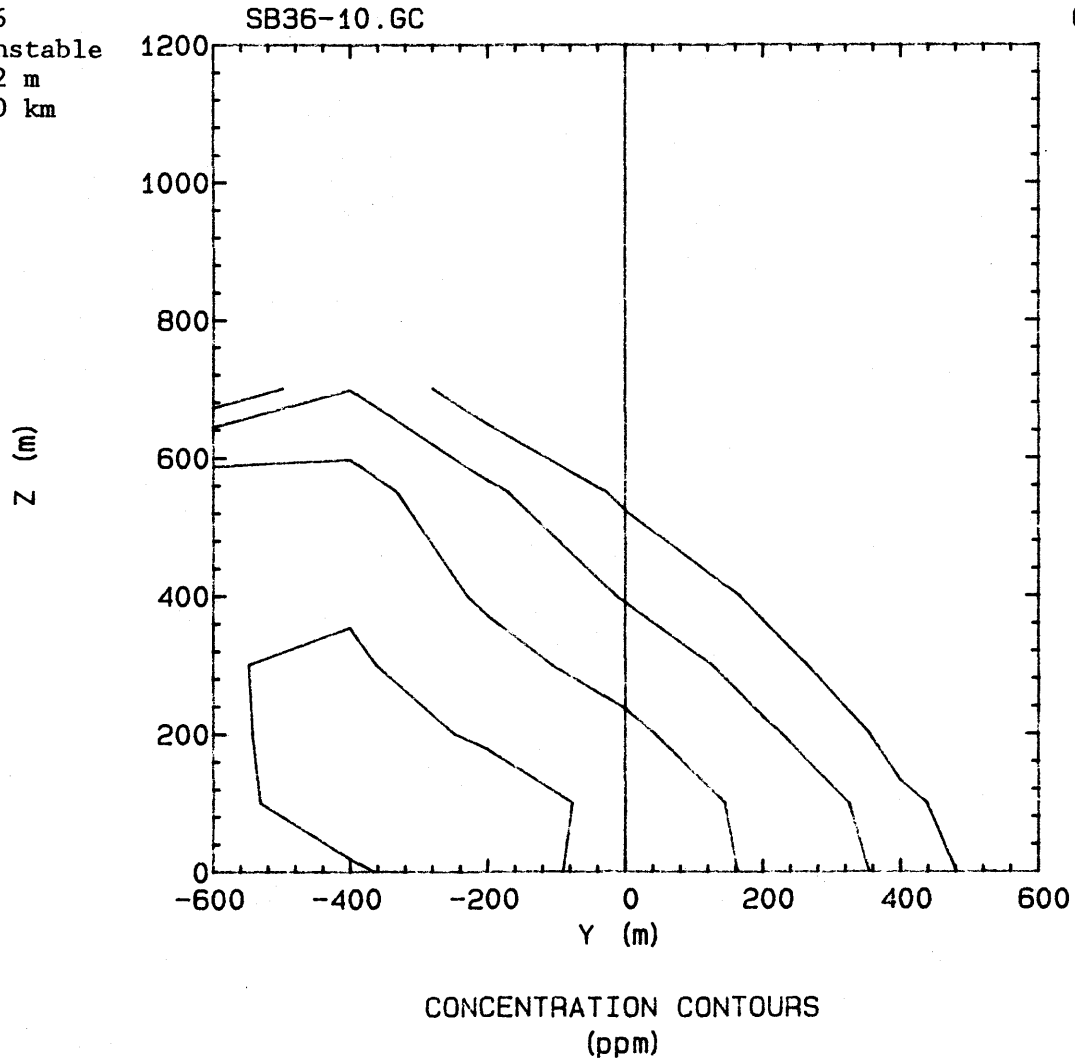
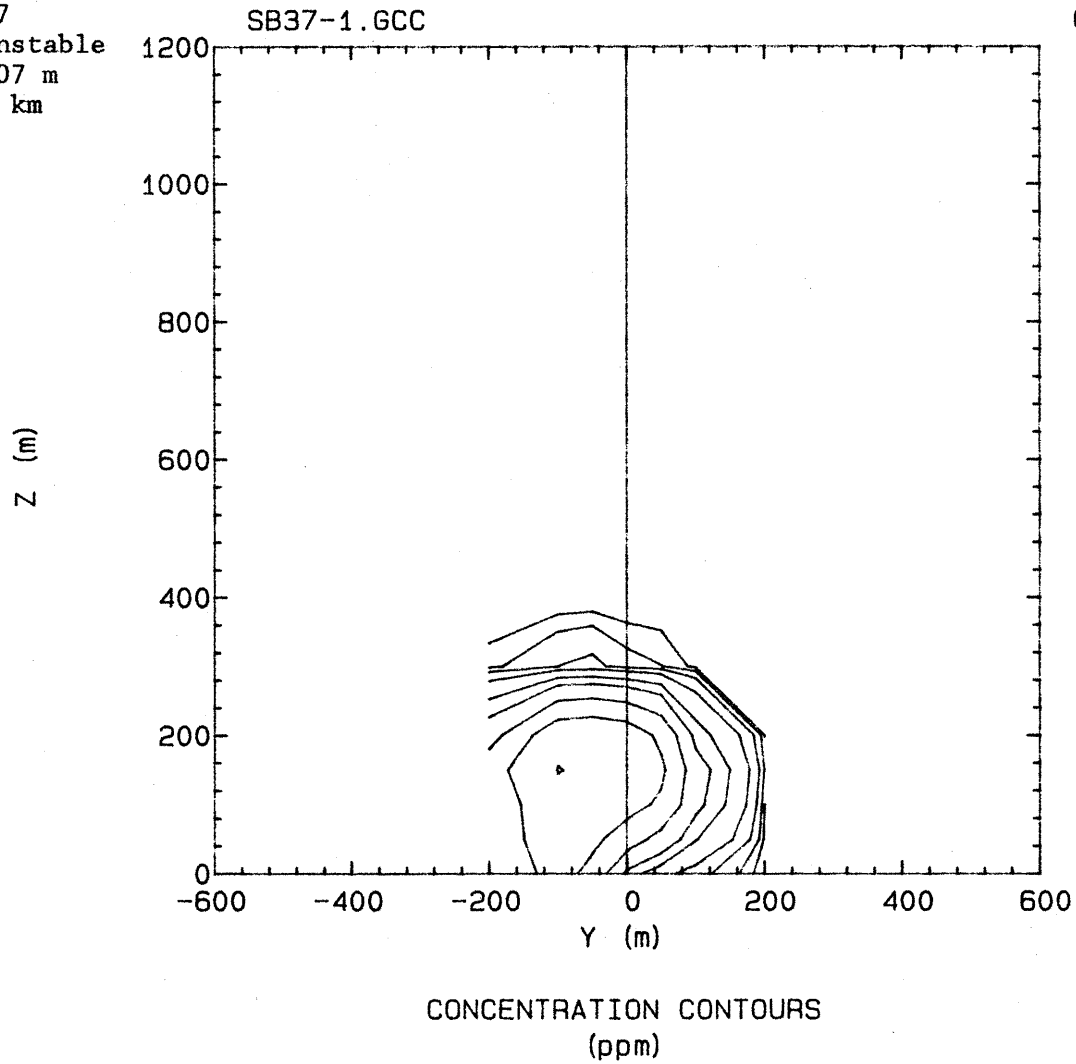


Figure 21-21. Concentration Contour Plots

Run 37
Flow Unstable
Stack Height 107 m
Downwind Distance 1 km



CONTOUR LEVELS

5.0
5.0
10.0
20.0
40.0
80.0
120.0
200.0
200.0
300.0
400.0

Figure 21-22. Concentration Contour Plots

Run 37
Flow Unstable
Stack Height 107 m
Downwind Distance 4 km

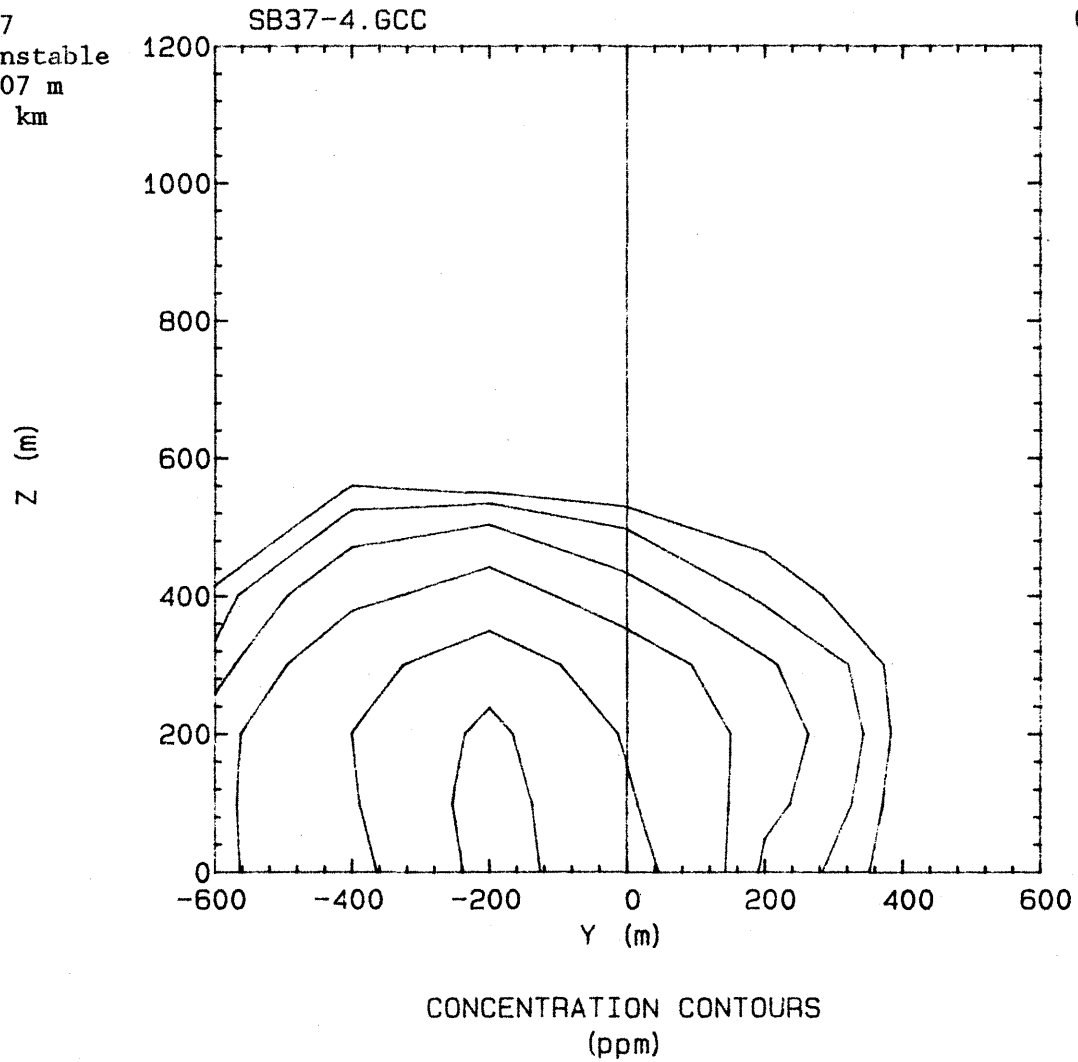


Figure 21-23. Concentration Contour Plots

Run 37
Flow Unstable
Stack Height 107 m
Downwind Distance 10 km

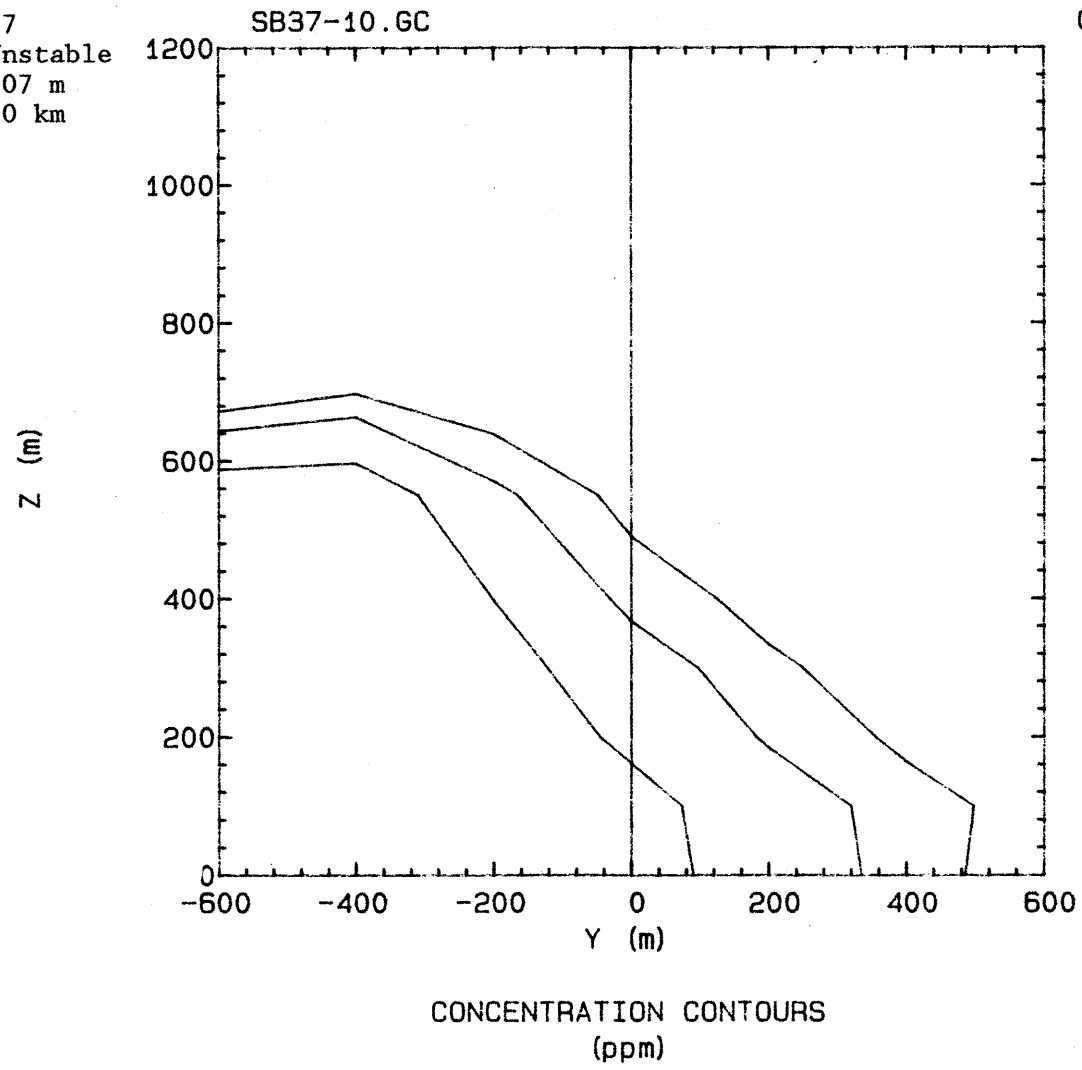


Figure 21-24. Concentration Contour Plots

Run 38
Flow Unstable
Stack Height 152 m
Downwind Distance 1 km

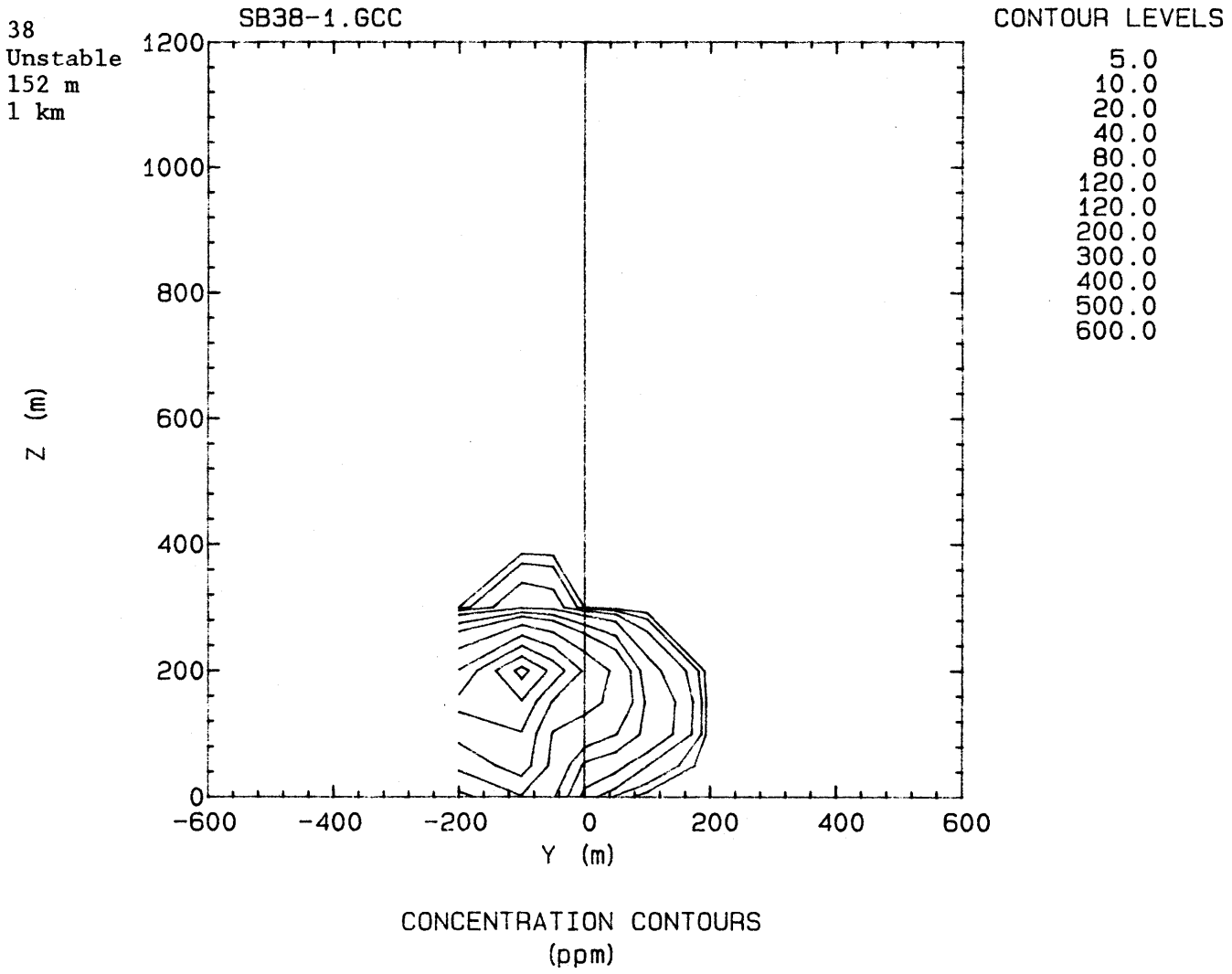


Figure 21-25. Concentration Contour Plots

Run 38
Flow Unstable
Stack Height 152 m
Downwind Distance 4 km

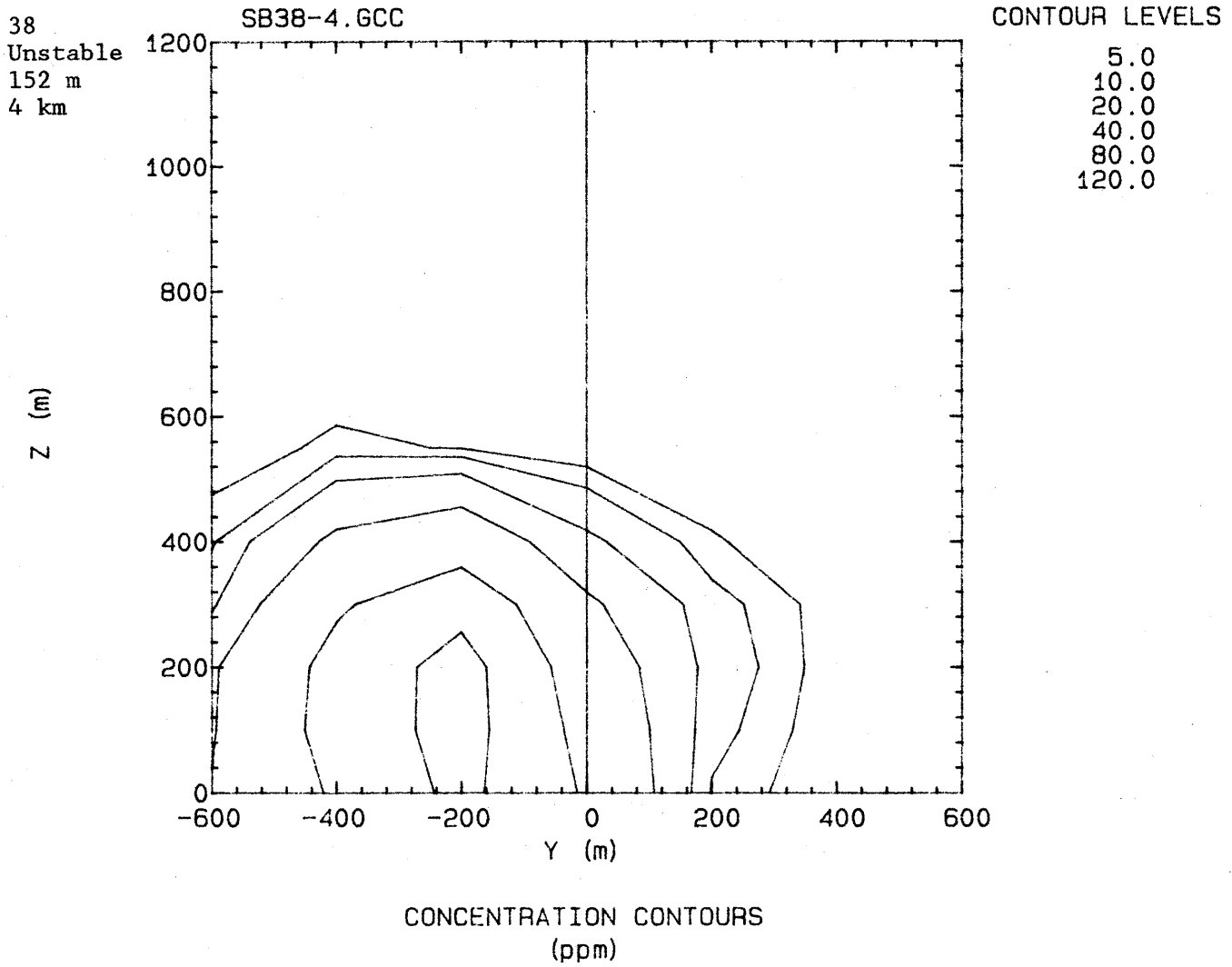
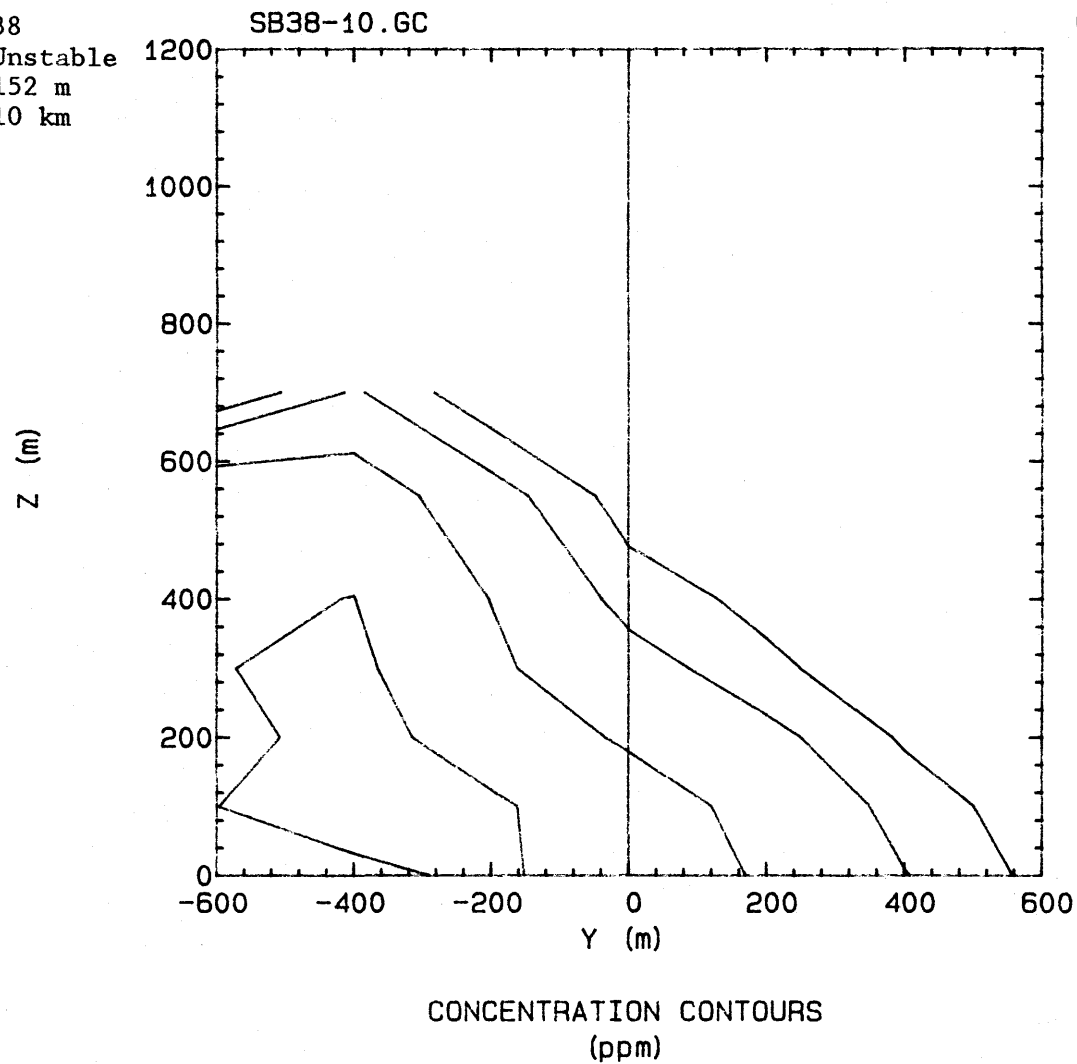


Figure 21-26. Concentration Contour Plots

Run 38
Flow Unstable
Stack Height 152 m
Downwind Distance 10 km



CONTOUR LEVELS
5.0
5.0
10.0
10.0
20.0
30.0

Figure 21-27. Concentration Contour Plots